CBX 2008-033
Qing He
David Asner
Edward Thorndike
October 10, 2008

Impact on γ/ϕ_3 measurement from CLEO-c binned $D^0 \to K^0_{S,L}\pi^+\pi^-$ Dalitz analysis

Abstract

This note describes CLEO-c impact on γ/ϕ_3 measurement using a Binned Dalitz analysis for $D^0 \to K^0_{S,L}\pi^+\pi^-$. We used the 818 pb^{-1} data sample collected at the $\psi(3770)$ resonance.

Contents

Chapter 1

Model independent approach to determine γ/ϕ_3

The Dalitz plot analysis of the three-body $\tilde{D}^0$ (D^0 or $\bar{D}^0$) decay from $B^\pm \to DK^\pm$ process provides today the best measurement of the CKM angle γ/ϕ_3

$$\gamma \equiv \arg\left(-\frac{V_{ud}V_{ub}^*}{V_{cd}V_{cb}^*}\right).$$

The unbinned $\tilde{D}^0 \to K_S^0\pi^+\pi^-$ Dalitz analysis has been implemented by BaBar [1] and Belle [2]. However, the unbinned technique is sensitive to the choice of the model used to describe the three-body D^0 decay, which introduce $7^\circ \sim 10^\circ$ uncertainty on γ determination. For LHCb and future Super-B factories, this uncertainty will become a major limitation. A model independent approach was introduced by Giri *et al.* [10] and investigated by A. Bondar *et al.* [11]. The model independent approach make use of charm factory data to obtain the missing information about the D^0 decay amplitude.

1.1 Model Independent Determination of γ

Here we repeat the procedure developed in [10], [11]. The cascade decay,

$$B^+ \to DK^+ \to (K_S^0\pi^-\pi^+)_D K^+, \tag{1.1}$$

is used to measure the angle,

$$\gamma = \arg\left(-\frac{V_{ud}V_{ub}^*}{V_{cd}V_{cb}^*}\right). \tag{1.2}$$

Define the amplitudes,

$$A(B^+ \to D^0K^+) \equiv A_B, \tag{1.3}$$
$$A(B^+ \to \bar{D}^0K^+) \equiv A_B r_b e^{i(\delta_B+\gamma)}, \tag{1.4}$$

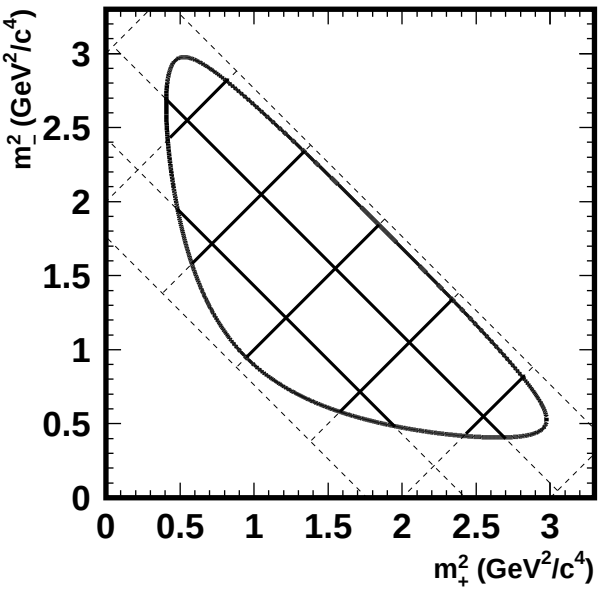

Figure 1.1: Binning of the $D^0 \to K^0_S\pi^+\pi^-$ Dalitz plot. $M^2_+ = M^2_{K^0_S\pi^+}$, $M^2_- = M^2_{K^0_S\pi^-}$

and

$$\begin{aligned} x &\equiv m^2_{K^0_S\pi^+}, && (1.5)\\ y &\equiv m^2_{K^0_S\pi^-}, && (1.6)\\ A_D(x,y) &\equiv A_{x,y}e^{i\delta_{x,y}} \\ &\equiv A(D^0 \to K^0_S\pi^-\pi^+) \\ &= A(\bar{D^0} \to K^0_S\pi^+\pi^-). && (1.7) \end{aligned}$$

Note here we made the assumption that there is no CP violation in D meson system. The amplitude for the cascade decay is,

$$A(B^+ \to (K^0_S\pi^-\pi^+)_D K^+) = A_B\mathcal{P}_D(A_D(x,y) + r_B e^{i(\delta_B+\gamma)}A_D(y,x)), \quad (1.8)$$

where $\mathcal{P}_D$ is the D meson propagator. Using the extremely accurate narrow width approximation for the D meson propagator, we get the expression for the reduced partial decay width:

$$\begin{aligned} &d\Gamma(B^+ \to (K^0_S\pi^-\pi^+)_D K^+) = \\ &(A^2_{x,y} + r^2_B A^2_{y,x} + 2r_B\mathrm{Re}[A_D(x,y)A^*_D(y,x)e^{-i(\delta_B+\gamma)}])dp, \end{aligned} \quad (1.9)$$

where dp denotes the phase space variables.

We partition the Dalitz plot into $2\mathcal{N}$ bins which are symmetric under exchange of x and y, as shown in Fig. 1.1. The $\mathcal{N}$ bins lying below the symmetry axis are denoted by the index i,

while the remaining bins are indexed with $\bar{i}$. Define quantities,

$$T_i \equiv \int_i |A_D(x,y)|^2 dxdy, \tag{1.10}$$

$$G_i \equiv \int_i A_D(x,y)A_D^*(y,x)dxdy, \tag{1.11}$$

and,

$$c_i \equiv \frac{\mathrm{Re}[G_i]}{\sqrt{T_i T_{\bar{i}}}} = \frac{1}{\sqrt{T_i T_{\bar{i}}}} \int_{D_i} |A_D(x,y)||A_D(y,x)| \cos(\delta_{x,y} - \delta_{y,x}) dxdy \tag{1.12}$$

$$s_i \equiv \frac{\mathrm{Im}[G_i]}{\sqrt{T_i T_{\bar{i}}}} = \frac{1}{\sqrt{T_i T_{\bar{i}}}} \int_{D_i} |A_D(x,y)||A_D(y,x)| \sin(\delta_{x,y} - \delta_{y,x}) dxdy, \tag{1.13}$$

where $\delta_{x,y}$ and $\delta_{y,x}$ are the phases for $A_D(x,y)$ and $A_D(y,x)$, respectively. The variables c_i, s_i of the i-th bin are related to the variables of the $\bar{i}$-th bin by

$$c_{\bar{i}} = c_i, \qquad\qquad s_{\bar{i}} = -s_i, \tag{1.14}$$

while there is no relation between T_i and $T_{\bar{i}}$. Then,

$$\begin{aligned} \Gamma_i^+ &\equiv \int_i d\Gamma(B^+ \to (K_S^0\pi^-\pi^+)_D K^+) \\ &= T_i + r_B^2 T_{\bar{i}} + 2r_B\sqrt{T_i T_{\bar{i}}}[\cos(\delta_B+\gamma)c_i + \sin(\delta_B+\gamma)s_i], \end{aligned} \tag{1.15}$$

$$\begin{aligned} \Gamma_{\bar{i}}^+ &\equiv \int_{\bar{i}} d\Gamma(B^+ \to (K_S^0\pi^-\pi^+)_D K^+) \\ &= T_{\bar{i}} + r_B^2 T_i + 2r_B\sqrt{T_i T_{\bar{i}}}[\cos(\delta_B+\gamma)c_i - \sin(\delta_B+\gamma)s_i] \end{aligned} \tag{1.16}$$

In order to express these variables in terms of yields in Dalitz plot, we need to define the number of events in the i-th bin

$$K_i = a_D \int_i |A_D(x,y)|^2 dxdy = a_D T_i. \tag{1.17}$$

The normalization factor a_D is just defined so that

$$\sum_i K_i = a_D \sum_i T_i = N, \tag{1.18}$$

where N is the total number of events in the Dalitz plot.

The number of events in the i-th bin of a Dalitz plot originating from a B^+ decay is similarly,

$$\begin{aligned} N_i^+ &= a_B \int_i |A_{B^+}(x,y)|^2 dxdy \\ &= a_B \int_i (|A_D(x,y)|^2 + r_B^2 |A_D(y,x)|^2 + 2r_B \mathrm{Re}[A_D(x,y)A_D(y,x)^* e^{-i(\delta_B+\gamma)}]) dxdy \\ &= a_B [T_i + r_B^2 T_{\bar{i}} + 2r_B \sqrt{T_i T_{\bar{i}}}([\cos(\delta_B+\gamma)c_i + \sin(\delta_B+\gamma)s_i)] \\ &= \frac{a_B}{a_D}[K_i + r_B^2 K_{\bar{i}} + 2r_B \sqrt{K_i K_{\bar{i}}}(\cos(\delta_B+\gamma)c_i + \sin(\delta_B+\gamma)s_i)]. \end{aligned} \tag{1.19}$$

T_i can be obtained from flavor tagged $D \to K_S^0\pi^+\pi^-$ decays, and c_i can be obtained from CP tagged $D \to K_S^0\pi^+\pi^-$ decays.

1.2 Phase bins

While the original idea of Giri *et al.* [10] is to divide the Dalitz plot into square bins, as shown in Fig. 1.1, Bondar *et al.* proposed to use model dependent strong phase bins, which will provide higher sensitivity to the γ measurement [11].

In this note, we adapt Bondar *et al.*'s idea, use uniform $\Delta\delta_D$ bin based on the BaBar model [1], where $\Delta\delta_D = \delta_D(m^2_{K_S^0\pi^+}, m^2_{K_S^0\pi^-}) - \delta_D(m^2_{K_S^0\pi^-}, m^2_{K_S^0\pi^+})$. In the half of the Dalitz plot $m^2_{K_S^0\pi^+} < m^2_{K_S^0\pi^-}$, the bin $\mathcal{D}_i$ is defined by condition

$$2\pi(i-1/2)/N < \Delta\delta_D < 2\pi(i+1/2)/N, \tag{1.20}$$

where $i = 0, 1, 2\cdots, N$. In the remaining part of Dalitz plot, the bins are defined symmetrically. Such binning choice with $N = 8$ is shown in Fig. 1.2. The plot is produced by dividing the phase space into 1000×1000 bins. The $\Delta\delta_D$ is calculated in each point(bin). When counting the number of events, the $\Delta\delta_D$ for the every single event is calculated based on its $M^2_{K_S^0\pi^+}$, $M^2_{K_S^0\pi^-}$ values.

1.3 Determining c_i from CP tagged $K_S^0\pi^+\pi^-$ decays

For $\psi(3770)$ decaying into a $D\bar{D}$ pair, since $\psi(3770)$ is produced through a virtual photon ($CP = +1$), if one D meson is detected in a CP eigenstate, the other D is also a CP eigenstate with opposite CP eigenvalue. The amplitude and partial decay width are,

$$A_{CP\pm}(x,y) = \frac{1}{\sqrt{2}}|A_D(x,y) \pm A_D(y,x)|, \tag{1.21}$$

$$d\Gamma_{CP\pm} = (\frac{1}{2}(A_{x,y}^2 + A_{y,x}^2) \pm A_{x,y}A_{y,x}\cos(\delta_{x,y} - \delta_{y,x}))dp. \tag{1.22}$$

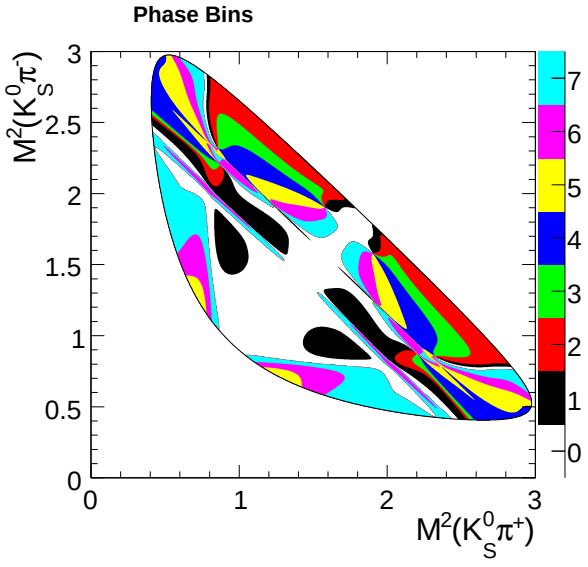

Figure 1.2: δ_D binning in Dalitz plot for 8 bin case. (The plots are produced by dividing the phase space into 1000×1000 bins. The $\Delta\delta_D$ is calculated in each point(bin).)

Define $M_i^{\pm}$ as the number of events in the i-th bin of a CP-tagged Dalitz plot, then

$$\begin{aligned} M_i^{\pm} &= a_{\pm} \int_i |A_{CP\pm}(x,y)|^2 dxdy \\ &= \frac{a_{\pm}}{2}(T_i \pm 2\mathrm{Re}[G_i] + T_{\bar{i}}) \\ &= \frac{a_{\pm}}{2a_D}(K_i \pm 2c_i\sqrt{K_iK_{\bar{i}}} + K_{\bar{i}}). \end{aligned} \tag{1.23}$$

Define

$$\bar{M_i^{\pm}} \equiv \frac{2a_D M_i^{\pm}}{a_{\pm}}, \tag{1.24}$$

then,

$$\bar{M_i^{+}} = K_i + 2c_i\sqrt{K_iK_{\bar{i}}} + K_{\bar{i}}, \tag{1.25}$$

$$\bar{M_i^{-}} = K_i - 2c_i\sqrt{K_iK_{\bar{i}}} + K_{\bar{i}}. \tag{1.26}$$

Add Equation 1.25 and Equation 1.26, we have,

$$\bar{M_i^{+}} + \bar{M_i^{-}} = 2(K_i + K_{\bar{i}}). \tag{1.27}$$

Subtract Equation 1.26 from Equation 1.25, we have,

$$\bar{M_i^+} - \bar{M_i^-} = 4c_i\sqrt{K_i K_{\bar{i}}}. \tag{1.28}$$

Then,

$$\begin{aligned} c_i &= \frac{(\bar{M_i^+} - \bar{M_i^-})}{4\sqrt{K_i K_{\bar{i}}}} \\ &= \frac{(\bar{M_i^+} - \bar{M_i^-})}{(\bar{M_i^+} + \bar{M_i^-})}\frac{2(K_i + K_{\bar{i}})}{4\sqrt{K_i K_{\bar{i}}}} \\ &= \frac{(\bar{M_i^+} - \bar{M_i^-})}{(\bar{M_i^+} + \bar{M_i^-})}\frac{(K_i + K_{\bar{i}})}{2\sqrt{K_i K_{\bar{i}}}} \\ &= \frac{(a_- M_i^+ - a_+ M_i^-)}{(a_- M_i^+ + a_+ M_i^-)}\frac{(K_i + K_{\bar{i}})}{2\sqrt{K_i K_{\bar{i}}}}. \end{aligned} \tag{1.29}$$

The coefficients, $a_\pm$, are not known, we need to represent them with known variables. Since,

$$\begin{aligned} M_i^\pm &= a_\pm \int_i |A_{CP\pm}(x,y)|^2 dxdy \\ &= S_\pm \mathcal{B}_\pm \frac{\int_i |A_{CP\pm}(x,y)|^2 dxdy}{\int |A_{CP\pm}(x,y)|^2 dxdy}, \end{aligned} \tag{1.30}$$

where $S_\pm$ is the number of single tags and $\mathcal{B}_\pm$ is the branching fraction of $K^0_S\pi\pi$ mode in CP even and CP odd samples. Note that here all the numbers are already efficiency corrected.

Since $\Gamma(D^0 \to CP+) = \Gamma(D^0 \to CP-)$ (if no mixing), then,

$$\frac{\mathcal{B}_+}{\mathcal{B}_-} = \frac{\int |A_{CP+}(x,y)|^2 dxdy}{\int |A_{CP-}(x,y)|^2 dxdy}. \tag{1.31}$$

Then,

$$\frac{a_+}{a_-} = \frac{S_+}{S_-}, \tag{1.32}$$

similarly, we can get,

$$\frac{a_\pm}{a_D} = \frac{S_\pm}{S_f}, \tag{1.33}$$

where S_f is number of single tags for flavor modes. Then c_i can be calculated using,

$$c_i = \frac{(M_i^+/S_+ - M_i^-/S_-)}{(M_i^+/S_+ + M_i^-/S_-)}\frac{(K_i + K_{\bar{i}})}{2\sqrt{K_i K_{\bar{i}}}}. \tag{1.34}$$

Equation 1.34 compute c_i by combining both CP even and CP odd samples together. Actually,

either CP even or CP odd samples can determine c_i separately, from Equation 1.23,

$$\frac{M_i^{\pm}}{S^{\pm}} = \frac{K_i \pm 2c_i\sqrt{K_iK_{\bar{i}}} + K_{\bar{i}}}{2S_f}. \tag{1.35}$$

By counting the yields in each bin of the Dalitz plot, we can get $M_i^{\pm}$ and $K_{i/\bar{i}}$. Combining with the tags number of CP modes, we can calculate c_i according Equation 1.34.

1.4 Determining c_i and s_i from $K^0_S\pi^+\pi^-$ vs. $K^0_S\pi^+\pi^-$ decay

Using CP tagged $K^0_S\pi^+\pi^-$, one can only determine c_i. Using $K^0_S\pi^+\pi^-$ vs. $K^0_S\pi^+\pi^-$ data, one can determine c_i and s_i simultaneously with the mechanism explained below.

When both D (denote as D and D') mesons from the $\psi(3770)$ decay into the $K^0_S\pi^+\pi^-$ final state, the amplitude and partial decay width are

$$A_{corr}(x,y,x',y') = \frac{1}{\sqrt{2}}(A_D(x,y)A_D(y',x') - A_D(x',y')A_D(y,x)), \tag{1.36}$$

$$\begin{aligned} d\Gamma_{corr} &= \frac{1}{2}(A^2_{x,y}A^2_{y',x'} + A^2_{y,x}A^2_{x',y'} - \\ &\quad 2A_{x,y}A_{y',x'}A_{y,x}A_{x',y'}\cos[(\delta_{x,y}-\delta_{y,x}) - (\delta_{x',y'}-\delta_{y',x'})])dp. \end{aligned} \tag{1.37}$$

Define $M_{i,j}$ as the number of events with D in the i-th bin and D' in the j-th bin, then

$$\begin{aligned} M_{i,j} &= \frac{1}{2}a_{corr}\int_i\int_j |A_D(x,y)A_D(y',x') - A_D(x',y')A_D(y,x)|^2 dxdydx'dy' \\ &= \frac{1}{2}a_{corr}(T_iT_{\bar{j}} + T_{\bar{i}}T_j - 2\sqrt{T_iT_{\bar{j}}T_{\bar{i}}T_j}(c_ic_j + s_is_j)) \\ &= \frac{a_{corr}}{2a_D^2}(K_iK_{\bar{j}} + K_{\bar{i}}K_j - 2\sqrt{K_iK_{\bar{j}}K_{\bar{i}}K_j}(c_ic_j + s_is_j)). \end{aligned} \tag{1.38}$$

Now we need to figure out what is a_{corr}/a_D^2.

$$M = a_{corr}\int |A_{corr}(x,y,x',y')|^2 dxdydx'dy' \tag{1.39}$$

$$K = a_D\int |A_D(x,y)|^2 dxdy \tag{1.40}$$

On the other hand, if assume 100% efficiency,

$$M = N_{D,\bar{D}}\mathcal{B}_{doub} = N_{D,\bar{D}}\frac{\int |A_{corr}(x,y,x',y')|^2 dxdydx'dy'}{\int |A_{D,\bar{D}}|^2 dp} \tag{1.41}$$

$$K = 2N_{D,\bar{D}}\mathcal{B}_f\mathcal{B}_s = 2N_{D,\bar{D}}\frac{\int |A_f|^2 dp \int |A_D(x,y)|^2 dxdy}{\int |A_{D,\bar{D}}|^2 dp}. \tag{1.42}$$

Then,

$$\frac{a_{corr}}{a_D^2} = \frac{N_{D,\bar{D}}}{\int |A_{D,\bar{D}}|^2 dp}\frac{(\int |A_{D,\bar{D}}|^2 dp)^2}{(2N_{D,\bar{D}}\int |A_f|^2 dp)^2} \quad (1.43)$$

$$= \frac{\int |A_{D,\bar{D}}|^2 dp}{4N_{D,\bar{D}}(\int |A_f|^2 dp)^2} \quad (1.44)$$

$$= \frac{1}{4N_{D,\bar{D}}\mathcal{B}_f^2}, \quad (1.45)$$

$$M_{i,j} = \frac{1}{8N_{D,\bar{D}}\mathcal{B}_f^2}(K_iK_{\bar{j}} + K_{\bar{i}}K_j - 2\sqrt{K_iK_{\bar{j}}K_{\bar{i}}K_j}(c_ic_j + s_is_j))$$

$$= \frac{N_{D,\bar{D}}}{2S_f^2}(K_iK_{\bar{j}} + K_{\bar{i}}K_j - 2\sqrt{K_iK_{\bar{j}}K_{\bar{i}}K_j}(c_ic_j + s_is_j)), \quad (1.46)$$

where in the last step, we used $S_f = 2N_{D,\bar{D}}\mathcal{B}_f$. Note that $M_{i,j}$, K_i, K_j etc. need to be corrected by double tag efficiencies.

In contrast to CP tagged analysis, where the sign of s_i in each bin was undetermined and has to be fixed using model assumptions, $K^0_S\pi^+\pi^-$ vs. $K^0_S\pi^+\pi^-$ analysis has only a four-fold ambiguity: change of the sign of all c_i or all s_i. In combination with CP tagged analysis, where the sign of c_i is fixed, this ambiguity reduces to two-fold. One of the two solutions can be chosen based on a weak model assumption. This approach allows to extract both c_i and s_i simultaneously without additional model uncertainties. One can use the same binning of $K^0_S\pi^+\pi^-$ Dalitz plot for both CP tagged $K^0_S\pi^+\pi^-$ strategy and $K^0_S\pi^+\pi^-$ vs. $K^0_S\pi^+\pi^-$ strategy to improve the statistical accuracy.

1.5 Make use of $D^0/\bar{D}^0 \to K^0_L\pi^+\pi^-$ decay

1.5.1 $K^0_S\pi^+\pi^-$ and $K^0_L\pi^+\pi^-$ difference

Though only $K^0_S\pi^+\pi^-$ is used for γ measurement by B-factories, $K^0_L\pi^+\pi^-$, because of its close relationship to $K^0_S\pi^+\pi^-$, is useful in improving the c_i, s_i determination. We made use of both $D^0 \to K^0_S\pi^+\pi^-$ data and $D^0 \to K^0_L\pi^+\pi^-$ data in this analysis. Here, we study the difference between $K^0_S\pi^+\pi^-$ and $K^0_L\pi^+\pi^-$.

First, let's start from the K^0_S and K^0_L definition,

$$K^0_S = (K^0 + \bar{K}^0)/\sqrt{2}, \quad (1.47)$$

$$K^0_L = (K^0 - \bar{K}^0)/\sqrt{2}. \quad (1.48)$$

The relative sign between K^0 and $\bar{K}^0$ components for K^0_S and K^0_L is different. Apparently, this makes the CP eigenvalues for K^0_S eigenstates and K^0_L eigenstates differ by a sign. Since we

follow the convention $A(D^0 \to K^0_S\pi^+\pi^-) = A(\bar{D}^0 \to K^0_S\pi^-\pi^+)$, then

$$A(D^0 \to K^0_L\pi^+\pi^-) = -A(\bar{D}^0 \to K^0_L\pi^-\pi^+). \tag{1.49}$$

This will give us a sign change in some of the calculations associated with $K^0_L\pi^+\pi^-$.

Besides the difference stated above, doubly Cabibbo suppressed decay of $D^0/\bar{D}^0$ will introduce a second order differences between $K^0_S\pi^+\pi^-$ and $K^0_L\pi^+\pi^-$ Dalitz plot. For the process $\bar{D}^0 \to K^0_S\pi^+\pi^-$, $\bar{D}^0$ mainly go through $K^0\pi^+\pi^-$, with a small part go through $\bar{K}^0\pi^+\pi^-$, which is doubly Cabibbo suppressed. The wrong sign $\bar{K}^0$ decay introduce 180° of difference between the phase of K^0_S and K^0_L. For charged K^* resonances, this difference change the phase of all wrong sign K^* decay by 180°. For neutral resonances, such as ρ^0, the situation is more complicated, the difference not only affect the phase, it may also affect the magnitude of the amplitude. Similar effect has been studied in $D^0/\bar{D}^0 \to K_{S,L}\pi^0$ and $D^\pm \to K_{S,L}\pi^\pm$ decays [15]. While the internal interfere mechanism of $D^0 \to K_{S,L}\pi^+\pi^-$ is not clear, as in $D \to K_{S,L}\pi$ system, we investigate the difference by varying the amplitude of the resonances of $K^0_S\pi^+\pi^-$ to see how big is the change for the c_i and s_i, which are the values we are after.

1.5.2 CP tagged $K^0_L\pi^+\pi^-$

Let's denote c_i and s_i for $K^0_L\pi^+\pi^-$ as c'_i and s'_i.

The deduction of equations for CP tagged $K^0_L\pi^+\pi^-$ sample is very similar to that of CP tagged $K^0_S\pi^+\pi^-$ sample, which is shown in Section 1.3. The only difference is that there is a sign change between the two amplitudes in Equation 1.21. Here, we will only quote the final equaitons for CP tagged $K^0_L\pi^+\pi^-$,

$$\frac{M^\pm_i}{S^\pm} = \frac{K_i \mp 2c'_i\sqrt{K_iK_{\bar{i}}} + K_{\bar{i}}}{2S_f}. \tag{1.50}$$

1.5.3 $K^0_S\pi^+\pi^-$ vs. $K^0_L\pi^+\pi^-$

The situation for $K^0_S\pi^+\pi^-$ vs. $K^0_L\pi^+\pi^-$ is a little bit different from the case of $K^0_S\pi^+\pi^-$ vs. $K^0_S\pi^+\pi^-$.

$$\begin{aligned} A_{corr}(x,y,x',y') &= \frac{1}{\sqrt{2}}(A_D(K^0_S\pi^+\pi^-)A'_{\bar{D}}(K^0_L\pi^+\pi^-) - A'_D(K^0_L\pi^+\pi^-)A_{\bar{D}}(K^0_S\pi^+\pi^-)) \\ &= -\frac{1}{\sqrt{2}}(A_D(x,y)A'_D(y',x') + A'_D(x',y')A_D(y,x)), \end{aligned} \tag{1.51}$$

where A'_D is the amplitude for $K^0_L\pi^+\pi^-$.

$$\begin{aligned} d\Gamma_{corr} &= \frac{1}{2}(A^2_{x,y}A'^2_{y',x'} + A^2_{y,x}A'^2_{x',y'} + \\ &\quad 2A_{x,y}A'_{y',x'}A_{y,x}A'_{x',y'}\cos[(\delta_{x,y} - \delta_{y,x}) - (\delta'_{x',y'} - \delta'_{y',x'})])dp. \end{aligned}$$

Define $M_{i,j}$ as the number of events with $D(K^0_S\pi^+\pi^-)$ in the i-th bin and $D'(K^0_L\pi^+\pi^-)$ in the j-th bin, then

$$\begin{aligned} M_{i,j} &= \frac{1}{2}a_{corr}\int_i\int_j |A'_D(x,y)A_D(y',x') + A'_D(x',y')A_D(y,x)|^2 dxdydx'dy' \\ &= \frac{1}{2}a_{corr}(T_iT'_{\bar{j}} + T_{\bar{i}}T'_j + 2\sqrt{T_iT'_{\bar{j}}T_{\bar{i}}T'_j}(c_ic'_j + s_is'_j)) \\ &= \frac{a_{corr}}{2a_D^2}(K_iK'_{\bar{j}} + K_{\bar{i}}K'_j + 2\sqrt{K_iK'_{\bar{j}}K_{\bar{i}}K'_j}(c_ic'_j + s_is'_j)) \\ &= \frac{N_{D,\bar{D}}}{2S_fS'_f}(K_iK'_{\bar{j}} + K_{\bar{i}}K'_j + 2\sqrt{K_iK'_{\bar{j}}K_{\bar{i}}K'_j}(c_ic'_j + s_is'_j)). \end{aligned} \tag{1.52}$$

All the notations with a superscript ' are related to $K^0_L\pi^+\pi^-$.

1.5.4 Relations between (c_i, s_i) and (c'_i, s'_i)

Consider the amplitude for $D^0 \to \bar{K}^0\pi^+\pi^-$ (a Cabibbo-favored decay), and for $D^0 \to K^0\pi^+\pi^-$ (a DCSD decay). Then

$$A(D^0 \to K^0_S\pi^+\pi^-) = \frac{1}{\sqrt{2}}[A(D^0 \to \bar{K}^0\pi^+\pi^-) + A(D^0 \to K^0\pi^+\pi^-)], \tag{1.53}$$

and

$$A(D^0 \to K^0_L\pi^+\pi^-) = \frac{1}{\sqrt{2}}[A(D^0 \to \bar{K}^0\pi^+\pi^-) - A(D^0 \to K^0\pi^+\pi^-)], \tag{1.54}$$

thus,

$$A(D^0 \to K^0_L\pi^+\pi^-) = A(D^0 \to K^0_S\pi^+\pi^-) - \sqrt{2}A(D^0 \to K^0\pi^+\pi^-). \tag{1.55}$$

The decay $D^0 \to \bar{K}^0\pi^+\pi^-$ will include final state of the form $K^{*-}\pi^+$, "ρ^0"$\bar{K}^0$, and "f_0"$\bar{K}^0$, where "ρ^0" stands for $\pi^+\pi^-$ in a L=odd state, and "f_0" stands for $\pi^+\pi^-$ in a L=even state, where L is the angular momentum. The decay $D^0 \to K^0\pi^+\pi^-$ will include final states of the form $K^{*+}\pi^-$, also "ρ^0"K^0 and "f_0"K^0. Thus we write

$$A(D^0 \to \bar{K}^0\pi^+\pi^-) = \sum_i a_iK^{*-}_i\pi^+ + \sum_j a_j\rho^0_j\bar{K}^0 + \sum_k a_kf^0_k\bar{K}^0, \tag{1.56}$$

and

$$A(D^0 \to K^0\pi^+\pi^-) = \sum_i b_iK^{*+}_i\pi^- + \sum_j b_j\rho^0_jK^0 + \sum_k b_kf^0_kK^0. \tag{1.57}$$

From this it follows

$$\begin{aligned} A(D^0 \to K^0_S\pi^+\pi^-) &= \frac{1}{\sqrt{2}}\sum_i a_i K^{*-}_i\pi^+ + \frac{1}{\sqrt{2}}\sum_i b_i K^{*+}_i\pi^- \\ &\quad + \sum_j (a_j + b_j)\rho^0_j K^0_S + \sum_k (a_k + b_k) f^0_k K^0_S, \end{aligned} \tag{1.58}$$

and

$$\begin{aligned} A(D^0 \to K^0_L\pi^+\pi^-) &= \frac{1}{\sqrt{2}}\sum_i a_i K^{*-}_i\pi^+ - \frac{1}{\sqrt{2}}\sum_i b_i K^{*+}_i\pi^- \\ &\quad + \sum_j (a_j - b_j)\rho^0_j K^0_L + \sum_k (a_k - b_k) f^0_k K^0_L. \end{aligned} \tag{1.59}$$

So, in going from $K^0_S\pi^+\pi^-$ to $K^0_L\pi^+\pi^-$

1. The K^{*-} terms do not change;
2. The K^{*+} terms change sign;
3. The ρ^0 terms change, from $a_j + b_j$ to $a_j - b_j$;
4. The f_0 terms change, from $a_k + b_k$ to $a_k - b_k$;

If we call the $K^0_S\pi^+\pi^-$ coefficients d_j, d_k, then the $K^0_L\pi^+\pi^-$ coefficients are $d_j - 2b_j$, $d_k - 2b_k$. With the proceeding as introduction, we are now in a position to compute the difference between c_i for $K^0_S\pi^+\pi^-$ and c'_i for $K^0_L\pi^+\pi^-$.

Though flipping the signs of the $K^{*+}\pi^-$ terms is straight forward, handling the ρ^0 and f_0 terms is *not*. We need to determine the change in the c_i's when the d_j's are replaced by $d_j - 2b_j$, and the d_k's are replaced by $d_k - 2b_k$. We know the d_j, d_k from the BaBar Dalitz plot fit. But, we have very limited knowledge of b_j, b_k. Since they are from DCSD, they should be down, relative to a_j, a_k, by a factor $\sim (V_{cd}V_{us})/(V_{cs}V_{ub}) \sim 1/20$. But that is about all we know, absent more theoretical work.

So for each ρ^0_j in turn, we replace d_j with $d_j(1 - 2re^{i\alpha})$, and see how much the c_i's change. Here r is the ratio of DCSD to favored amplitude, which we take to be $\tan^2\theta_C$ (θ_C is the Cabibbo angle), and α is a (totally unknown) phase, which we set it as 0°.

The procedure just described for the $\rho^0 K^0_S$ terms is repeated for the $f_0 K^0_S$ terms, with each d_k replaced with $d_k(1 - 2re^{i\alpha})$.

We start with the BaBar Dalitz plot analysis and make the following changes to $K^0_S\pi^+\pi^-$.

- $K^{*-}\pi^+$ terms unchanged
- Flipping the signs of the $K^{*+}\pi^-$ terms
- All ρ^0, f_0 terms time a same factor $1 - 2re^{i\alpha}$, where $r = \tan^2\theta_C \sim 0.0557$, $\alpha = 0°$.
- Non resonant component treated same as ρ^0 and f_0 terms.

The (c_i, s_i) and (c'_i, s'_i) for the BaBar model are shown in Table 1.1.

Table 1.1: The BaBar model predictions for (c_i, s_i) and (c'_i, s'_i).

i	c_i	s_i	c'_i	s'_i
1	0.769	0.032	0.868	-0.002
2	0.570	0.396	0.737	0.332
3	-0.044	0.765	0.283	0.752
4	-0.570	0.644	-0.317	0.777
5	-0.842	-0.152	-0.765	-0.111
6	-0.626	-0.574	-0.406	-0.612
7	-0.006	-0.766	0.410	-0.671
8	0.410	-0.386	0.594	-0.371

1.5.5 Model dependence

The corrections we applied are model dependent. It introduces the first systematic error for the corrections. We choose BaBar model to give us the corrections, while using Belle and CLEO models to estimate the systematic errors. BaBar and Belle models are fitted from high statistics samples, while CLEO model is extracted from very low statistics sample. The reason to include CLEO model is that BaBar and Belle models both include the controversial σ's, while CLEO model doesn't. The corrections for different models are shown in Table 1.2. The largest variation (away from Babar model predictions) is taken as the systematic error.

Table 1.2: BaBar, Belle, and CLEO model predictions for the corrections $\Delta c_i = c'_i - c_i$ and $\Delta s_i = s'_i - s_i$. The largest deviations from BaBar model predictions are taken as systematic errors.

	Δc_1	Δc_2	Δc_3	Δc_4	Δc_5	Δc_6	Δc_7	Δc_8
BaBar	0.099	0.167	0.327	0.253	0.077	0.22	0.416	0.184
Belle	0.104	0.16	0.217	0.087	0.03	0.153	0.353	0.189
CLEO II.V	0.06	0.143	0.234	0.084	0.111	0.211	0.259	0.17
Sys.	0.039	0.024	0.11	0.169	0.047	0.067	0.157	0.014
	Δs_1	Δs_2	Δs_3	Δs_4	Δs_5	Δs_6	Δs_7	Δs_8
BaBar	-0.034	-0.064	-0.013	0.133	0.041	-0.038	0.095	0.015
Belle	-0.056	-0.146	-0.031	0.006	0.004	-0.091	0.036	-0.01
CLEO II.V	0.032	-0.025	0.083	0.091	-0.02	-0.035	0.081	0.099
Sys.	0.066	0.082	0.096	0.127	0.061	0.053	0.059	0.084

1.5.6 Systematics from ρ^0, f_0 corrections

For all ρ^0 and f_0 type resonances, we have used the same r and α, which are supposed to be resonance dependent. To estimate the systematic errors, we no longer assume that all ρ^0 and f_0 have the same values of r and α. Rather, we assume they each vary from our "best guess" ($r = \tan^2\theta_C$, $\alpha = 0$), randomly and independently, according to a Gaussian distribution for r, with width 0.025 (conservatively take half size of r) and a uniform distribution in α $0 \sim 360°$,

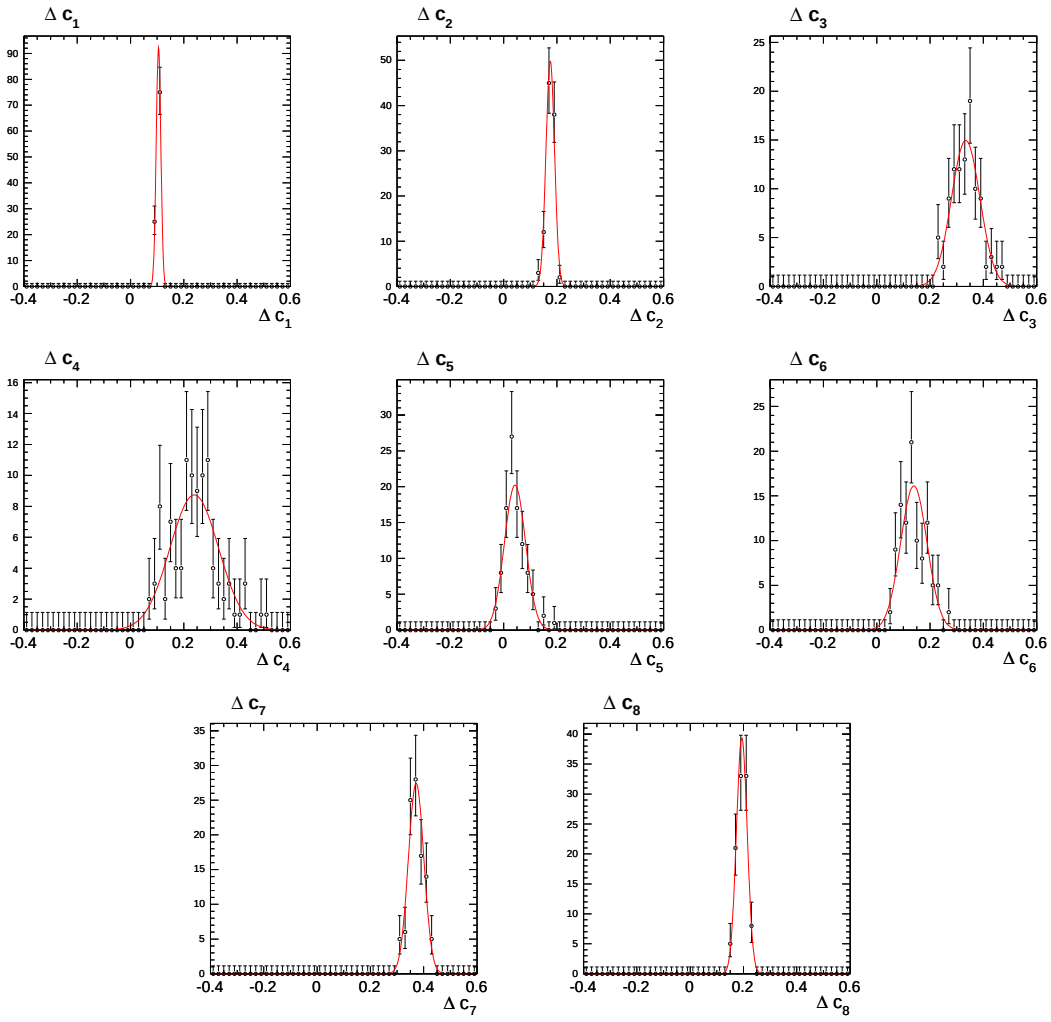

Figure 1.3: Δc_i distributions when randomly varying r and α for 100 times.

respectively. 100 samples are calculated and the Δc_i and Δs_i distributions are fitted with Gaussian distributions. The widths of the distributions are taken as systematic error. The results are shown in Fig. 1.3, Fig. 1.4 and Table 1.3.

1.5.7 Systematics

The sum of the systematics are shown in Table 1.4. In principle, there exists uncertainties for BaBar model itself, however, this uncertainty is much smaller than the systematics on model dependence. To avoid double counting the uncertainty on model, this part of uncertainty is not included.

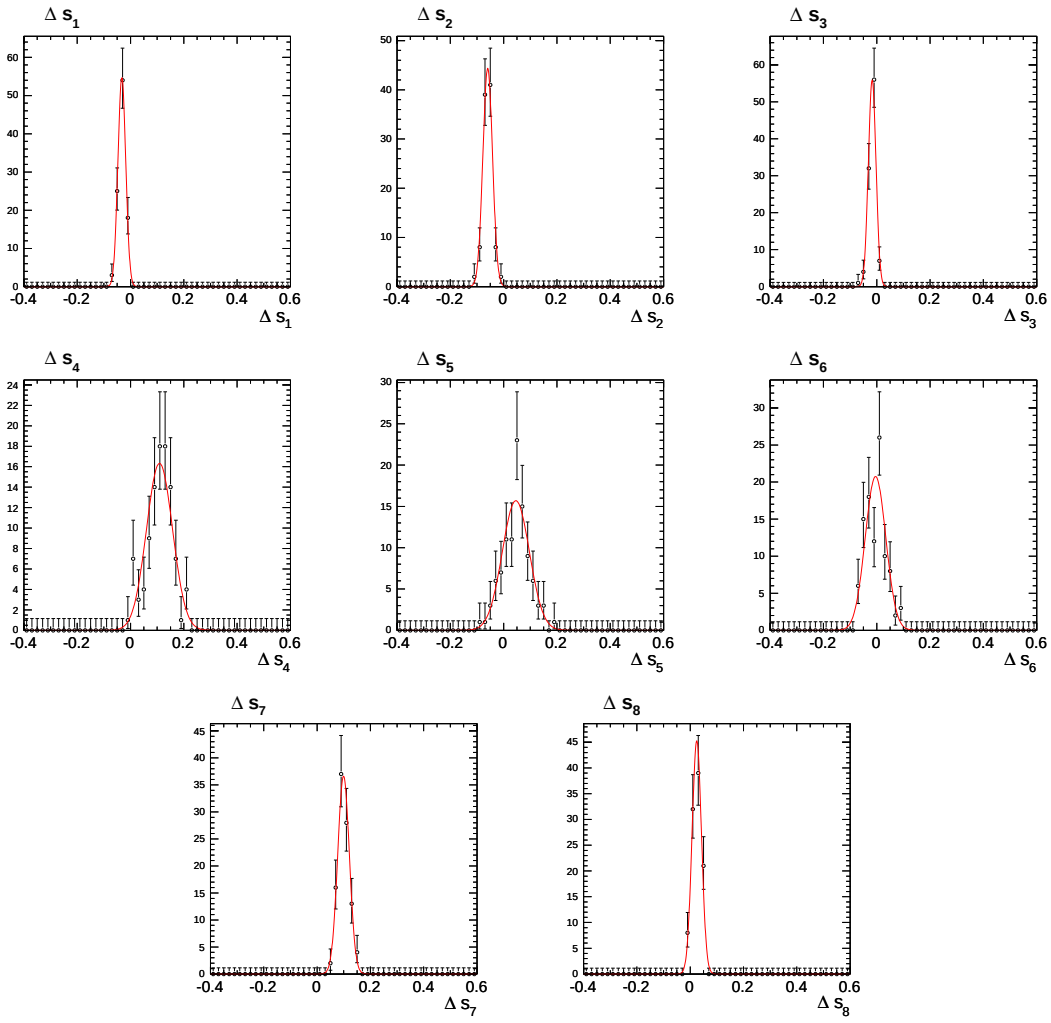

Figure 1.4: Δs_i distributions when randomly varying r and α for 100 times.

Table 1.3: Mean and central values for Δc_i and Δs_i distributions.

	mean	width		mean	width
Δc_1	0.105 ± 0.001	0.009 ± 0.001	Δs_1	-0.033 ± 0.001	0.015 ± 0.001
Δc_2	0.175 ± 0.002	0.016 ± 0.001	Δs_1	-0.060 ± 0.002	0.018 ± 0.001
Δc_3	0.334 ± 0.005	0.053 ± 0.004	Δs_1	-0.017 ± 0.001	0.014 ± 0.001
Δc_4	0.239 ± 0.009	0.091 ± 0.006	Δs_1	0.109 ± 0.005	0.049 ± 0.003
Δc_5	0.043 ± 0.004	0.039 ± 0.003	Δs_1	0.046 ± 0.005	0.051 ± 0.004
Δc_6	0.139 ± 0.005	0.050 ± 0.004	Δs_1	-0.005 ± 0.004	0.038 ± 0.003
Δc_7	0.372 ± 0.003	0.029 ± 0.002	Δs_1	0.099 ± 0.002	0.022 ± 0.002
Δc_8	0.194 ± 0.002	0.020 ± 0.001	Δs_1	0.025 ± 0.002	0.018 ± 0.001

Table 1.4: Systematic errors for $\Delta c_i = c_i' - c_i$ and $\Delta s_i = s_i' - s_i$

	Δc_1	Δc_2	Δc_3	Δc_4	Δc_5	Δc_6	Δc_7	Δc_8
Model Depen.	0.039	0.024	0.11	0.169	0.047	0.067	0.157	0.014
ρ, f_0	0.010	0.018	0.041	0.072	0.037	0.055	0.026	0.018
Sum	0.040	0.029	0.122	0.192	0.061	0.084	0.160	0.024
	Δs_1	Δs_2	Δs_3	Δs_4	Δs_5	Δs_6	Δs_7	Δs_8
Model Depen.	0.066	0.082	0.096	0.127	0.061	0.053	0.059	0.084
ρ, f_0	0.011	0.015	0.011	0.044	0.055	0.037	0.018	0.017
Sum	0.068	0.084	0.097	0.136	0.080	0.065	0.063	0.086

1.6 Global fit

The idea for doing a combined fit is shown in Fig. 1.5. There are two sets of c_i, s_i in Fig. 1.5. (c_i, s_i) are associated with $K^0_S\pi^+\pi^-$, while (c_i', s_i') are associated with $K^0_L\pi^+\pi^-$. Using CP tagged $K^0_S\pi^+\pi^-$ and $K^0_L\pi^+\pi^-$ data, one can determine c_i and c_i', respectively. Using $K^0_S\pi^+\pi^-$ vs. $K^0_S\pi^+\pi^-$ data, one can determine both c_i and s_i. Using $K^0_S\pi^+\pi^-$ vs. $K^0_L\pi^+\pi^-$ data, one can constrain all the variables, (c_i, s_i) and (c_i', s_i'). There are additional constrains from the relationship between (c_i, c_i') and (s_i, s_i'), which we studied in Section 1.5. Using all the relations shown in Fig. 1.5, we can perform a combined fit to all the data samples to extract all the parameters (c_i, s_i) and (c_i', s_i').

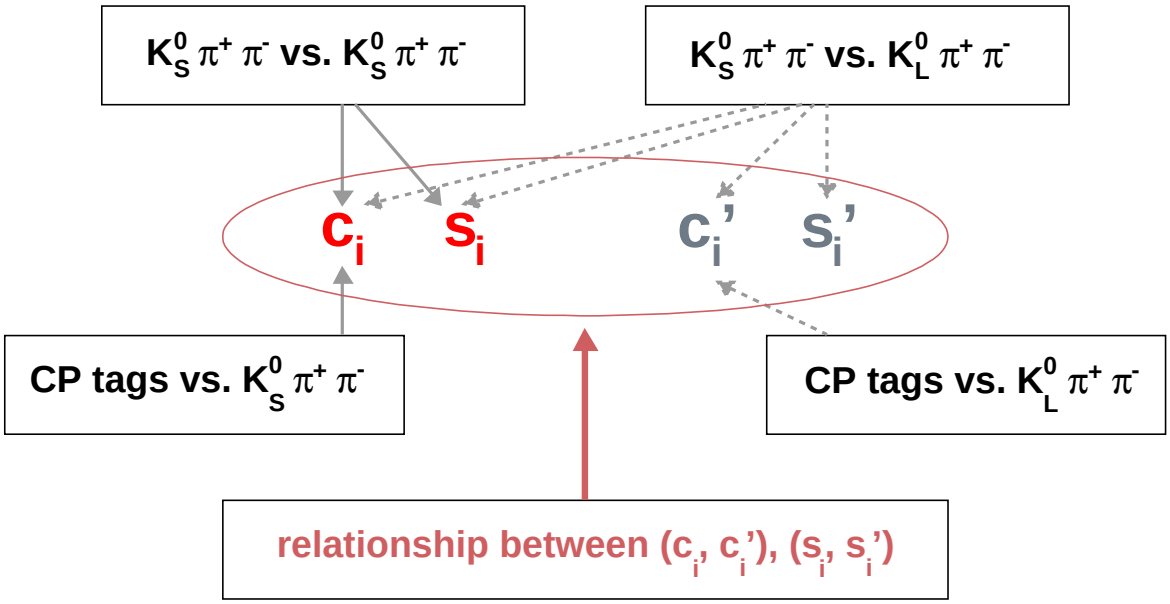

Figure 1.5: The idea for the global fit.

In terms of formulas, all the relations are listed below:

- CP tagged $K^0_S\pi^+\pi^-$, from Equation 1.35,

$$\frac{M_i^{\pm}}{S^{\pm}} = \frac{K_i \pm 2c_i\sqrt{K_iK_{\bar{i}}} + K_{\bar{i}}}{2S_f}$$

- CP tagged $K^0_L\pi^+\pi^-$

$$\frac{M_i^{\pm}}{S^{\pm}} = \frac{K'_i \mp 2c'_i\sqrt{K'_iK'_{\bar{i}}} + K'_{\bar{i}}}{2S'_f}$$

- $K^0_S\pi^+\pi^-$ vs. $K^0_S\pi^+\pi^-$, from Equation 1.46,

$$M_{i,j} = \frac{N_{D,\bar{D}}}{2S_f^2}(K_iK_{\bar{j}} + K_{\bar{i}}K_j - 2\sqrt{K_iK_{\bar{j}}K_{\bar{i}}K_j}(c_ic_j + s_is_j)),$$

- $K^0_S\pi^+\pi^-$ vs. $K^0_L\pi^+\pi^-$

$$M_{i,j} = \frac{N_{D,\bar{D}}}{2S_fS'_f}(K_iK'_{\bar{j}} + K_{\bar{i}}K'_j + 2\sqrt{K_iK'_{\bar{j}}K_{\bar{i}}K'_j}(c_ic'_j + s_is'_j)).$$

where $M_i^{\pm}$ is the number of CP tagged $K^0_{S,L}\pi^+\pi^-$ events in the i-th bin, $M_{i,j}$ is the number of events with D in the i-th bin and D' in the j-th bin, K_i is the number of flavor tagged $K^0_S\pi^+\pi^-$ events in the i-th bin, $S^{\pm}$ is the number of CP tags, S_f is the number of flavor tags.

The negative logarithmic likelihood function is constructed as follows:

$$\begin{aligned}
-2\log\mathcal{L} &= -2\sum_i \log P(M_i^{\pm}, \langle M_i^{\pm}\rangle)_{(CP,K^0_S\pi^+\pi^-)} \\
&\quad -2\sum_i \log P(M_i^{\pm}, \langle M_i^{\pm}\rangle)_{(CP,K^0_L\pi^+\pi^-)} \\
&\quad -2\sum_{i,j} \log P(M_{i,j}, \langle M_{i,j}\rangle)_{(K^0_S\pi^+\pi^-,K^0_S\pi^+\pi^-)} \\
&\quad -2\sum_{i,j} \log P(M_{i,j}, \langle M_{i,j}\rangle)_{(K^0_S\pi^+\pi^-,K^0_L\pi^+\pi^-)} \\
&\quad +\chi^2, \qquad (1.60)
\end{aligned}$$

where $P(M, \langle M\rangle)$ is the Poisson probability to get M events with the expected number of $\langle M\rangle$ events, χ^2 is the constrain term,

$$\chi^2 = \sum_i (\frac{c'_i - c_i - \Delta c_i}{\delta\Delta c_i})^2 + \sum_i (\frac{s'_i - s_i - \Delta s_i}{\delta\Delta s_i})^2,$$

where $\Delta c_i, \Delta s_i, \delta\Delta c_i, \delta\Delta s_i$ are calculated in Section 1.5.

Chapter 2

Data selection & Monte Carlo generation

All the notations include charge conjugate if not otherwise specified.

2.1 Tagged analysis

The 818±8 pb^{-1} $\psi(3770)$ data collected by CLEO-c detector is used for this analysis. We reconstruct the final states shown in Table 2.1, with $\pi^0 \to \gamma\gamma$, $\eta \to \gamma\gamma$, $K^0_S \to \pi^+\pi^-$, and $\omega \to \pi^+\pi^-\pi^0$. Since K^0_L and neutrinos don't leave evidence in our detector, we do not reconstruct $K^0_L\pi^0$ and semileptonic single tag modes; they are only included in double tag modes, with the other D fully reconstructed. We denote CP even modes, K^+K^-, $\pi^+\pi^-$, and $K^0_S\pi^0\pi^0$, by S_+; denote CP odd modes, $K^0_S\pi^0$, $K^0_S\eta$, and $K^0_S\omega$, by S_-. For CP eigenstates, we choose modes with unambiguous CP content. In addition to two-body decays, we also include $K^0_S\pi^0\pi^0$, which is a pure CP-even eigenstate because the two identical π^0's must have even angular momentum in order to satisfy Bose symmetry.

Table 2.1: D final states reconstructed in this analysis.

Type	Final States
Flavored	$K^-\pi^+$, $K^-\pi^+\pi^0$, $K^-\pi^+\pi^+\pi^-$
S_+	K^+K^-, $\pi^+\pi^-$, $K^0_S\pi^0\pi^0$, $K^0_L\pi^0$
S_-	$K^0_S\pi^0$, $K^0_S\eta$, $K^0_S\omega$
$e^\pm$	$K^-e^+\nu_e$

The single tags reconstruction are implemented by CLEO-c specific software [6]. DTags are the standard way of CLEO-c to reconstruct events from tracks and showers and other information collected by the detector. The DTag code identifies D-meson by making combinations of different final state particles. Most common particles used are: $\pi^\pm$, $K^\pm$, K^0_S, π^0, and η. Note K^0_S is actually detected as a pair of $\pi^+\pi^-$ in the detector, since it only travels a very short distance before it decays. Different DTags in one single event can be joined together to form double tags, which fully described the event. The DTag code prevents using common

constituents (i.e. tracks or showers) in both DTags. The default DTag cuts for tracks and showers and other related variables are shown in Table 2.2, with details explained below. d_b is

Table 2.2: Default selection requirements on DTag object.

	DTag requirements
Track quality	$\chi^2 < 10000$
	hit fraction > 0.5
	$\lvert\cot\theta\rvert < 2.53$
	$\lvert\vec{p}\rvert_{max} < 2.00\text{GeV}/c$
	$\lvert\vec{p}\rvert_{min} > 0.05\text{GeV}/c$
	$\lvert z_0\rvert < 0.050\text{m}$
	$\lvert d_b\rvert < 0.005\text{m}$
	Standard PID
π^0/η	$\chi^2 < 10000$
	$\sigma \leq 1000$
	$M_{\text{unconstrained}} < 1000$ GeV/c^2
	Pull Mass ≤ 3.0
	Min. Shower Energy $= 30/50$ MeV
K^0_S	$\chi^2 < 1000$
	Pull Mass ≤ 3.0
	$M_{\text{unconstrained}} < 1000$ GeV/c^2
DTag object	$M_{bc} > 1.83$ GeV/c^2
	$\lvert\Delta E\rvert < 0.100$ GeV

the signed distance of closest approach of the helical fit to the beamspot in the radial direction and must be less than 5 mm, while z_0 is the distance of closest approach of the fit to the beamspot in the direction of the beam-axis and must be within 50 mm. There is a fiducial requirement that $|\cot\theta|$ must be less than 2.53, where θ is with respect to the beam-axis. "hit fraction" is the ratio of the number of hits used in the fit to the expected number of hits based on the last layer of the detector recording hits and must be greater than 50%.

The standard PID consists of a number of particle identification requirements which test the hypothesis for the track being a particular charged particle. For charged kaons, there are three requirements:

$$\sigma_K^2 - \sigma_\pi^2 + L_K - L_\pi \;<\; 0, \tag{2.1}$$

$$|\sigma_K| \leq 3.0, \tag{2.2}$$

$$n_\gamma \geq 3.0, \tag{2.3}$$

where $\sigma_{K/\pi}$ is the difference between the expected specific ionization (dE/dx) and the measured value, $L_{K/\pi}$ is the likelihood variable from RICH information, and n_γ is the number of photons associated with the track in the RICH. When the momentum of the track is less than 700 MeV/c, only dE/dx information is used. Charged pion identification is similar, with K and π

swapped:

$$\sigma_\pi^2 - \sigma_K^2 + L_\pi - L_K \;<\; 0, \tag{2.4}$$

$$|\sigma_\pi| \leq 3.0, \tag{2.5}$$

$$n_\gamma \geq 3.0. \tag{2.6}$$

The pull mass of π^0 and η candidates are required less than 3, where pull mass is the difference between the measured and nominal masses, divided by the resolution (σ). The minimum shower energy for π^0 reconstruction is 30 MeV, while for η reconstruction is 50 MeV.

Single D candidates are identified using two kinematic variables that express momentum and energy conservation: the beam-constrained candidate mass M and the energy difference ΔE. These variables are defined to be

$$M \equiv \sqrt{E_0^2/c^4 - \vec{p}_D^{\,2}/c^2} \tag{2.7}$$

$$\Delta E \equiv E_D - E_0, \tag{2.8}$$

where $\vec{p}_D$ and E_D are the total momentum and energy of the D candidate, and E_0 is the beam energy. Correctly reconstructed D candidates produce a peak in M at the D mass and in ΔE at zero.

The main purpose of this thesis is to study the structure of $K^0_{S,L}\pi^+\pi^-$ Dalitz decay in different quantum states. Since D^0 and $\bar{D}^0$ are produced quantum coherently from $\psi(3770)$, we use one side D to identify the quantum state of the other D, which decays to $K^0_{S,L}\pi^+\pi^-$. The following double tags are studied in this analysis, grouped in different categories according the quantum state of the tags.

- Flavor Tags
  - $K^-e^+\nu$ vs. $K^0_S\pi^+\pi^-$
  - $K^-\pi^+$ vs. $K^0_{S,L}\pi^+\pi^-$
  - $K^-\pi^+\pi^0$ vs. $K^0_{S,L}\pi^+\pi^-$
  - $K^-\pi^+\pi^+\pi^-$ vs. $K^0_{S,L}\pi^+\pi^-$
- CP even Tags
  - $\pi^+\pi^-$ vs. $K^0_{S,L}\pi^+\pi^-$
  - K^+K^- vs. $K^0_{S,L}\pi^+\pi^-$
  - $K^0_S\pi^0\pi^0$ vs. $K^0_S\pi^+\pi^-$
  - $K^0_L\pi^0$ vs. $K^0_S\pi^+\pi^-$
- CP odd Tags
  - $K^0_S\pi^0$ vs. $K^0_{S,L}\pi^+\pi^-$
  - $K^0_S\eta$ vs. $K^0_{S,L}\pi^+\pi^-$

  - $K^0_S\omega$ vs. $K^0_S\pi^+\pi^-$

- Double Dalitz
  - $K^0_S\pi^+\pi^-$ vs. $K^0_{S,L}\pi^+\pi^-$

Any modes having a K^0_L or neutrino are reconstructed using a missing mass technique, which will be explained later.

2.2 Single tags

We determine single tag yields by fitting the M_{bc} distribution with the mode-dependent requirements on ΔE listed in Table 2.3, which are applied to both single tag and double tag D candidates. The limits are set at approximately three standard deviations. Modes with π^0 and η, which decay to two photons, have asymmetric limits to allow for partially contained showers in the electromagnetic calorimeter.

For K^0_S candidates, we require $|M_{\pi^+\pi^-} - M_{K^0_S}| < 7.5$ MeV/c^2, and we require the decay vertex to be separated from the interaction region with a significance greater than two standard deviation (flight significance > 2). We accept ω candidates with $|M_{\pi^+\pi^-\pi^0} - M_\omega| < 20$ MeV/c^2. Reconstruction of $\eta \to \gamma\gamma$ proceeds analogously to $\pi^0 \to \gamma\gamma$. In addition, we require $|M_{\gamma\gamma} - M_\eta| < 42$ MeV/c^2.

For $K^-\pi^+$, K^+K^-, and $\pi^+\pi^-$ single tag modes, in events containing only two tracks, we suppress cosmic muons and beam-energy Bhabhas by vetoing tracks that are identified as muons or electrons and by requiring at least one electromagnetic shower in the calorimeter above 50 MeV not associated with the signal tracks. For K^+K^- single tag candidates, additional geometric requirements are needed to remove doubly radiative Bhabhas followed by pair conversion of a radiated photon. Also, we accept only one candidate per mode per event; when multiple candidates are present, we choose the one with smallest $|\Delta E|$.

Table 2.3: Requirements on ΔE for D candidates.

Mode	Requirement(GeV)
$K^-\pi^+$	$\lvert\Delta E\rvert < 0.025$
$K^-\pi^+\pi^0$	$\lvert\Delta E\rvert < 0.030$
$K^-\pi^+\pi^+\pi^-$	$\lvert\Delta E\rvert < 0.020$
$K^0_S\pi^0$	-0.071$< \Delta E <$ 0.045
$K^0_S\eta$	-0.055$< \Delta E <$ 0.035
$K^0_S\omega$	$\lvert\Delta E\rvert <$0.025
K^+K^-	$\Delta E <$0.020
$\pi^+\pi^-$	$\Delta E <$0.030
$K^0_S\pi^0\pi^0$	-0.055$< \Delta E <$0.045
$K^0_S\pi^+\pi^-$	$\Delta E <$0.020

Tag side M_{bc} distributions are shown in Fig. 2.1 and Fig. 2.2 for Monte Carlo and Data, respectively. The solid lines show the total fits, and the dashed lines show the background shapes.

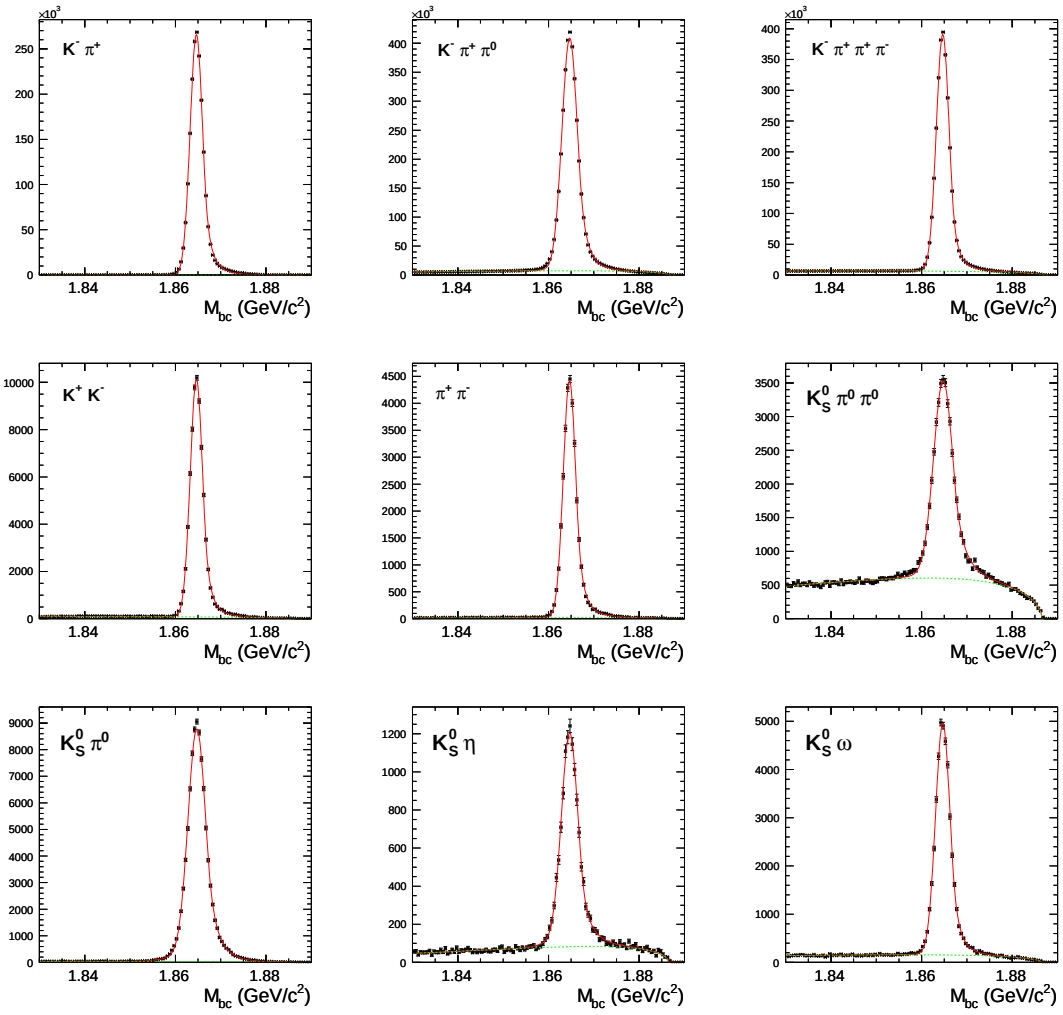

Figure 2.1: Monte Carlo M_{bc} distributions for various tag modes. The solid lines show the total fits, and the dashed lines show the background shapes.

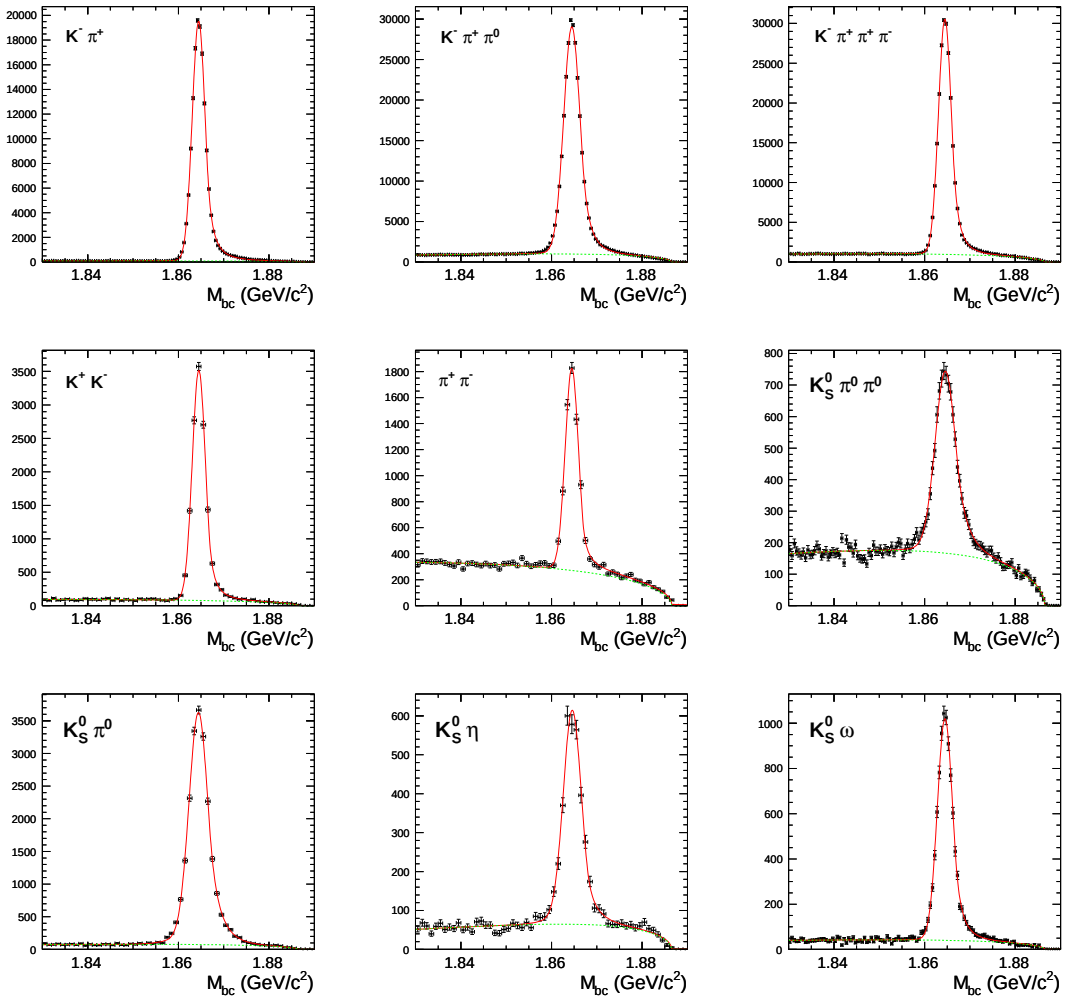

Figure 2.2: Data M_{bc} distribution for various tag modes. The solid lines show the total fits, and the dashed lines show the background shapes.

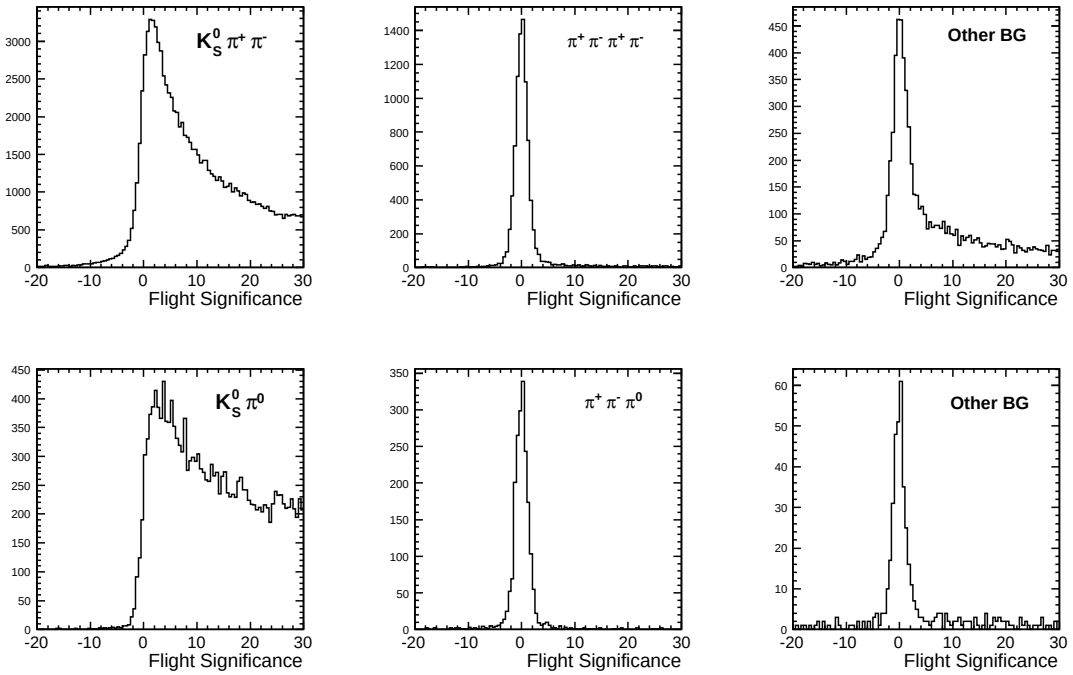

Figure 2.3: K^0_S flight significance distributions for $K^0_S\pi^+\pi^-$ mode (Upper row) and $K^0_S\pi^0$ mode (Lower row) in MC. The distributions for Monte Carlo truth signal are shown in the left column. The distributions for peaking background are shown in the middle column. The distributions for the background (except peaking background) are shown in the right column.

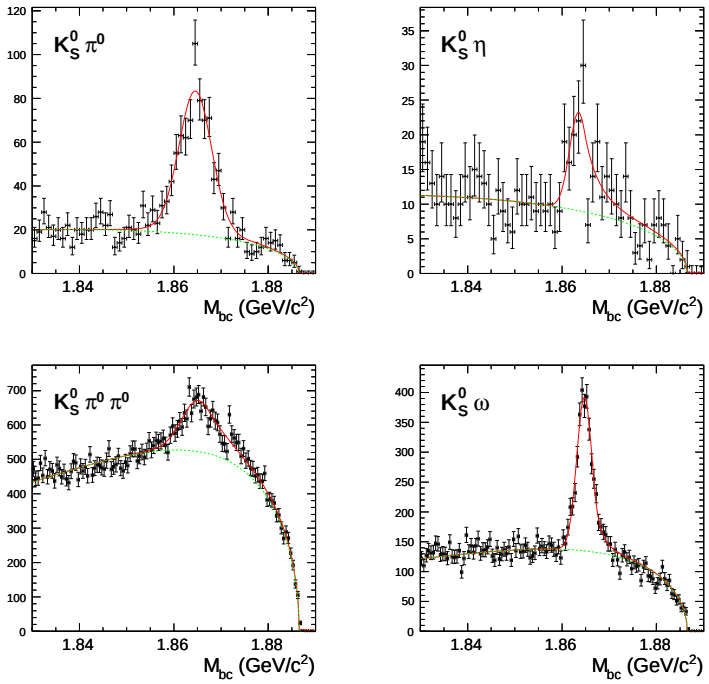

Figure 2.4: Peaking background fits for $K^0_S\pi^0$, $K^0_S\eta$, $K^0_S\pi^0\pi^0$, $K^0_S\omega$ modes. $K^0_S\pi^0$ and $K^0_S\eta$ modes are studied using $M(\pi^+\pi^-)$ mass sidebands in data, while $K^0_S\pi^0\pi^0$ and $K^0_S\omega$ modes are studied using Quantum Correlated Monte Carlo.

Table 2.4: Monte Carlo and Data single tag yields. M_{bc} is required within 1.860 GeV/c^2 and 1.870 GeV/c^2.

Mode	Monte Carlo	Data
$K^-\pi^+$	1925497.2 ± 1370.3	144563.4 ± 403.1
$K^-\pi^+\pi^0$	3535525.2 ± 2027.6	258938.0 ± 580.6
$K^-\pi^+\pi^+\pi^-$	2821064.8 ± 1839.3	220831.3 ± 540.6
$K^0_S\pi^0$	88223.8 ± 303.3	19058.7 ± 150.1
$\pi^+\pi^-$	31901.6 ± 185.4	5950.4 ± 111.6
K^+K^-	71991.5 ± 278.7	12867.1 ± 125.8
$K^0_S\eta$	10703.0 ± 129.1	2792.9 ± 69.4
$K^0_S\pi^0\pi^0$	31707.9 ± 264.7	6562.3 ± 130.9
$K^0_S\omega$	39880.2 ± 224.8	8512.4 ± 107.1

Table 2.5: Peaking background yields for K^0_S modes. $K^0_S\pi^0$ and $K^0_S\eta$ modes are studied using $M(\pi^+\pi^-)$ mass sidebands in data, while $K^0_S\pi^0\pi^0$ and $K^0_S\omega$ modes are studied using Quantum Correlated Monte Carlo, then normalized to Data according number of tags.

Mode	MC	Data
$K^0_S\pi^0$	/	485.2 ± 31.7
$K^0_S\eta$	/	78.7 ± 14.7
$K^0_S\pi^0\pi^0$	2270.6 ± 153.2	470.0 ± 31.7
$K^0_S\omega$	2167.6 ± 78.2	462.3 ± 16.7

The tag yields are extracted from a fit to the M_{bc} distribution. The fit function is Crystal Ball plus Gaussian for signal and ARGUS function [7] for background.

$$CB(x:\mu_1,\sigma_1,n,\alpha) = \begin{cases} \exp(-\frac{(x-\mu_1)^2}{2\sigma_1^2}) & \text{if } x < \mu_1 + \alpha\sigma_1 \\ \frac{(n/\alpha)^n \exp(-\alpha^2/2)}{[(x-\mu_1)/\sigma_1 + n/\alpha - \alpha]^n} & \text{if } x \geq \mu_1 + \alpha\sigma_1 \end{cases} \tag{2.9}$$

$$G(x:\mu_2,\sigma_2) = \frac{1}{\sqrt{2\pi}\sigma_2}\exp(-\frac{(x-\mu_2)^2}{2\sigma_2^2}) \tag{2.10}$$

$$ARGUS(x:C,E,\xi) = Cx\sqrt{1-(\frac{x}{E})^2}\exp(\frac{\xi(1-x^2)}{E^2}) \tag{2.11}$$

The fits were done in two steps. First, we fit the Monte Carlo truth matched single tag events. Using the result from the first step, we fixed the parameters determining the split of the yield between Crystal Ball and Gaussian in generic Monte Carlo and data. Then, we did a second fit to get the yield.

We require 1.86 GeV/c^2 < M_{bc} < 1.87 GeV/c^2, the event yields are shown in Table 2.4.

For tags with a K^0_S, there are peaking backgrounds presented in ΔE and M_{bc} distributions. The peaking backgrounds are from a pair of $\pi^+\pi^-$ faking a K^0_S. Specifically, for $K^0_S\pi^+\pi^-$ tag, the peaking background channel is $\pi^+\pi^-\pi^+\pi^-$, for $K^0_S\pi^0$ tag, the background channels are $\rho^+(\rho^+ \to \pi^+\pi^0)\pi^-$, $\rho^0(\rho^0 \to \pi^+\pi^-)\pi^0$, and $\pi^+\pi^-\pi^0$. The background is about 5% in $K^0_S\pi^+\pi^-$

tag mode, 4% in $K^0_S\pi^0$ tag mode. The K^0_S flight significance requirement is utilized to remove the background. The K^0_S flight significance distributions in Monte Carlo are shown in Fig. 2.3. The distributions for Monte Carlo truth signal are shown in the left column. The distributions for peaking background are shown in the middle column. The distributions for the background (except peaking background) are shown in the right column. Various cut criteria are studied and we choose to require flight significance of K^0_S greater than 2 in both signal and tag sides.

With the K^0_S flight significance requirement, the peaking background has been greatly suppressed, though not completely. The residue peaking background is extracted by doing a fit to either K^0_S mass sidebands ($K^0_S\pi^0$, $K^0_S\eta$ case) or the isolated true background events in QCMC ($K^0_S\pi^0\pi^0$, $K^0_S\omega$ case). The fit plots are shown in Fig. 2.4 and the yields are shown in Table 2.5. For $K^0_S\pi^0$ and $K^0_S\eta$ modes, the peaking background come from non resonant $\pi^+\pi^-$ pair faking a K^0_S. Using K^0_S mass sidebands is an effective way to estimate the background. For $K^0_S\pi^0\pi^0$ and $K^0_S\omega$ modes, the peaking background components are more complicated. Quantum Correlated Monte Carlo is utilized to study the peaking backgrounds, then normalized to data according to the number of tags.

2.3 Double tags

2.3.1 $K^0_S\pi^+\pi^-$ double tag yields

Tag side ΔE sidebands are used for tag side background subtraction. The mode dependent ΔE sidebands are shown in Table 2.6. For $K^0_S\pi^0$, $K^0_S\eta$, $K^0_S\pi^0\pi^0$ modes, K^0_S sideband (12 MeV/c^2 < $|M_{K^0_S} - 0.4976|$ < 19.5 MeV/c^2) is also selected for peaking background consideration. For $K^0_S\omega$ mode, ω mass sideband (30 MeV/c^2 < $|M_\omega - 0.782|$ < 50 MeV/c^2)is used for background subtraction.

Whether the background is flat for $K^0_S\omega$ is one concern for using ω sidebands. In order to check this, we produced the $M(\pi^+\pi^-\pi^0)$ mass plots in Fig.2.5. The background in Monte Carlo is shown as a shaded histogram in the left plot. The background distribution is roughly flat with a tendency increasing steadily from the low mass region to the high mass region. Using a low mass sideband and a high mass sideband is safe to cover the discrepancy.

Table 2.6: ΔE sidebands selection.

Mode	low-side(GeV)	high-side(GeV)
$K^-\pi^+$	-0.075∼-0.050	0.050∼0.075
$K^-\pi^+\pi^0$	-0.080∼-0.050	0.050∼0.080
$K^-\pi^+\pi^+\pi^-$	-0.060∼-0.040	0.040∼0.060
$K^0_S\pi^0$	-0.100∼-0.071	0.045∼0.100
$K^0_S\eta$	-0.100∼-0.055	0.040∼0.085
$K^0_S\omega$	-0.075∼-0.050	0.050∼0.075
K^+K^-	-0.060∼-0.040	0.040∼0.060
$\pi^+\pi^-$	-0.080∼-0.050	0.050∼0.080
$K^0_S\pi^0\pi^0$	-0.100∼-0.055	0.045∼0.100

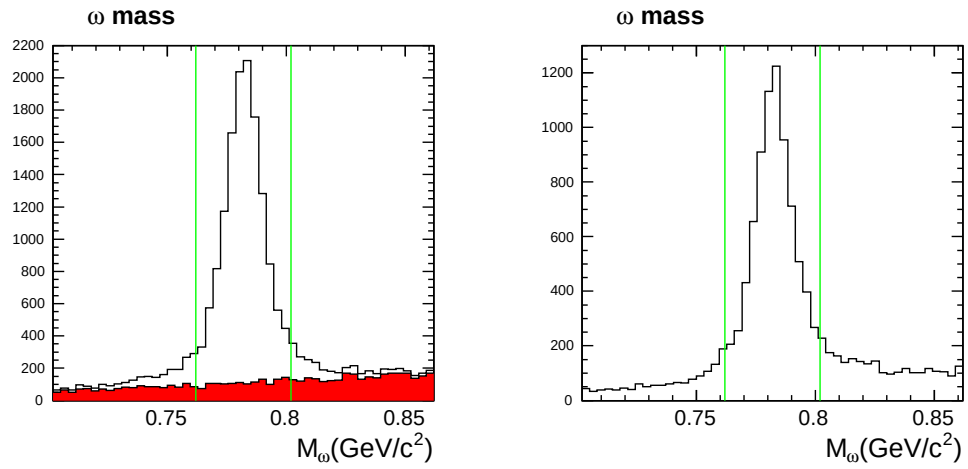

Figure 2.5: $\pi^+\pi^-\pi^0$ invariant mass distributions for $K^0_S\omega$ tag in Monte Carlo (left) and data (right), the shaded histogram is background.

In Table 2.7, we show the double tag yields for $K^0_S\pi^+\pi^-$ vs. various tags, and the expected background levels, which is estimated from Quantum Correlated Monte Carlo samples.

Table 2.7: Data yields of $K^0_S\pi^+\pi^-$ vs. various tag modes and the estimate background level from QCMC.

Mode	Yield	B/(S+B)
$K^-\pi^+$	1447	1.6%
$K^-\pi^+\pi^0$	2776	2.5%
$K^-\pi^+\pi^+\pi^-$	2250	4.4%
$\pi^+\pi^-$	62	0.3%
K^+K^-	124	1.0%
$K^0_S\pi^0\pi^0$	56	12.5%
$K^0_S\pi^0$	189	2.8%
$K^0_S\eta$	39	5.6%
$K^0_S\omega$	83	7.2%

The $D^0 \to K^0_S\pi^+\pi^-$ Dalitz plots and the projections for flavor tagged $K^0_S\pi^+\pi^-$, CP even tagged $K^0_S\pi^+\pi^-$, and CP odd tagged $K^0_S\pi^+\pi^-$ samples are shown in Fig. 2.6, Fig. 2.7 and Fig. 2.8, respectively. The Dalitz plots of our flavor tagged $K^0_S\pi^+\pi^-$ samples are very similar to the Dalitz plots in [1] and [2]. The quantum correlation shows up in CP tagged $K^0_S\pi^+\pi^-$ samples. In Fig. 2.7, the $M^2(\pi^+\pi^-)$ projection has an enhanced $K^0_S\rho$ peak, while in Fig. 2.8, the $K^0_S\rho$ peak vanishes. This is because $K^0_S\rho$ is a CP odd eigenstate, it gets enhanced in CP even tagged samples and vanishes in CP odd tagged samples.

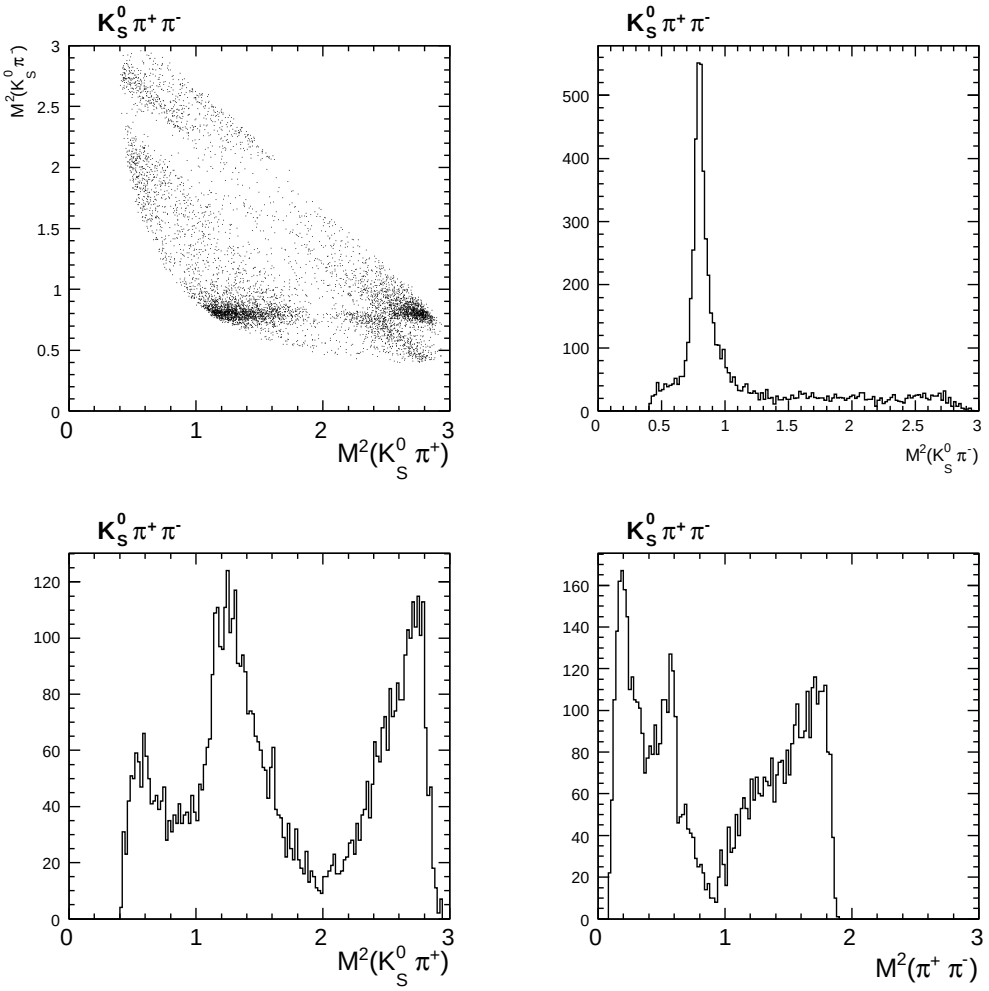

Figure 2.6: $K^0_S\pi^+\pi^-$ Dalitz plot and $M^2(K^0_S\pi^+)$, $M^2(K^0_S\pi^-)$, $M^2(\pi^+\pi^-)$ projections in flavor tagged ($\bar{D}^0 \to K^+\pi^-$, $\bar{D}^0 \to K^+\pi^-\pi^0$, $\bar{D}^0 \to K^+\pi^-\pi^+\pi^-$) sample.

2.3.2 $K^0_L\pi^+\pi^-$ double tag yields

Since K^0_L travels through our detector before it decays, it leaves no signal in our detector, we use missing mass technique to find $K^0_L\pi^+\pi^-$. Our procedure is as follows. First, we tag an event containing a D^0 (or $\bar{D}^0$), using the decay modes $D^0 \to K^-\pi^+$, $D^0 \to K^-\pi^+\pi^0$, $D^0 \to K^-\pi^+\pi^+\pi^-$, $D^0 \to K^0_S\pi^0$, $D^0 \to K^0_S\eta$, $D^0 \to K^+K^-$, and $D^0 \to \pi^+\pi^-$. Then we look for $\bar{D}^0 \to K^0_L\pi^+\pi^-$ (or $D^0 \to K^0_L\pi^+\pi^-$) on the "other side". We do this by requiring that the "other side" contain only two tracks, and little else. We applied π^0 and η and K^0_S veto in the other side, we also have special shower energy requirement in the calorimeter which will be discussed in a minute. Using the tag D measured momentum, we compute the missing momentum of the "other side", and compute the mass from the missing momentum.

Fig. 2.9 show the $\cos\theta$ vs. shower energy scatter plots in MC. "θ" is the angle between shower and the predicted K^0_L direction. The signal events are shown on the left while the background events are shown on the right. The dashed red line represents the cut we make.

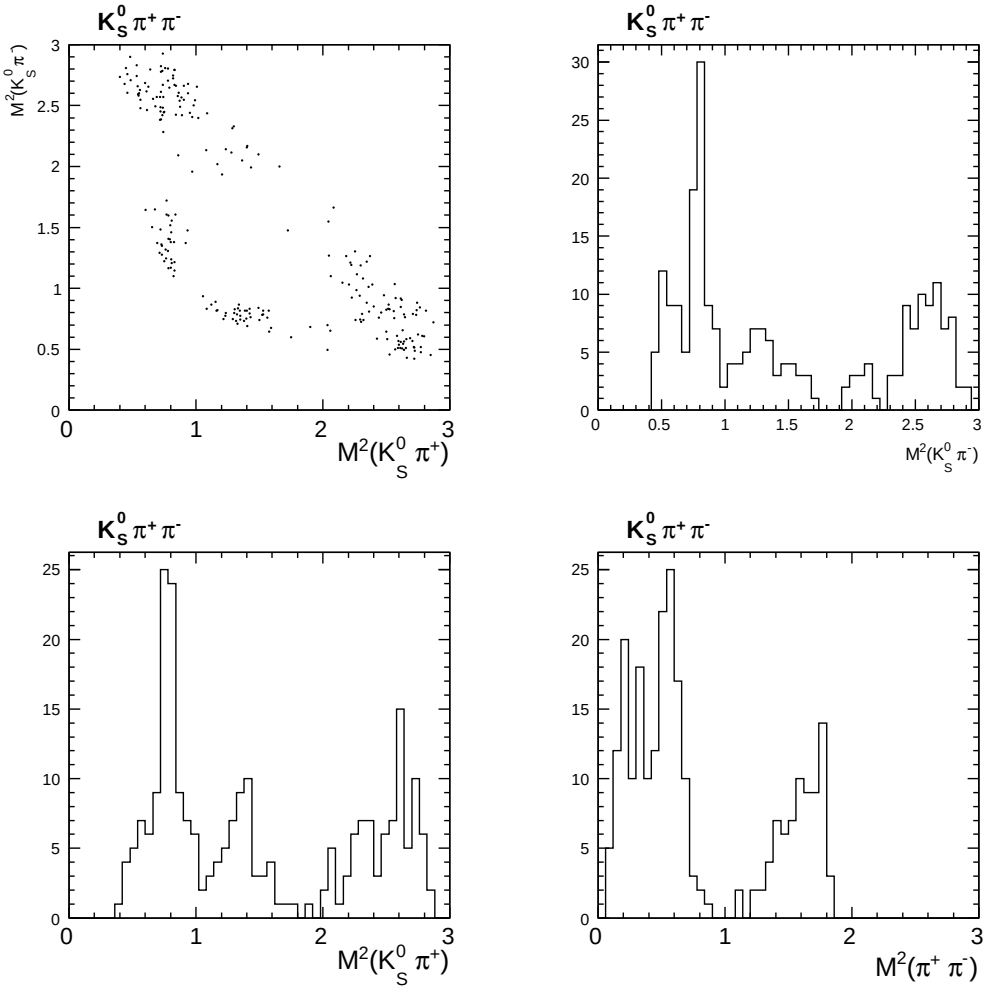

Figure 2.7: $K^0_S\pi^+\pi^-$ Dalitz plot and $M^2(K^0_S\pi^+)$, $M^2(K^0_S\pi^-)$, $M^2(\pi^+\pi^-)$ projections in CP even tagged $(K^+K^-, \pi^+\pi^-, K^0_S\pi^0\pi^0)$ sample

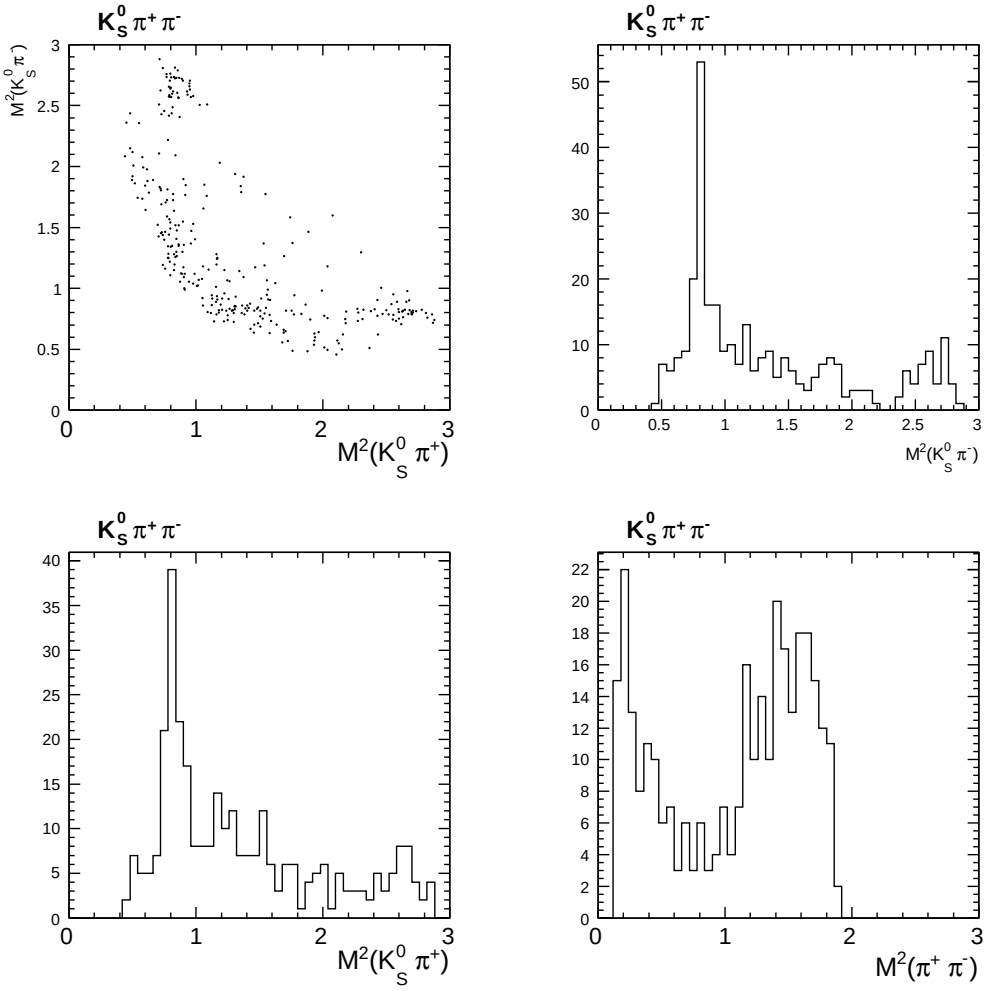

Figure 2.8: $K^0_S\pi^+\pi^-$ Dalitz plot and $M^2(K^0_S\pi^+)$, $M^2(K^0_S\pi^-)$, $M^2(\pi^+\pi^-)$ projections in CP odd tagged ($K^0_S\pi^0, K^0_S\eta, K^0_S\omega$) sample.

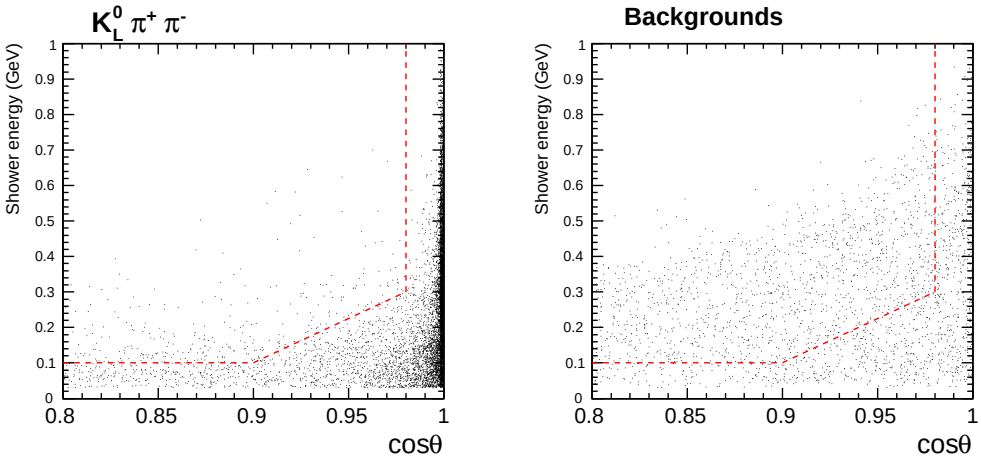

Figure 2.9: MC $\cos\theta$ vs. shower energy scatter plot when one D is identified as $K^-\pi^+$ mode, where θ is the angle between the shower and the predicted K^0_L direction. Signal events are shown on the left, background events are shown on the right. Tag side ΔE, m_{bc} cuts applied. Signal side require only two pions, π^0 veto, η veto, missing mass square between 0.21 $\sim$ 0.29 GeV$^2/c^4$.

Any event with a shower located above the dashed red line is rejected. Note that the red dashed line extend to the left which is not shown in the plot. This requirement effectively removes the backgrounds, especially for $K^0_S\pi^+\pi^-$, which is the most significant background. By applying this cut, the background has been reduced from 15% to 5%. No cut is free, we also lose about 10% signal events.

The Missing mass distributions are shown in Fig. 2.10, Fig. 2.11, solid line is Monte Carlo, dots are real data, and the shaded histogram is background.

After applying all the cuts, the background of $K^0_L\pi^+\pi^-$ reduces to 5% level. We separate the the backgrounds into two categories:

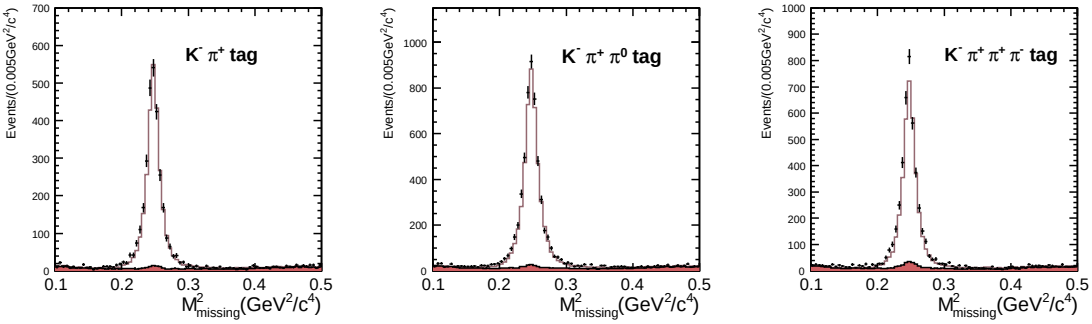

Figure 2.10: $M^2_{missing}$ distributions when one D is identified as $K^-\pi^+$ (left), $K^-\pi^+\pi^0$ (middle), $K^-\pi^+\pi^+\pi^-$ (right). Solid histogram is Monte Carlo, dots are data, shaded histogram is background.

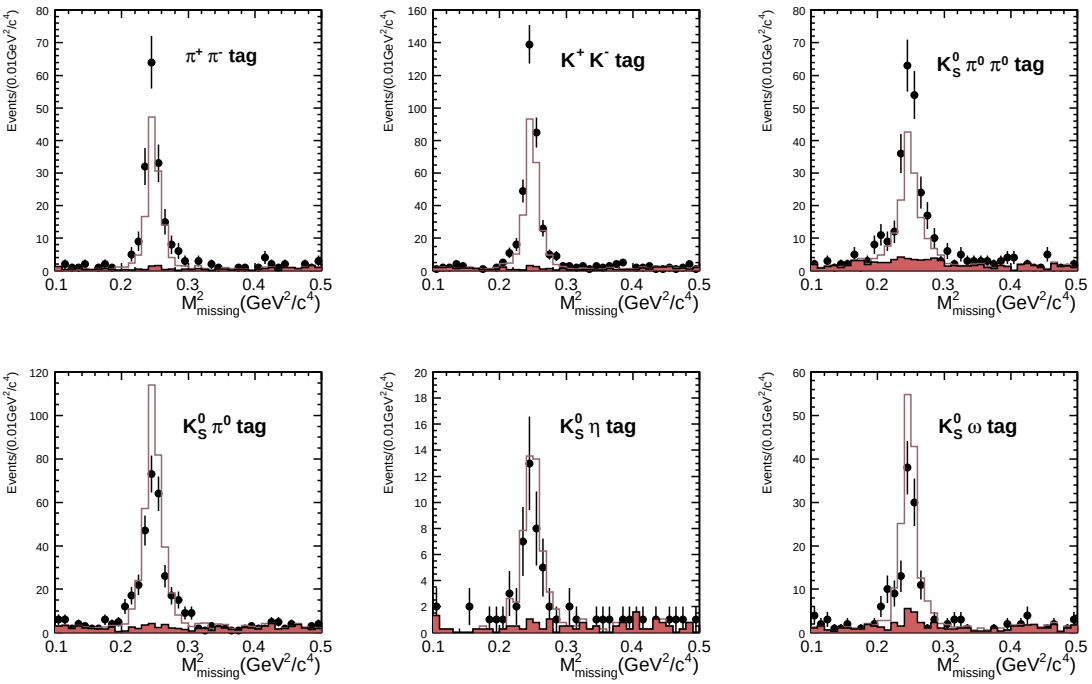

Figure 2.11: MC $M^2_{missing}$ distributions when one D is identified as $\pi^+\pi^-$ (top left), K^+K^- (top middle), $K^0_S\pi^0\pi^0$ (top right), $K^0_S\pi^0$ (down left) , $K^0_S\eta$ (down middle), $K^0_S\omega$ (down right). Solid histogram is Monte Carlo, dots are data, shaded histogram is background.

Table 2.8: Data yields of $K^0_L\pi^+\pi^-$ vs. various tag modes and the estimate background level from QCMC.

Mode	Yield	B/(S+B)
$K^-\pi^+$	2858	5.2%
$K^-\pi^+\pi^0$	5130	6.5%
$K^-\pi^+\pi^+\pi^-$	4110	8.2%
$\pi^+\pi^-$	172	4.3%
K^+K^-	345	4.4%
$K^0_S\pi^0$	281	6.2%
$K^0_S\eta$	41	8.4%

- $K^0_S\pi^+\pi^-$, which is about 2%.
- The others, $K^-\pi^+\pi^0$, $K^0_L\eta'$, $K^-\mu^+\nu$, $\rho^-\mu^+\nu$ etc..

The reason why $K^0_S\pi^+\pi^-$ shows up as a peaking background is that we fail to find the π^0's from $K^0_S \to \pi^0\pi^0$ decay. Later we subtract this part of background using $K^0_S\pi^+\pi^-$ real data distributions.

In Table 2.8, we show the yields of $K^0_L\pi^+\pi^-$ vs.various tag modes, and the estimated background level from QCMC. The $D^0 \to K^0_L\pi^+\pi^-$ Dalitz plots and the projections for flavor tagged $K^0_L\pi^+\pi^-$, CP even tagged $K^0_L\pi^+\pi^-$, and CP odd tagged $K^0_L\pi^+\pi^-$ samples are shown in Fig. 2.12, Fig. 2.14 and Fig. 2.13, respectively. The Dalitz plots of flavor tagged $K^0_L\pi^+\pi^-$ sample looks similar to the Dalitz plots of flavor tagged $K^0_S\pi^+\pi^-$ sample. The quantum correlation shows up in CP tagged $K^0_L\pi^+\pi^-$ samples. The $K^0_L\rho$ peak gets enhanced in CP odd tagged sample, while it vanishes in CP even tagged sample. This is opposite to $K^0_S\pi^+\pi^-$ since $K^0_L\rho$ and $K^0_S\rho$ has opposite CP eigenvalues.

2.3.3 $K^0_L\pi^0$ vs. $K^0_S\pi^+\pi^-$

We also include $K^0_L\pi^0$ as a CP even tag in this note. $K^0_L\pi^0$ is reconstructed by missing mass technique. First we tag $K^0_S\pi^+\pi^-$ in the event, then look for K^0_L missing mass peak in the rest of the event. After selecting a $K^0_S\pi^+\pi^-$ tag, we require there are no tracks, only one π^0 in the "other" side, we veto events with extra π^0 and η. We also apply the shower energy requirement, same as in $K^0_L\pi^+\pi^-$ reconstruction. The $\cos\theta$ vs. shower energy scatter plot is shown in Fig. 2.15. Any event with a shower located above the dashed red line is rejected.

The missing mass plot after all cuts is shown in Fig. 2.16. The solid line represents Monte Carlo, the points represent data, and the shaded histograms represent background in Monte Carlo. There is a slight shift between data and Monte Carlo, which is due to a minor discrepancy in our calorimeter simulation at large photon energies [15]. The data yields and estimated background are shown in Table 2.9. From Monte Carlo study, approximate 6% background is present. The Dalitz plot and the projections of $K^0_S\pi^+\pi^-$ is shown in Fig. 2.17.

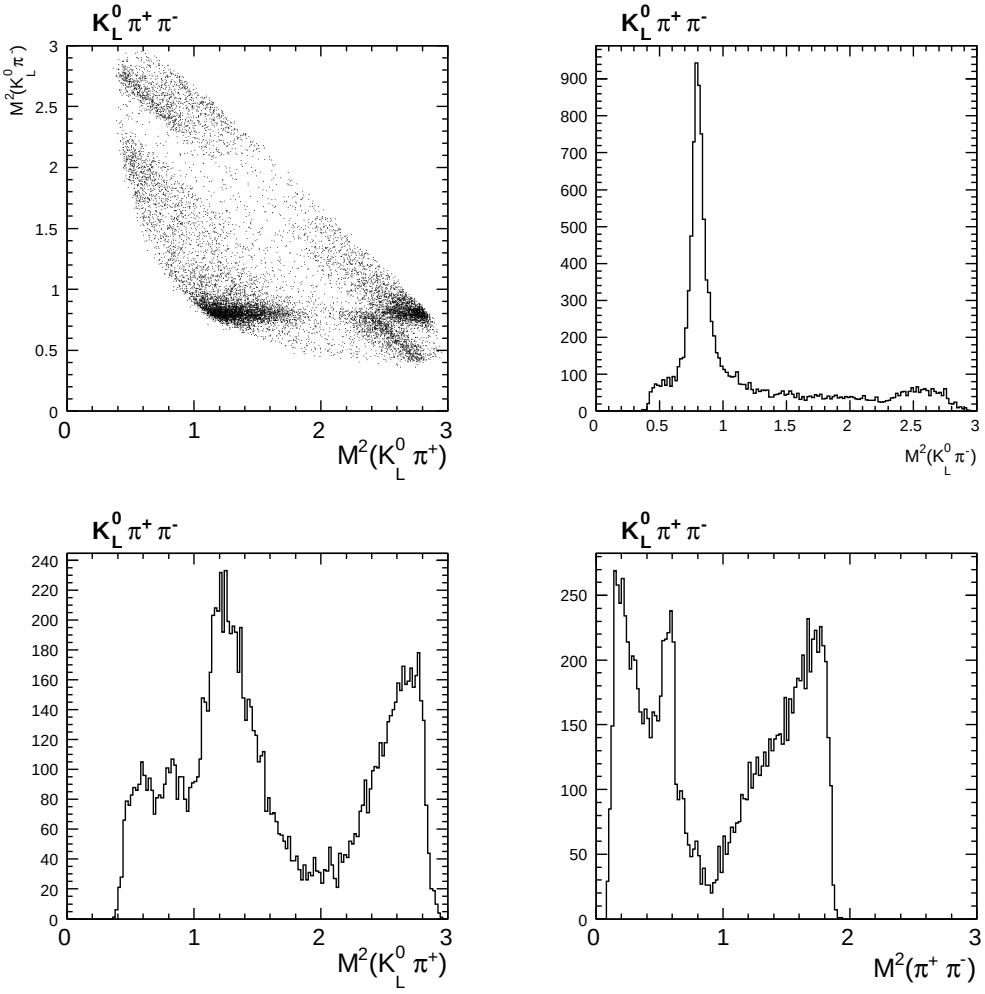

Figure 2.12: $K^0_L\pi^+\pi^-$ Dalitz plot and $M^2(K^0_L\pi^+)$, $M^2(K^0_L\pi^-)$, $M^2(\pi^+\pi^-)$ projections in flavor tagged $(K^-\pi^+, K^-\pi^+\pi^0, K^-\pi^+\pi^+\pi^-)$ sample.

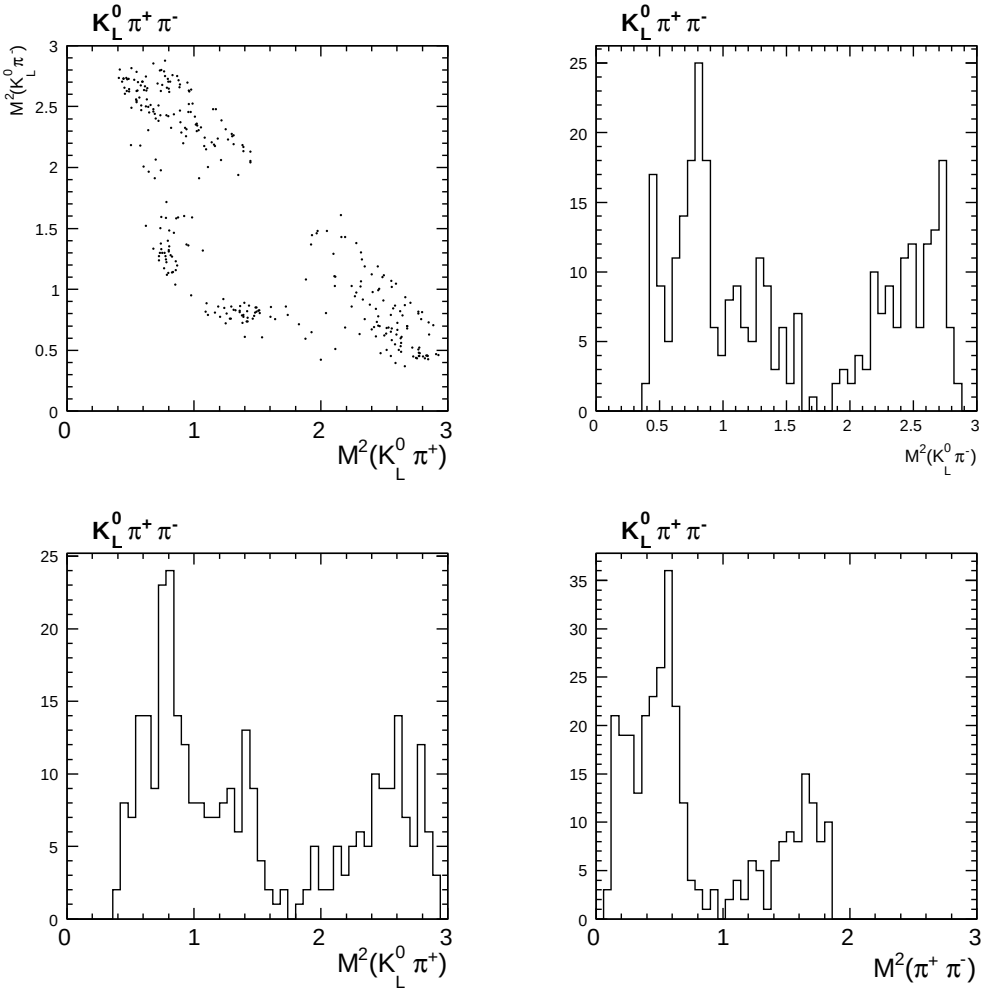

Figure 2.13: $K^0_L\pi^+\pi^-$ Dalitz plot and $M^2(K^0_L\pi^+)$, $M^2(K^0_L\pi^-)$, $M^2(\pi^+\pi^-)$ projections in CP odd tagged ($K^0_S\pi^0$, $K^0_S\eta$) sample.

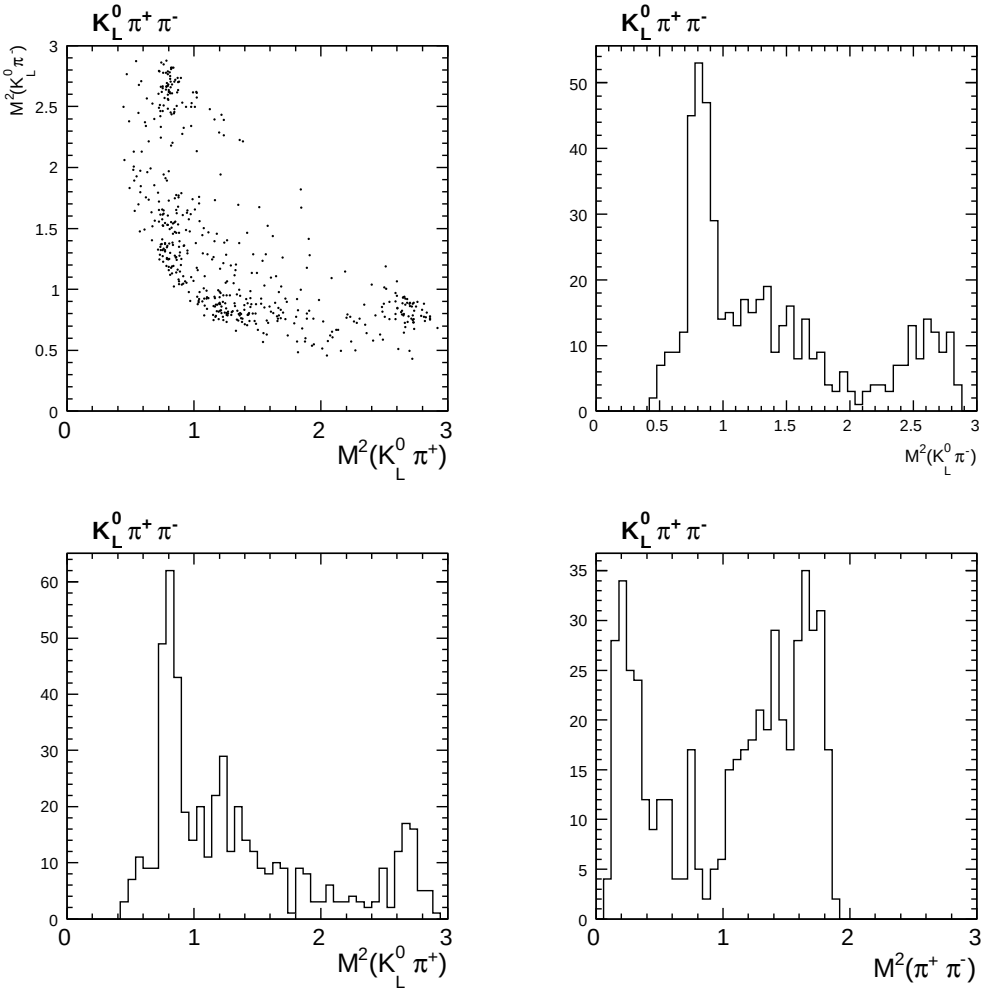

Figure 2.14: $K^0_L\pi^+\pi^-$ Dalitz plot and $M^2(K^0_L\pi^+)$, $M^2(K^0_L\pi^-)$, $M^2(\pi^+\pi^-)$ projections in CP even tagged ($\pi^+\pi^-$, K^+K^-) sample.

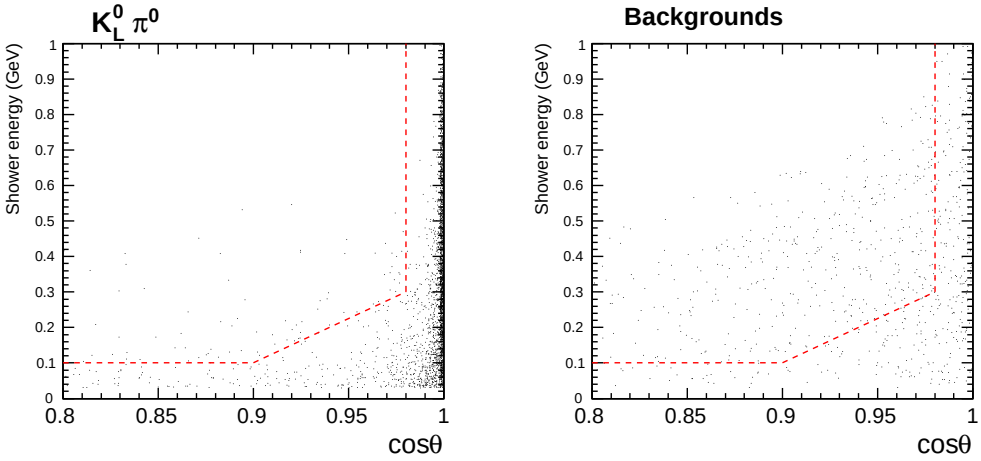

Figure 2.15: MC $\cos\theta$ vs. shower energy scatter plot when one D is identified as $K^-\pi^+$ mode, where θ is the angle between the shower and the predicted K^0_L direction. Signal events are shown on the left, background events are shown on the right. Tag side ΔE, m_{bc} cuts applied. Signal side require only one π^0, track veto, η veto, missing mass square between 0.1 $\sim$ 0.5 GeV$^2/c^4$.

Table 2.9: $K^0_L\pi^0$ vs. $K^0_S\pi^+\pi^-$ yield and expected background level from QCMC

Mode	Data	B/(S+B)
$K^0_S\pi^+\pi^-$	229	5.8%

2.3.4 $K^-e^+\nu$ vs. $K^0_S\pi^+\pi^-$

The reconstruction technique for $K^-e^+\nu$ is same as in [8]. First, we find $K^0_S\pi^+\pi^-$ tag, then search for a positron and a kaon. The energy lost by positrons to bremsstrahlung photons is partially recovered by adding showers that are within 5° of the positron momentum and are not matched to any other particles. Every possible pair of kaon and positron with opposite charge is considered, multiple candidates are found rare. Semileptonic decays are identified using the variable $U_{miss} \equiv E_{miss} - c|\vec{p}_{miss}|$, where E_{miss} and $\vec{p}_{mjiss}$ are the missing energy and momentum of the D meson decaying semileptonically. The U_{miss} distributions are shown in Fig. 2.18. The U_{miss} distributions shown in log scale (left) and linear scale (right). The shaded histograms are background channels. The red histogram represents $\pi e\nu$, the green histogram represents $K^*e\nu$, and the brown histogram represents other backgrounds. Less than 1% background is seen in Monte Carlo. We require $|U_{miss}| < 50$ MeV, the yields are shown in Table 2.10.

Table 2.10: $K^-e^+\nu$ vs. $K^0_S\pi^+\pi^-$ yield and expected background level from Monte Carlo

Mode	Data	B/(S+B)
$K^-e^+\nu$	1356	0.55%

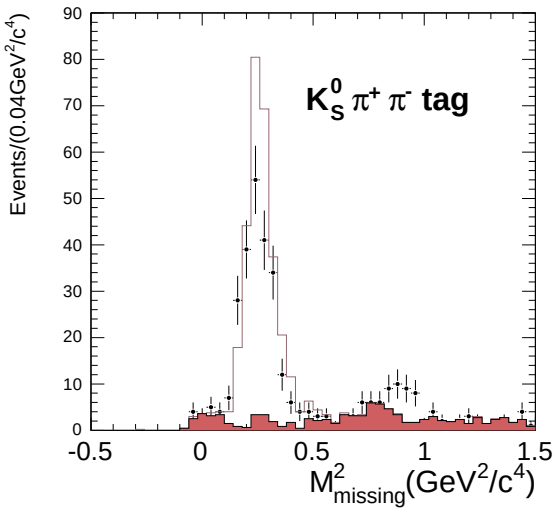

Figure 2.16: Missing mass square distributions for $K^0_L\pi^0$ when one D is identified as $K^0_S\pi^+\pi^-$. Solid histogram is Monte Carlo, dots are data, shaded histogram is background.

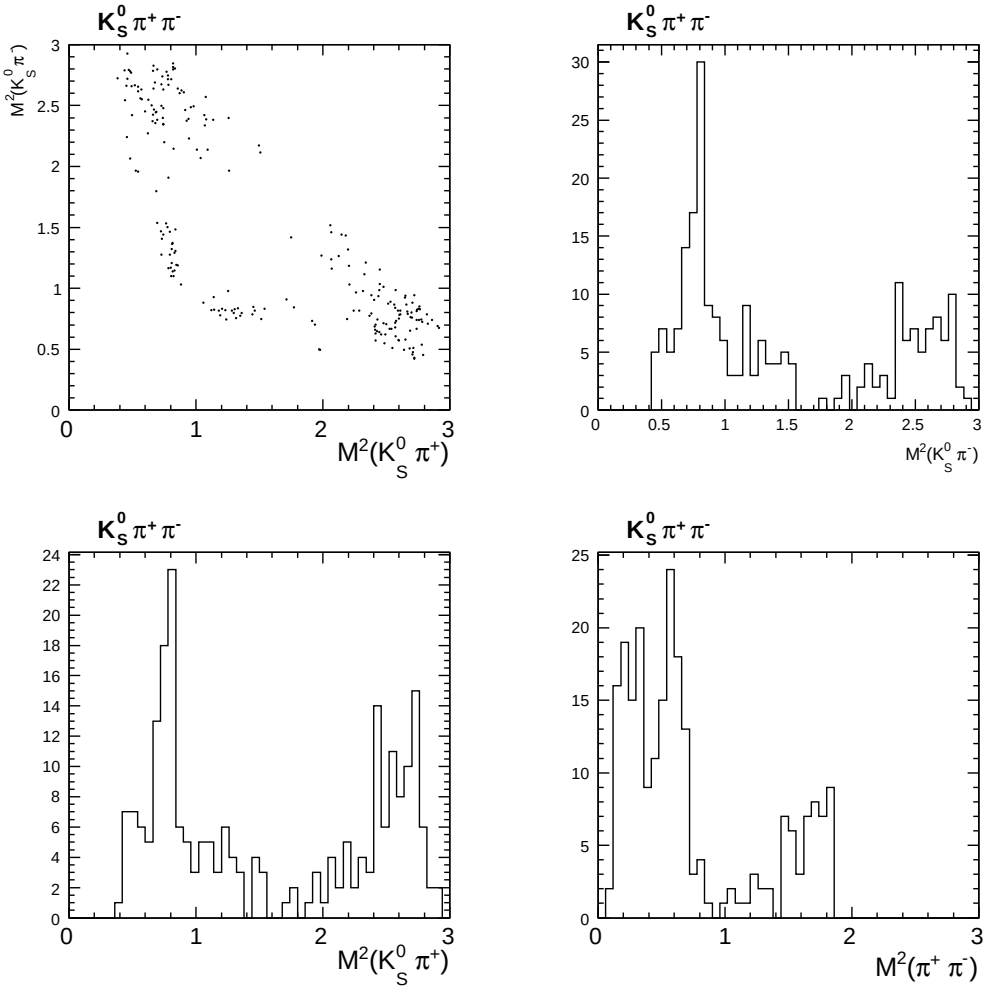

Figure 2.17: $K^0_S\pi^+\pi^-$ Dalitz plot and $M^2(K^0_S\pi^+)$, $M^2(K^0_S\pi^-)$, $M^2(\pi^+\pi^-)$ projections in $K^0_L\pi^0$ tagged sample.

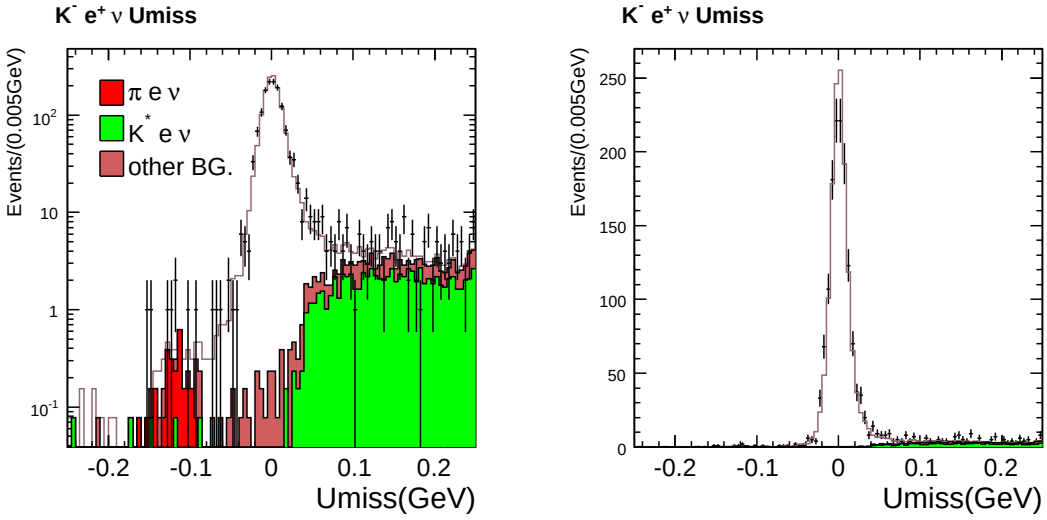

Figure 2.18: U_{miss} distributions for $K^- e^+ \nu$ in both Monte Carlo and data. U_{miss} distributions are shown in log scale (left) and linear scale (right). The shaded histograms are background channels(Red: $\pi e \nu$; Green: $K^* e \nu$; Brown: other backgrounds).

2.4 Double Dalitz $K^0_S\pi^+\pi^-$ vs. $K^0_{S,L}\pi^+\pi^-$

2.4.1 Using NoPID data

We use $K^0_S\pi^+\pi^-$ vs. $K^0_S\pi^+\pi^-$ data to extract both c_i and s_i. In order to get more statistics, we selected $K^0_S\pi^+\pi^-$ vs. $K^0_S\pi^+\pi^-$ events without applying particle identification to the tracks. And we also don't apply the flight significance cut to both K^0_S's. The yield of $K^0_S\pi^+\pi^-$ vs. $K^0_S\pi^+\pi^-$ is shown in Table 2.11. The Dalitz plot and its projections are shown in Fig. 2.19. Note that the two Dalitz decays are drawn in the same plot since we can't distinguish these two processes.

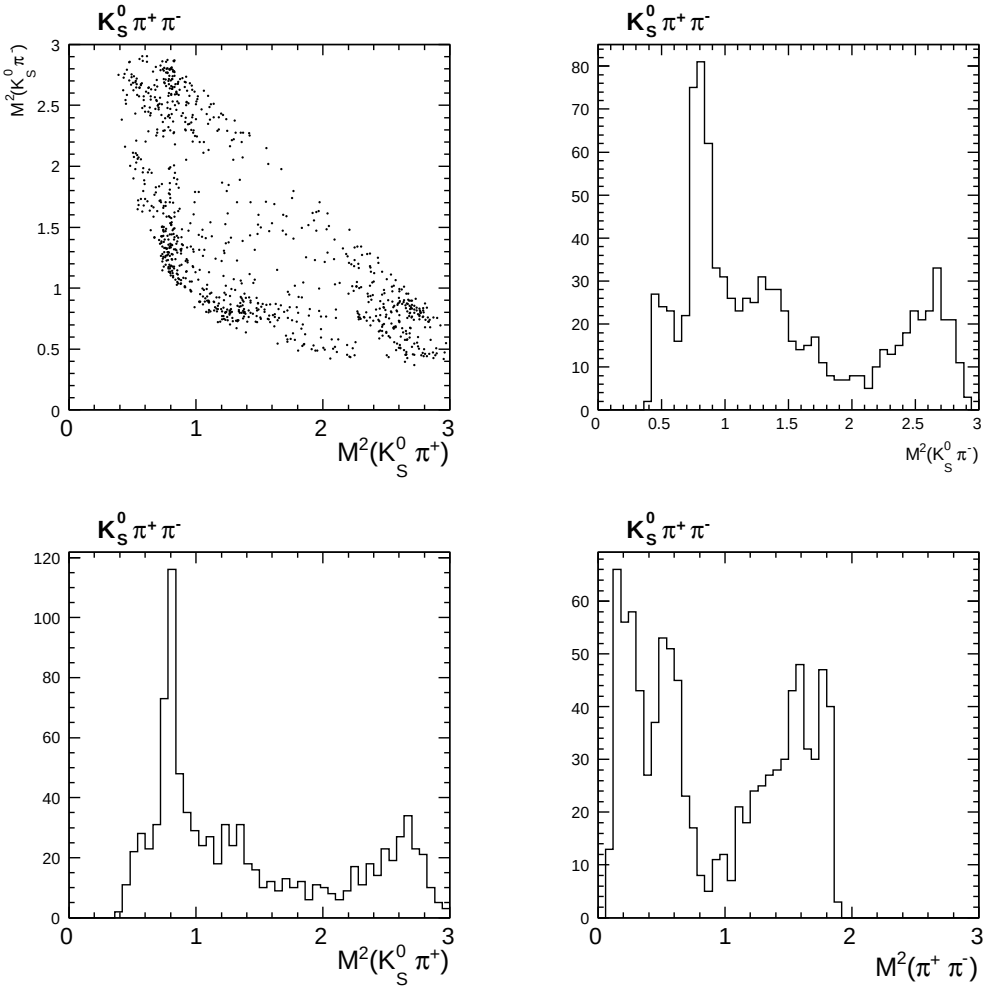

Figure 2.19: $K^0_S\pi^+\pi^-$ Dalitz plot $M^2(K^0_S\pi^+)$, $M^2(K^0_S\pi^-)$, $M^2(\pi^+\pi^-)$ projections for $K^0_S\pi^+\pi^-$ vs. $K^0_S\pi^+\pi^-$ sample. The two Dalitz decays are drawn in the same plot since one can't distinguish these two processes.

The major background for $K^0_S\pi^+\pi^-$ is four charged pion decay. From Monte Carlo study, most of the background events are due to $\pi^+\pi^+\pi^-\pi^-$ faking $K^0_S\pi^+\pi^-$. K^0_S mass sidebands and

ΔE sidebands are selected to estimate the background level. The first $M_{K^0_S}$ vs. second $M_{K^0_S}$ scatter plot is shown in Fig. 2.20. The middle box is the signal region and the adjacent four boxes are sideband regions. Also shown on the right of Fig. 2.20 is the sideband selection for ΔE, which is chosen to account for the continuum background. The sideband yields are shown in Table 2.11. The background level is around 9%.

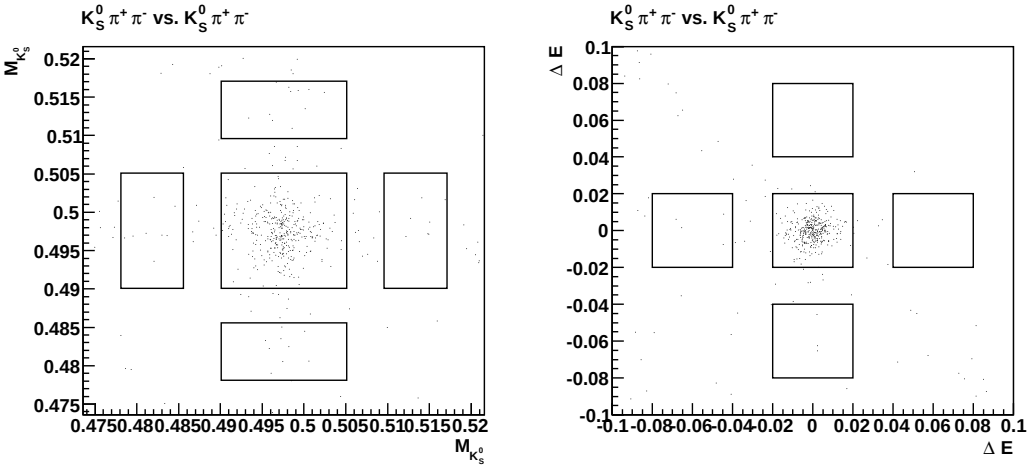

Figure 2.20: $K^0_S\pi^+\pi^-$ vs. $K^0_S\pi^+\pi^-$ sidebands selection for background estimation.

Table 2.11: $K^0_S\pi^+\pi^-$ vs. $K^0_S\pi^+\pi^-$ yield and background estimation.

	Yield	K^0_S sideband	ΔE sideband	Background
Data	421	35	7/2	9.1±1.5%

2.4.2 Partial reconstruction

We also reconstruct $K^0_S\pi^+\pi^-$ vs. $K^0_S\pi^+\pi^-$ events using partial reconstruction. The strategy is as follows: First find a $K^0_S\pi^+\pi^-$ tag in the event, then in the rest of the event, find a K^0_S and a charged π and calculate the missing mass. We require there are only 3 tracks found in the other side, all tracks should be consistent with pion identification, and one K^0_S should be found. We veto events with π^0's and η's.

The missing mass square distribution is shown in Fig. 2.21. The solid line is Monte Carlo, the points with error bars are data, the shaded histogram is Monte Carlo background. There is a small amount of peaking background shown in the signal region. It is $D^0 \to \pi^+\pi^+\pi^-\pi^-$ after checking the Monte Carlo truth information. The continuum background is fitted with a 2nd order polynomial function, as shown in Fig. 2.22. We ignored the peaking background, which will be subtracted later using Monte Carlo information, in the fit. The yields and background level for partial reconstruction are shown in Table 2.12.

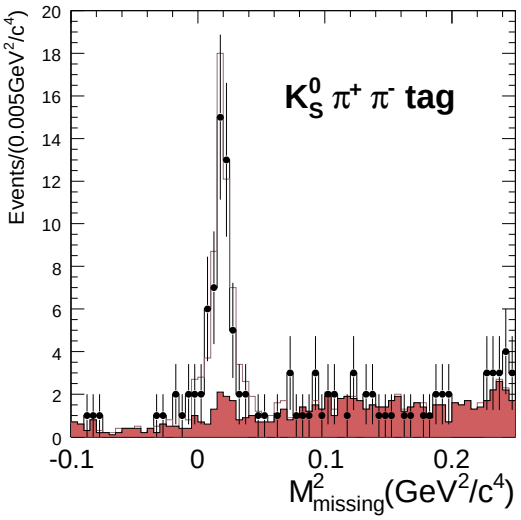

Figure 2.21: $M^2_{missing}$ distribution for $K^0_S\pi^+\pi^-$ vs. $K^0_S\pi^+\pi^-$ partial reconstruction. The shaded histogram is Monte Carlo background.

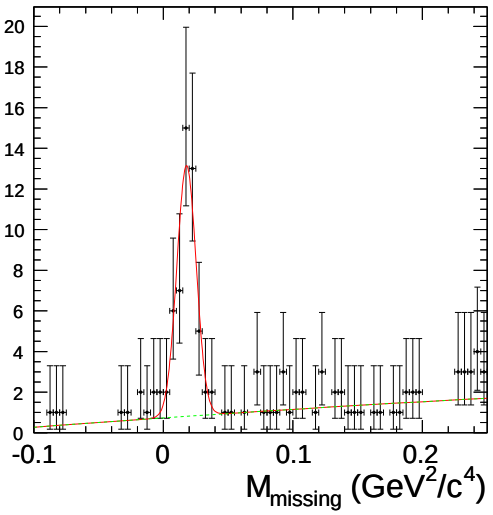

Figure 2.22: Fit to $M^2_{missing}$ distribution. The continuum background is parameterized using a 2nd order polynomial function.

Table 2.12: $K^0_S\pi^+\pi^-$ vs. $K^0_S\pi^+\pi^-$ partial reconstruction yield. Note that in the fit, the peaking background has been neglected. It will be considered later using Monte Carlo.

	Yield	$\pi^+\pi^+\pi^-\pi^-$	Other BG	B/(S+B)
MC	556	33	70	18.5%
Data	54.4	/	8.4	15.4%

Table 2.13: $K^0_S\pi^+\pi^-$ vs. $K^0_L\pi^+\pi^-$ yield and background level estimation from QCMC.

Mode	Data	B/(S+B)
$K^0_S\pi^+\pi^-$	867	7.7%

2.4.3 $K^0_S\pi^+\pi^-$ vs. $K^0_L\pi^+\pi^-$

$K^0_S\pi^+\pi^-$ and $K^0_L\pi^+\pi^-$ selections are same as before. The missing mass square distribution when only two tracks are found in addition to a $K^0_S\pi^+\pi^-$ tag is shown in Fig. 2.23. Solid line is Monte Carlo, dots are data, shaded histogram is Monte Carlo background. The yields and background level are shown in Table 2.13. The Dalitz plot of $K^0_S\pi^+\pi^-$ is shown in Fig. 2.24, and the Dalitz plot of $K^0_L\pi^+\pi^-$ is shown in Fig. 2.25.

2.5 Signal Monte Carlo generation

2.5.1 Single $K^0_S\pi^+\pi^-$ generation

The Dalitz decay model of $D^0 \to K_S\pi^+\pi^-$ in EvtGen has only two resonances, $K^*(892)$ and $\rho^0(770)$. In order to simulate real data better, we made modifications to the $K^0_S\pi^+\pi^-$ decay model, using the BaBar fit result [1], which includes 16 resonances. All of the resonances are parameterized using a Breit-Wigner function except $\rho^0(770)$ and $\rho^0(1450)$. $\rho^0(770)$ and $\rho^0(1450)$ are parameterized using the Gounaris-Sakurai function [9]. Flavor and CP tagged $K^0_S\pi^+\pi^-$ samples are generated. The $K^0_S\pi^+\pi^-$ CP eigenstate tagged samples are generated according to the amplitude

$$f_{CP\pm}(x,y) = f_D(x,y) \pm \bar{f}_D(y,x).$$

Note here the non resonant part is treated as a scaler particle.

The flavor and CP tagged $K^0_S\pi^+\pi^-$ Dalitz plots in both data and Monte Carlo are shown in Fig. 2.26.

2.5.2 Double $K^0_S\pi^+\pi^-$ generation

The situation is more complicated for $K^0_S\pi^+\pi^-$ vs. $K^0_S\pi^+\pi^-$ correlated Monte Carlo. We need to generate the Monte Carlo of $D^0/\bar{D}^0$ system according the antisymmetric wave function:

$$f_{corr}(x,y,x',y') = f_D(x,y)\bar{f}'_D(y',x') - f'_D(x',y')\bar{f}_D(y,x). \tag{2.12}$$

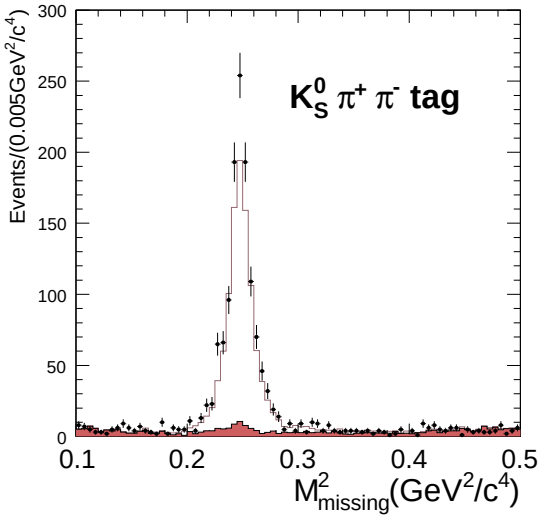

Figure 2.23: Missing mass square distribution for $K^0_L\pi^+\pi^-$ when one D is identified as $K^0_S\pi^+\pi^-$. Solid histogram is Monte Carlo, dots are data, shaded histogram is background.

This can't be realized by modifying an existing EvtGen model since all the models decay D^0 and $\bar{D}^0$ separately. Instead, we start from $\psi(3770)$, let $\psi(3770) \to (D^0, \bar{D}^0) \to (K^0_S\pi^+\pi^-, K^0_S\pi^+\pi^-)$ inside the new model. We make the two step process $(\psi(3770) \to (D^0, \bar{D}^0)$, $D^0/\bar{D}^0 \to K^0_S\pi^+\pi^-)$ realized in one step. Since D^0 and $\bar{D}^0$ now only appear as a intermedia state inside the model, in Monte Carlo tree, only $\psi(3770) \to (K^0_S\pi^+\pi^-, K^0_S\pi^+\pi^-)$ is shown. All the other things are same as usual Monte Carlo, the analysis code doesn't need change.

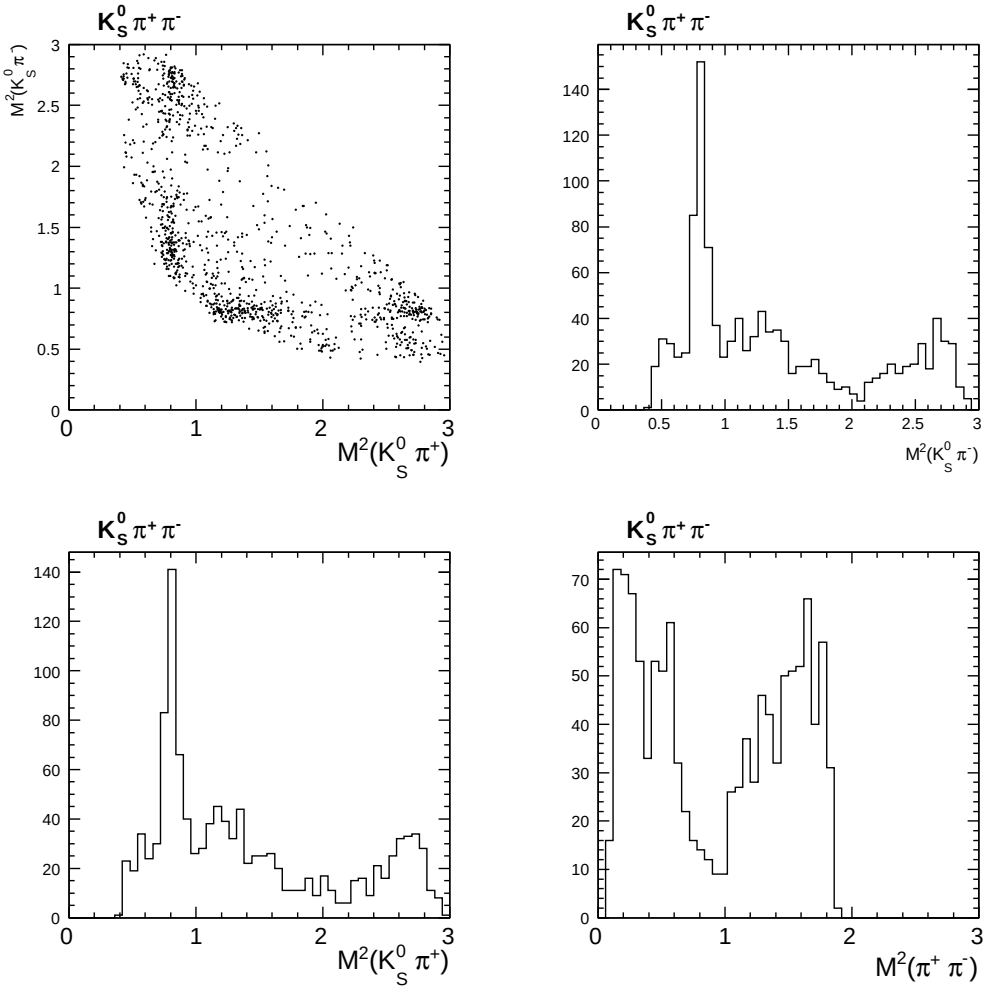

Figure 2.24: $K^0_S\pi^+\pi^-$ Dalitz plot and projections for $K^0_S\pi^+\pi^-$ vs. $K^0_L\pi^+\pi^-$ data sample.

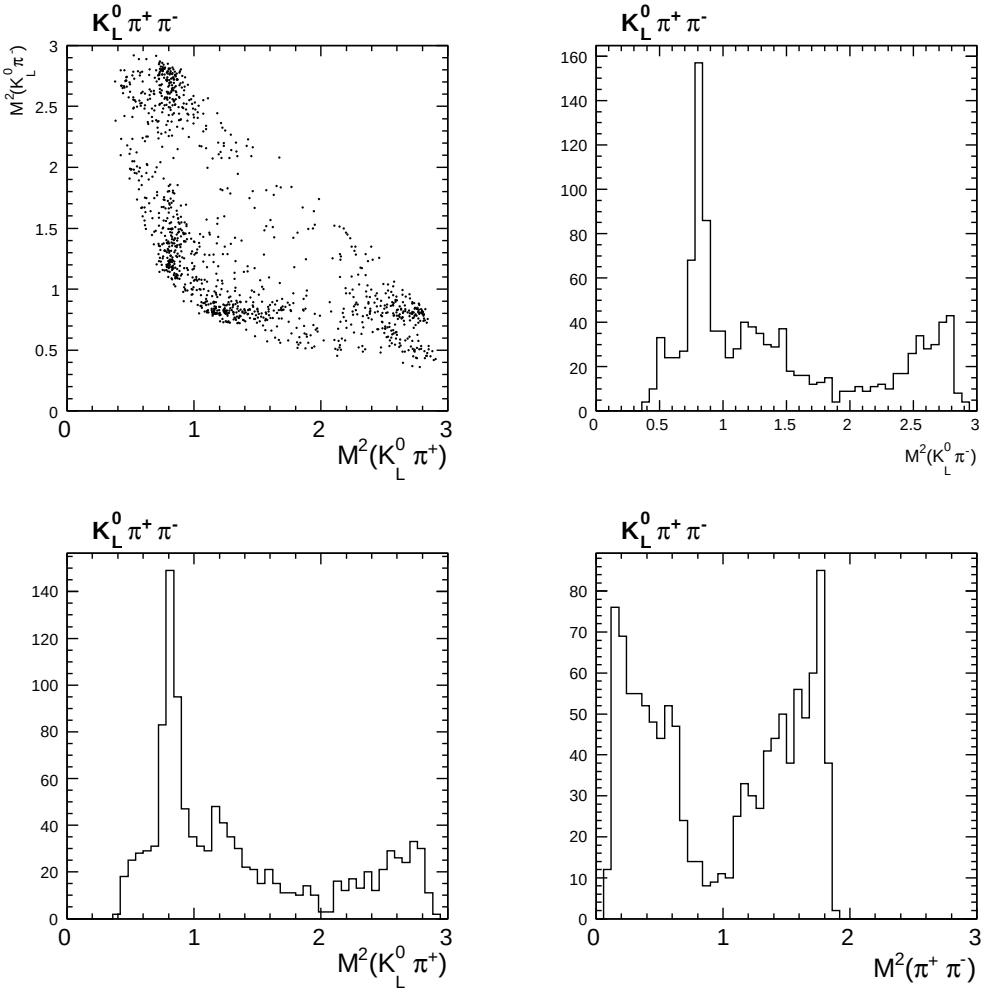

Figure 2.25: $K_L^0\pi^+\pi^-$ Dalitz plot and projections for $K_S^0\pi^+\pi^-$ vs. $K_L^0\pi^+\pi^-$ data sample.

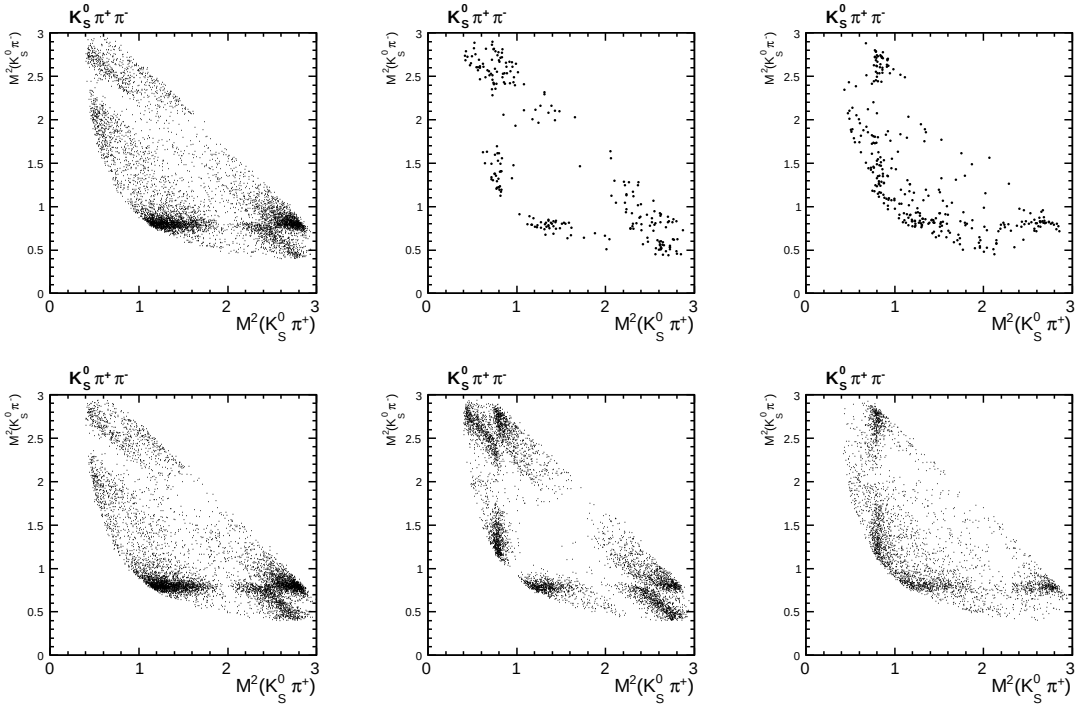

Figure 2.26: $K^0_S\pi^+\pi^-$ Dalitz plots in both data (top row) and Monte Carlo (bottom row) for flavor tagged sample (first column), CP even tagged sample (second column) and CP odd tagged sample (third column).

Chapter 3

Input Data & Fit

3.1 Efficiencies

The efficiency is defined as the ratio of reconstructed events to generated events in each bin. Large data sets are generated to calculate the efficiencies.

The $K^0_S\pi^+\pi^-$ efficiencies for different tag modes are shown in Table 3.1 and Table 3.2. The $K^0_L\pi^+\pi^-$ efficiencies for different tag modes are shown in Table 3.3 and Table 3.4. The events density is not symmetric in the lower half ($M_{K^0\pi^+} > M_{K^0_S\pi^-}$) and upper half ($M_{K^0\pi^+} < M_{K^0_S\pi^-}$) for flavor tagged $K^0_{S,L}\pi^+\pi^-$ samples, so the efficiencies for the lower half and upper half are calculated separately. While for CP tagged $K^0_{S,L}\pi^+\pi^-$ samples, the lower half and upper half are merged together, since the events population is symmetric.

For $K^0_L\pi^+\pi^-$ efficiencies, there are some relatively large variations among the bins. We further investigate this issue by generating phase space Monte Carlo samples, then fitting with a cubic polynomial function

$$\begin{aligned}\varepsilon(x,y) &= 1 + E_x x + E_y y + E_{xy} xy + E_{xx} x^2 + E_{yy} y^2 + E_{xxy} x^2 y + E_{xyy} x y^2 \\ &\quad + E_{xxx} x^3 + E_{yyy} y^3, \end{aligned} \tag{3.1}$$

where $x = M^2(K^0\pi^+)$, $y = M^2(K^0\pi^-)$. The fit results are shown in Fig. 3.1. The efficiency shape is basically symmetric with the center having the highest efficiency, the two corners having the lowest efficiencies. The flavor tagged $K^0_L\pi^+\pi^-$ Dalitz plot overlay on the 8 bins is shown in Fig. 3.2. The efficiency for each bin is the weighted average according the events population. So the efficiencies for flavor tagged and CP tagged samples are not the same, since the events populations are not the same.

Before we calculate $K^0_S\pi^+\pi^-$ vs. $K^0_S\pi^+\pi^-$ efficiencies, there are some facts about $M_{i,j}$ (Equation 1.46) which we should know

1. $M_{i,j} \neq M_{\bar{i},j}$,
2. $M_{i,j} = M_{\bar{i},\bar{j}}$,
3. $M_{\bar{i},j} = M_{i,\bar{j}}$.

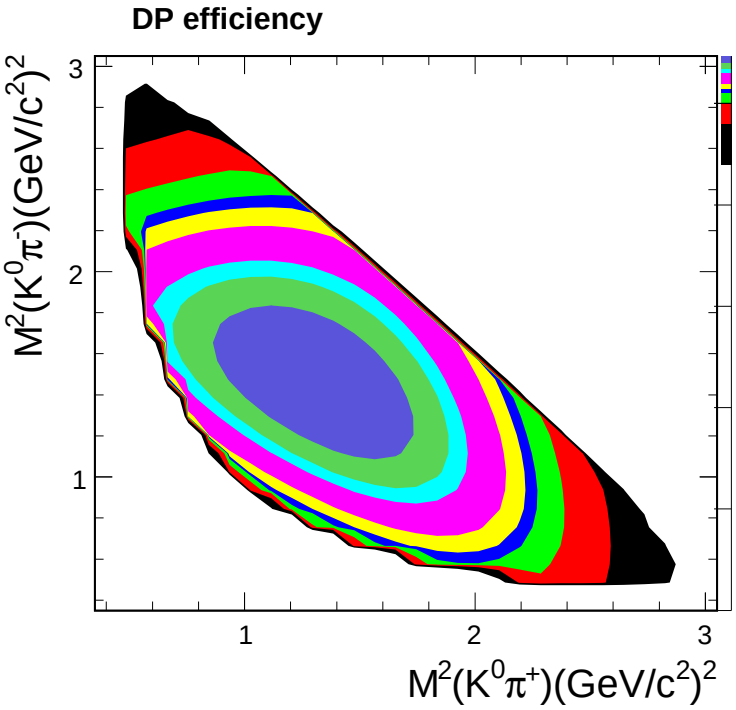

Figure 3.1: $K^0_L\pi^+\pi^-$ reconstruction efficiency. The efficiency is fitted to flavor tagged $K^0_L\pi^+\pi^-$ phase space Monte Carlo sample with a cubic polynomial function. The center has highest efficiency, while the two corners have lowest efficiencies.

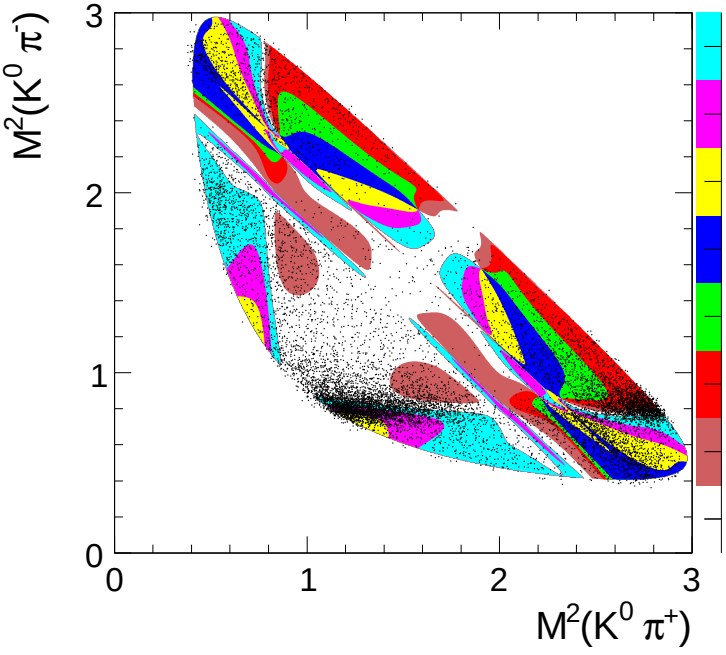

Figure 3.2: Flavor tagged $K^0_L\pi^+\pi^-$ Dalitz plot overlay on the 8 bins.

So in the efficiency calculations, we group $M_{i,j}$, $M_{\bar{i},\bar{j}}$ in one set, and $M_{\bar{i},j}$, $M_{i,\bar{j}}$ in another set. $K^0_S\pi^+\pi^-$ vs. $K^0_S\pi^+\pi^-$ efficiencies are shown in Table 3.5. $K^0_S\pi^+\pi^-$ vs. $K^0_L\pi^+\pi^-$ efficiencies are shown in Table 3.6.

3.2 Input Yields & Backgrounds

3.2.1 CP and flavor tagged $K^0_{S,L}\pi^+\pi^-$ data

We use tag side sidebands to subtract the tag side background. For flavor tags, tag side ΔE sidebands are used. For CP tags with a K^0_S in tag side, both ΔE and K^0_S sidebands of tag side are used to subtract the background. The signal and sideband yields of $K^0_S\pi^+\pi^-$ vs. tags in data are shown in Table 3.7. Some bins have very low statistics in CP tags. The backgrounds in signal side, which is very small, will be studied as systematic error. In order to combine $K^0_L\pi^0$ vs. $K^0_S\pi^+\pi^-$ data, we used the total number of $D^0/\bar{D}^0$, calculated from cross section and luminosity. The luminosity for the full dataset is 818 ± 8 pb^{-1}. We also used the branching fraction of $K^0_L\pi^0$ from [15], which is $\mathcal{B}_{K^0_L\pi^0} = 0.998 \pm 0.049 \pm 0.030 \pm 0.038\%$.

In Table 3.8, we show the signal and sideband yields of $K^0_L\pi^+\pi^-$ vs. tags in data. The sideband yields including both tag side sidebands, which is same as $K^0_S\pi^+\pi^-$ case, and $M^2_{missing}$ sidebands, which are $0.15 < M^2_{missing} < 0.18$ GeV$^2/c^4$ and $0.32 < M^2_{missing} < 0.37$ GeV$^2/c^4$.

3.2.2 $K^0_S\pi^+\pi^-$ vs. $K^0_{S,L}\pi^+\pi^-$ data

The events from NoPID $K^0_S\pi^+\pi^-$ vs. $K^0_S\pi^+\pi^-$ double tag reconstruction and the events from partial reconstruction are combined together to do the fit. $M_{(i,j),(\bar{i},\bar{j})}$, and $M_{(i,\bar{j}),(\bar{i},j)}$ yields are shown in Table 3.9.

There are peaking backgrounds from $\pi^+\pi^-\pi^+\pi^-$ faking $K^0_S\pi^+\pi^-$. We use Monte Carlo to study this piece of background. The $\pi^+\pi^-\pi^+\pi^-$ Dalitz structure is taken from recent Focus study [19]. The dominant component is the decay $D^0 \to a_1(1260)^+\pi^-$, accounting for 60% of the decay rate. The second most dominant contribution comes from the decay $D^0 \to \rho(770)^0\rho(770)^0$, with a fraction of 25%. For the remaining components, we use non-resonant decay model.

Correlated $K^0_S\pi^+\pi^-$ vs. $K^0_S\pi^+\pi^-$ Monte Carlo samples are generated with $\pi^+\pi^-\pi^+\pi^-$ background added in. After reconstruction, among 21367 double $K^0_S\pi^+\pi^-$ yields, the number of $\pi^+\pi^-\pi^+\pi^-$ background is 1296, which is about 6.1% of the toal yields. In Table 3.10, we show the expected background events, which is normalized from Monte Carlo, in data. This table is then subtracted from Table 3.9 in the global fit. Other kinds of background are considered in the systematic study.

$K^0_S\pi^+\pi^-$ vs. $K^0_L\pi^+\pi^-$ yields in both signal region and sideband region are shown in Table 3.11. Note here, we apply the K^0_S flight significance cut to $K^0_S\pi^+\pi^-$, so the peaking background from 4 charged pions is greatly suppressed.

In $K^0_L\pi^+\pi^-$ reconstruction, there is about 2% peaking background from $K^0_S\pi^+\pi^-$. In Table 3.12, we show $K^0_S\pi^+\pi^-$ data yields, efficiency of $K^0_S\pi^+\pi^-$ reconstruction, efficiency of $K^0_S\pi^+\pi^-$ being reconstructed as $K^0_L\pi^+\pi^-$. From these numbers, we can estimate the back-

Table 3.1: $K^0_S\pi^+\pi^-$ reconstruction efficiencies for the 8 bins in flavor tagged samples. The efficiencies for the upper half ($M_{K^0_S\pi^+} < M_{K^0_S\pi^-}$) and lower half ($M_{K^0_S\pi^+} > M_{K^0_S\pi^-}$) are computed separately.

	$M_{K^0_S\pi^+} > M_{K^0_S\pi^-}$			$M_{K^0_S\pi^+} < M_{K^0_S\pi^-}$		
$K^-\pi^+$	Rec.	Gen.	Eff.(%)	Rec.	Gen.	Eff.(%)
Bin[0]	3094.0	8842.0	35.0±0.5	970.0	2736.0	35.5±0.9
Bin[1]	1288.0	3676.0	35.0±0.8	289.0	869.0	33.3±1.6
Bin[2]	2204.0	6028.0	36.6±0.6	533.0	1389.0	38.4±1.3
Bin[3]	592.0	1694.0	34.9±1.2	196.0	558.0	35.1±2.0
Bin[4]	1219.0	3428.0	35.6±0.8	463.0	1335.0	34.7±1.3
Bin[5]	1564.0	4561.0	34.3±0.7	595.0	1635.0	36.4±1.2
Bin[6]	2050.0	6187.0	33.1±0.6	370.0	1101.0	33.6±1.4
Bin[7]	2257.0	6780.0	33.3±0.6	909.0	2626.0	34.6±0.9
$K^-\pi^+\pi^0$	Rec.	Gen.	Eff.(%)	Rec.	Gen.	Eff.(%)
Bin[0]	5586.0	16562.0	33.7±0.4	1805.0	5246.0	34.4±0.7
Bin[1]	2482.0	6987.0	35.5±0.6	542.0	1674.0	32.4±1.1
Bin[2]	4195.0	11370.0	36.9±0.5	974.0	2596.0	37.5±1.0
Bin[3]	1151.0	3170.0	36.3±0.9	393.0	1053.0	37.3±1.5
Bin[4]	2255.0	6361.0	35.5±0.6	897.0	2495.0	36.0±1.0
Bin[5]	2791.0	8438.0	33.1±0.5	1117.0	3333.0	33.5±0.8
Bin[6]	3964.0	12033.0	32.9±0.4	720.0	2059.0	35.0±1.1
Bin[7]	4273.0	12846.0	33.3±0.4	1807.0	5363.0	33.7±0.6
$K^-\pi^+\pi^+\pi^-$	Rec.	Gen.	Eff.(%)	Rec.	Gen.	Eff.(%)
Bin[0]	4222.0	12624.0	33.4±0.4	1393.0	3980.0	35.0±0.8
Bin[1]	1805.0	5331.0	33.9±0.6	404.0	1278.0	31.6±1.3
Bin[2]	3085.0	8716.0	35.4±0.5	732.0	2004.0	36.5±1.1
Bin[3]	855.0	2343.0	36.5±1.0	304.0	842.0	36.1±1.7
Bin[4]	1662.0	4835.0	34.4±0.7	639.0	1932.0	33.1±1.1
Bin[5]	2209.0	6530.0	33.8±0.6	799.0	2342.0	34.1±1.0
Bin[6]	2956.0	8917.0	33.2±0.5	519.0	1575.0	33.0±1.2
Bin[7]	3181.0	9724.0	32.7±0.5	1323.0	3877.0	34.1±0.8
$K^-e^+\nu$	Rec.	Gen.	Eff.(%)	Rec.	Gen.	Eff.(%)
Bin[0]	9427.0	49020.0	19.2±0.2	3000.0	15549.0	19.3±0.3
Bin[1]	4176.0	20910.0	20.0±0.3	1015.0	5235.0	19.4±0.5
Bin[2]	6910.0	33452.0	20.7±0.2	1738.0	7848.0	22.1±0.5
Bin[3]	1970.0	9452.0	20.8±0.4	653.0	3156.0	20.7±0.7
Bin[4]	3802.0	18982.0	20.0±0.3	1471.0	7466.0	19.7±0.5
Bin[5]	4761.0	25072.0	19.0±0.2	1811.0	9305.0	19.5±0.4
Bin[6]	6694.0	34863.0	19.2±0.2	1222.0	6169.0	19.8±0.5
Bin[7]	7135.0	37893.0	18.8±0.2	2888.0	15137.0	19.1±0.3

Table 3.2: $K^0_S\pi^+\pi^-$ reconstruction efficiencies for the 8 bins in CP tagged samples. Note here the column labeled with $K^0_L\pi^0$ is the double tag efficiency.

Bin	$K^0_L\pi^0$	K^+K^-	$\pi^+\pi^-$	$K^0_S\pi^0\pi^0$	$K^0_S\pi^0$	$K^0_S\eta$	$K^0_S\omega$
0	15.1±0.2	34.1±0.6	33.3±0.9	31.0±0.9	33.6±0.3	32.0±0.7	33.3±0.4
1	15.2±0.3	34.5±0.8	35.9±1.2	34.0±1.2	34.1±0.4	32.4±1.2	33.8±0.7
2	16.4±0.3	36.5±0.5	37.2±0.7	34.0±0.7	36.7±0.4	34.9±1.2	34.3±0.7
3	15.7±0.4	34.9±0.7	36.3±1.0	33.1±1.0	34.7±1.1	34.3±3.0	34.1±1.7
4	15.5±0.3	35.7±0.4	34.5±0.7	33.3±0.6	34.7±1.1	31.8±2.8	33.5±1.7
5	14.4±0.3	34.1±0.4	33.4±0.6	31.6±0.6	32.8±0.7	30.4±1.8	33.2±1.1
6	14.7±0.3	33.0±0.5	33.1±0.7	31.0±0.7	33.4±0.4	30.9±1.2	32.2±0.7
7	14.8±0.2	34.0±0.5	35.4±0.8	33.4±0.8	33.2±0.3	31.9±0.9	33.2±0.5

Table 3.3: $K^0_L\pi^+\pi^-$ reconstruction efficiencies for the 8 bins in flavor tagged samples. The efficiencies for the upper half ($M_{K^0_L\pi^+} < M_{K^0_L\pi^-}$) and lower half ($M_{K^0_L\pi^+} > M_{K^0_L\pi^-}$) are computed separately.

	$K^-\pi^+$		$K^-\pi^+\pi^0$		$K^-\pi^+\pi^+\pi^-$	
Bin	Lower half	Upper half	Lower half	Upper half	Lower half	Upper half
0	65.6±0.7	68.7±1.1	64.3±0.5	65.1±0.8	59.9±0.6	58.2±1.0
1	65.6±1.1	64.7±2.0	58.3±0.9	60.9±1.5	52.6±1.0	55.1±1.8
2	64.5±0.8	64.1±1.8	59.4±0.6	60.8±1.3	55.7±0.7	58.9±1.5
3	68.1±1.5	65.8±2.9	59.9±1.1	60.8±2.1	54.5±1.3	57.7±2.4
4	62.4±1.2	63.0±1.9	58.6±0.9	62.2±1.4	55.7±1.0	52.1±1.7
5	68.0±1.0	61.4±1.7	64.4±0.7	58.9±1.3	59.1±0.9	54.1±1.4
6	62.2±0.8	66.0±1.8	62.1±0.6	59.7±1.4	54.6±0.7	54.8±1.6
7	65.2±0.8	64.1±1.2	61.1±0.6	62.6±0.9	55.6±0.7	58.6±1.0

Table 3.4: $K^0_L\pi^+\pi^-$ reconstruction efficiencies for the 8 bins in CP tagged samples.

Bin	K^+K^-	$\pi^+\pi^-$	$K^0_S\pi^0$	$K^0_S\eta$
0	65.2±0.4	66.6±0.6	70.9±0.5	70.4±1.5
1	61.0±0.7	61.3±1.0	58.9±0.7	53.8±2.1
2	65.0±0.6	64.5±0.9	60.2±0.4	59.0±1.1
3	67.4±1.3	69.9±1.9	62.6±0.5	60.3±1.5
4	61.6±1.5	64.8±2.3	59.8±0.4	58.9±1.0
5	68.1±0.9	69.0±1.4	63.2±0.3	61.1±1.0
6	63.3±0.6	63.0±0.8	61.4±0.4	56.8±1.1
7	63.9±0.5	65.6±0.7	65.6±0.4	67.0±1.2

Table 3.5: $K^0_S\pi^+\pi^-$ vs. $K^0_S\pi^+\pi^-$ $M_{(i,j),(\bar{i},\bar{j})}$, and $M_{(i,\bar{j}),(\bar{i},j)}$ efficiencies, respectively. All numbers are in percentage.

i/j	0	1	2	3	4	5	6	7
0	17.3±0.4							
1	16.3±0.3	15.0±0.8						
2	16.8±0.2	16.4±0.4	18.5±0.6					
3	17.5±0.3	15.7±0.5	18.8±0.7	20.5±2.4				
4	15.9±0.2	15.0±0.3	16.1±0.3	16.9±0.7	15.7±0.9			
5	16.0±0.2	15.0±0.3	16.3±0.2	16.3±0.5	16.6±0.5	16.2±0.7		
6	16.7±0.2	16.0±0.3	16.3±0.2	17.0±0.4	15.8±0.3	16.1±0.4	16.1±0.6	
7	16.5±0.2	15.9±0.3	16.1±0.2	16.4±0.3	15.5±0.2	15.7±0.2	16.5±0.3	16.2±0.3
i/j	0	1	2	3	4	5	6	7
0	16.4±0.2							
1	16.2±0.2	15.8±0.4						
2	16.6±0.1	15.9±0.2	16.0±0.2					
3	16.9±0.2	16.1±0.4	16.8±0.3	16.8±0.8				
4	15.8±0.2	15.5±0.3	15.9±0.2	16.5±0.5	15.5±0.5			
5	16.3±0.1	15.5±0.2	16.6±0.2	16.8±0.5	16.0±0.3	16.0±0.3		
6	16.7±0.1	16.0±0.2	16.5±0.2	16.6±0.4	15.9±0.2	16.2±0.2	16.0±0.2	
7	16.4±0.2	16.1±0.2	16.6±0.2	16.5±0.3	15.7±0.2	15.8±0.2	16.2±0.2	16.4±0.2

Table 3.6: $K^0_S\pi^+\pi^-$ vs. $K^0_L\pi^+\pi^-$ $M_{(i,j),(\bar{i},\bar{j})}$, and $M_{(i,\bar{j}),(\bar{i},j)}$ efficiencies, respectively. All numbers are in percentage.

i/j	0	1	2	3	4	5	6	7
0	20.7±0.3	19.4±0.5	19.5±0.5	19.8±1.0	19.4±1.0	22.2±0.7	19.2±0.5	20.3±0.4
1	21.0±0.5	20.3±0.8	20.2±0.7	20.7±1.4	19.2±1.4	24.6±1.3	21.2±0.9	21.2±0.6
2	22.3±0.5	21.3±0.8	21.4±0.6	23.1±1.0	22.6±0.9	22.4±1.0	24.7±1.1	21.1±0.6
3	23.2±1.3	19.7±1.7	20.8±1.0	21.0±1.7	21.7±1.3	24.3±1.5	23.0±2.1	23.7±1.5
4	23.1±1.2	20.4±1.7	19.7±1.0	24.3±1.3	21.8±0.8	20.4±0.7	20.5±0.9	19.6±0.8
5	22.0±0.8	20.6±1.5	19.3±1.0	18.7±1.4	19.6±0.7	20.0±0.6	19.3±0.7	20.4±0.6
6	20.1±0.5	21.1±1.1	21.0±1.1	19.2±1.8	19.0±0.8	20.2±0.6	19.1±0.6	19.6±0.5
7	21.1±0.4	19.8±0.6	20.5±0.6	21.4±1.3	20.0±0.8	20.4±0.6	20.1±0.5	20.8±0.4
i/j	0	1	2	3	4	5	6	7
0	20.8±0.3	19.0±0.4	20.4±0.3	20.5±0.7	21.5±0.7	22.0±0.5	20.4±0.3	20.1±0.3
1	22.3±0.4	21.2±0.7	20.4±0.6	21.3±1.2	20.0±0.9	23.1±0.7	21.0±0.5	21.1±0.5
2	23.0±0.4	21.0±0.7	22.5±0.5	22.6±1.0	20.5±0.6	22.6±0.5	21.7±0.4	22.2±0.4
3	23.2±0.9	17.7±1.4	23.0±1.1	19.6±1.6	22.1±1.1	21.1±0.9	20.5±0.8	22.7±0.8
4	23.3±0.7	21.1±1.0	20.5±0.6	21.5±1.0	19.5±0.7	20.2±0.6	21.0±0.7	20.9±0.7
5	20.3±0.5	19.5±0.7	19.4±0.5	20.0±0.8	19.2±0.6	21.0±0.7	20.0±0.6	20.9±0.6
6	20.0±0.4	19.0±0.6	19.6±0.4	22.1±0.7	20.3±0.6	19.8±0.6	18.8±0.5	21.0±0.5
7	20.8±0.3	19.3±0.5	19.9±0.4	20.4±0.7	19.1±0.7	21.3±0.6	19.6±0.4	19.7±0.4

Table 3.7: Data yields of both signal and sideband $K^0_S\pi^+\pi^-$ vs. flavor tags, CP even, CP odd tags in each bin. For flavor tags, the yields in lower half (first row) and upper half (second row) Dalitz plot are shown separately, while for CP tags, they are summed.

Tag Mode	Bin(1)	Bin(2)	Bin(3)	Bin(4)	Bin(5)	Bin(6)	Bin(7)	Bin(8)
$K^-\pi^+$	237/2	96/1	167/2	58/0	70/1	93/0	155/0	187/2
	93/0	30/0	45/0	18/0	36/0	33/0	23/0	97/1
$K^-\pi^+\pi^0$	452/7	196/1	318/6	111/1	162/1	217/1	291/5	314/7
	137/4	43/1	87/3	31/1	74/3	66/2	59/0	172/3
$K^-\pi^+\pi^+\pi^-$	325/5	150/1	298/2	90/2	132/1	136/2	245/3	261/8
	123/1	52/1	63/2	31/0	68/0	57/2	47/0	136/2
K^+K^-	9/0	7/0	19/1	10/0	26/1	18/0	18/0	15/0
$\pi^+\pi^-$	8/0	2/0	7/0	5/1	9/1	15/0	10/0	4/0
$K^0_S\pi^0\pi^0$	3/0	1/0	12/0	4/0	12/0	9/0	4/3	8/0
$K^0_L\pi^0$	19/0	10/0	37/0	20/0	43/0	37/0	24/0	39/0
$K^0_S\pi^0$	59/1	25/0	27/1	4/0	3/0	5/0	23/1	39/0
$K^0_S\eta$	13/0	3/0	7/0	2/0	0/0	0/0	5/0	9/0
$K^0_S\omega$	22/3	6/0	12/1	3/0	0/0	3/0	8/2	23/0

ground yields, which are shown in the last column in Table 3.12. Using the expected peaking background yields, according the distribution of $K^0_S\pi^+\pi^-$ in the 8 bins, we get the peaking background yields in Table 3.13 and Table 3.14. These two tables are used in peaking background subtraction.

Table 3.8: Data yields of both signal and sideband $K^0_L\pi^+\pi^-$ vs. flavor tags, CP even, CP odd tags in each bin. For flavor tags, the yields in lower half (first row) and upper half (second row) Dalitz plot are shown separately, while for CP tags, they are summed.

Tag Mode	Bin(1)	Bin(2)	Bin(3)	Bin(4)	Bin(5)	Bin(6)	Bin(7)	Bin(8)
$K^-\pi^+$	469/23	164/8	319/15	104/7	161/3	230/9	294/0	326/9
	172/13	63/3	91/11	42/2	96/5	80/5	62/2	177/8
$K^-\pi^+\pi^0$	910/38	299/23	522/22	176/16	264/14	405/15	531/12	617/24
	318/23	115/8	186/21	64/13	145/16	148/12	110/10	299/24
$K^-\pi^+\pi^+\pi^-$	664/32	240/16	446/27	155/11	235/9	295/9	439/12	510/13
	272/23	91/8	157/12	61/7	108/7	94/13	98/7	232/15
K^+K^-	111/4	38/2	45/1	12/2	11/1	13/1	52/0	62/3
$\pi^+\pi^-$	47/3	23/1	25/0	5/1	5/0	8/0	22/0	37/1
$K^0_S\pi^0$	34/6	14/2	38/2	18/2	62/3	49/2	34/3	31/3
$K^0_S\eta$	4/1	0/0	9/0	7/1	10/0	5/1	3/0	2/0

Table 3.9: $K^0_S\pi^+\pi^-$ vs. $K^0_S\pi^+\pi^-$ $M_{(i,j),(\bar{\imath},\bar{\jmath})}$, and $M_{(i,\bar{\jmath}),(\bar{\imath},j)}$ yields in data.

$M_{(i,j),(\bar{\imath},\bar{\jmath})}$	0	1	2	3	4	5	6	7
0	3							
1	1	1						
2	8	4	3					
3	3	2	1	1				
4	17	3	6	1	0			
5	11	3	9	1	5	1		
6	5	2	6	2	3	5	1	
7	12	3	12	4	8	8	3	7
$M_{(i,\bar{\jmath}),(\bar{\imath},j)}$	0	1	2	3	4	5	6	7
0	16							
1	6	1						
2	27	8	10					
3	8	0	8	1				
4	18	7	9	2	1			
5	16	2	3	1	2	2		
6	16	4	9	7	5	8	12	
7	13	5	14	5	15	19	15	11

Table 3.10: Expected background yields from $D^0 \to \pi^+\pi^-\pi^+\pi^-$ in $K^0_S\pi^+\pi^-$ vs. $K^0_S\pi^+\pi^-$ events.

$M_{(i,j),(\bar{\imath},\bar{\jmath})}$	0	1	2	3	4	5	6	7
0	1.06							
1	1.45	0.33						
2	1.71	0.44	0.12					
3	0.89	0.30	0.27	0.12				
4	1.51	0.56	0.89	0.30	0.15			
5	1.69	0.80	0.47	0.24	0.68	0.24		
6	1.74	0.77	0.35	0.89	0.65	0.62	0.41	
7	1.60	1.54	1.69	0.41	1.24	0.86	1.09	0.30
$M_{(i,\bar{\jmath}),(\bar{\imath},j)}$	0	1	2	3	4	5	6	7
0	1.06							
1	0.44	0.12						
2	0.71	0.30	0.30					
3	0.18	0.15	0.12	0.03				
4	0.27	0.24	0.12	0.12	0.27			
5	0.44	0.15	0.24	0.09	0.15	0.12		
6	0.59	0.24	0.27	0.03	0.30	0.18	0.15	
7	1.01	0.56	0.33	0.18	0.24	0.27	0.33	0.47

Table 3.11: $K^0_S\pi^+\pi^-$ vs. $K^0_L\pi^+\pi^-$ $M_{(i,j),(\bar{i},\bar{j})}$, and $M_{(i,\bar{j}),(\bar{i},j)}$ yields in both signal region and sideband region in data.

$M_{(i,j),(\bar{i},\bar{j})}$	1	2	3	4	5	6	7	8
0	31/3	3/1	18/2	2/1	4/0	1/0	12/1	28/2
1	8/1	6/1	3/0	0/0	1/0	2/0	6/0	3/0
2	19/2	6/3	16/0	5/0	2/0	0/0	3/0	18/0
3	4/0	1/0	3/0	0/0	4/1	1/0	3/0	2/0
4	3/0	0/1	11/0	6/1	9/1	7/0	6/0	6/0
5	2/0	3/0	8/0	4/1	6/0	6/0	4/0	6/0
6	20/0	4/0	3/1	2/0	7/1	6/0	5/1	14/0
7	35/2	10/1	9/1	4/0	3/0	7/0	9/1	33/2
$M_{(i,\bar{j}),(\bar{i},j)}$	1	2	3	4	5	6	7	8
0	60/2	13/2	37/1	5/0	8/1	10/0	22/1	25/1
1	9/0	10/0	4/0	2/1	7/1	4/0	11/0	13/0
2	22/0	15/1	18/0	4/0	7/0	7/1	13/1	22/0
3	9/1	3/2	4/0	4/0	6/0	5/1	8/0	3/0
4	7/1	0/0	6/0	8/0	11/1	5/0	5/0	5/0
5	17/2	3/0	13/1	3/0	7/0	10/0	11/0	6/0
6	23/1	10/0	15/2	4/0	7/0	7/0	9/0	17/0
7	33/0	5/0	12/1	7/1	7/0	8/0	10/0	20/1

Table 3.12: $K^0_L\pi^+\pi^-$ peaking background ($K^0_L\pi^+\pi^-$) estimation. The "Yields" column show $K^0_S\pi^+\pi^-$ data yields vs. different tag modes. "ϵ" is the efficiency of $K^0_S\pi^+\pi^-$ reconstruction. "$\epsilon_{K^0_L\pi^+\pi^-}$" is the efficiency of $K^0_S\pi^+\pi^-$ being reconstructed as $K^0_L\pi^+\pi^-$. "Expect BG." is the expected $K^0_S\pi^+\pi^-$ background events in $K^0_L\pi^+\pi^-$ reconstruction.

Tag	Yields	ϵ	$\epsilon_{K^0_L\pi^+\pi^-}$	Expect BG.
$K^-\pi^+$	1438	0.348	0.011	44.3
$K^-\pi^+\pi^0$	2730	0.344	0.011	84.7
$K^-\pi^+\pi^+\pi^-$	2218	0.340	0.012	78.1
K^+K^-	122	0.347	0.011	3.7
$\pi^+\pi^-$	60	0.347	0.011	2.0
$K^0_S\pi^0$	186	0.340	0.011	6.3
$K^0_S\eta$	39	0.323	0.010	1.3
$K^0_S\pi^+\pi^-$	383	0.145	0.008	21.7

Table 3.13: Expected $K^0_L\pi^+\pi^-$ peaking background yields from $K^0_S\pi^+\pi^-$ events that pass the $K^0_L\pi^+\pi^-$ selection.

Tag	0	1	2	3	4	5	6	7
$K^-\pi^+$	8.42	1.93	4.17	1.70	2.94	3.48	5.33	5.41
	1.93	1.08	0.77	0.62	1.16	0.62	1.55	2.63
$K^-\pi^+\pi^0$	14.44	4.76	6.40	2.11	3.98	7.26	11.78	12.33
	5.70	1.56	1.56	1.40	2.03	3.28	1.64	3.90
$K^-\pi^+\pi^+\pi^-$	13.33	5.18	6.71	2.12	3.65	7.64	9.85	10.53
	4.76	1.02	2.21	0.85	1.19	2.63	1.87	3.74
K^+K^-	0.35	0.24	0.52	0.20	0.49	0.63	0.71	0.55
$\pi^+\pi^-$	0.16	0.07	0.25	0.08	0.37	0.34	0.38	0.30
$K^0_S\pi^0$	2.16	0.52	0.60	0.13	0.10	0.41	0.83	1.46
$K^0_S\eta$	0.47	0.08	0.15	0.07	0.01	0.12	0.12	0.20

Table 3.14: Expected $K^0_S\pi^+\pi^-$ vs. $K^0_L\pi^+\pi^-$ background yields from $K^0_S\pi^+\pi^-$ events that pass the $K^0_L\pi^+\pi^-$ selection.

i/j	0	1	2	3	4	5	6	7
0	0.20	0.06	0.20	0.09	0.17	0.28	0.21	0.23
1	0.12	0.01	0.02	0.02	0.06	0.13	0.11	0.08
2	0.29	0.05	0.04	0.03	0.12	0.19	0.28	0.24
3	0.12	0.03	0.03	0.00	0.03	0.05	0.08	0.11
4	0.21	0.09	0.13	0.01	0.01	0.03	0.10	0.19
5	0.30	0.12	0.14	0.03	0.03	0.04	0.10	0.17
6	0.20	0.10	0.16	0.04	0.08	0.07	0.06	0.13
7	0.28	0.10	0.23	0.08	0.16	0.19	0.15	0.22
i/j	0	1	2	3	4	5	6	7
0	0.38	0.19	0.35	0.13	0.27	0.38	0.42	0.46
1	0.20	0.09	0.17	0.09	0.12	0.15	0.18	0.18
2	0.50	0.20	0.33	0.10	0.15	0.20	0.26	0.34
3	0.22	0.04	0.10	0.02	0.05	0.06	0.08	0.10
4	0.34	0.14	0.12	0.02	0.07	0.12	0.17	0.34
5	0.41	0.11	0.17	0.04	0.06	0.22	0.28	0.44
6	0.48	0.18	0.18	0.08	0.15	0.23	0.33	0.39
7	0.44	0.11	0.26	0.11	0.22	0.38	0.45	0.34

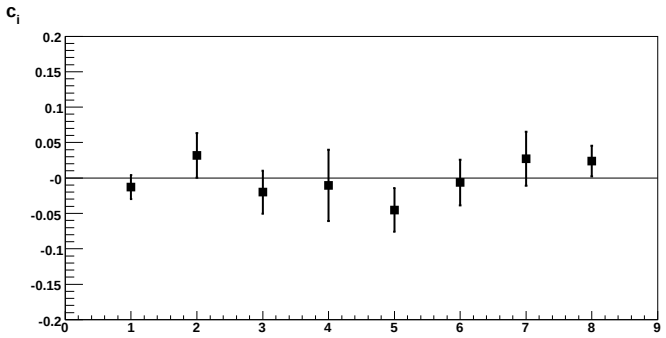

Figure 3.3: The difference between Monte Carlo output and input values for 8 $\Delta\delta_D$ bin case.

3.3 Monte Carlo Test

3.3.1 CP tagged $K^0_S\pi^+\pi^-$ Monte Carlo test

Using the generated flavor and CP tagged Monte Carlo samples, we can test our procedures for c_i calculation. We count the number of events in each bin of generated flavor tagged, CP tagged Monte Carlo samples, then plug all the efficiency corrected numbers into the following formula (Equation 1.34)

$$c_i = \frac{(M_i^+/S_+ - M_i^-/S_-)}{(M_i^+/S_+ + M_i^-/S_-)} \frac{(K_i + K_{\bar{i}})}{2\sqrt{K_i K_{\bar{i}}}}. \tag{3.2}$$

The Monte Carlo test results are shown in Table 3.15. In Fig. 3.3, we show the difference between the output values and the input values. The output values agree with input values pretty well.

Table 3.15: CP tagged $K^0_S\pi^+\pi^-$ MC test for c_i calculation.

	Input c_i	MC Output	σ off
c_1	0.769	0.756±0.017	-0.762
c_2	0.570	0.602±0.032	1.006
c_3	-0.044	-0.064±0.030	-0.656
c_4	-0.570	-0.580±0.050	-0.205
c_5	-0.842	-0.887±0.031	-1.464
c_6	-0.626	-0.632±0.032	-0.198
c_7	-0.006	0.021±0.038	0.715
c_8	0.410	0.434±0.022	1.092

3.3.2 $K^0_S\pi^+\pi^-$ vs $K^0_S\pi^+\pi^-$ Monte Carlo study

Using correlated $K^0_S\pi^+\pi^-$ vs. $K^0_S\pi^+\pi^-$ Monte Carlo samples, we extract both c_i and s_i.

Table 3.16: Fitted c_i and s_i central values for generator level Monte Carlo.

	Input	Output	Diff		Input	Output	Diff
c_1	0.769	0.767 ± 0.003	-0.002	s_1	0.032	0.043 ± 0.004	0.011
c_2	0.570	0.570 ± 0.006	-0.000	s_2	0.396	0.400 ± 0.007	0.004
c_3	-0.044	-0.049 ± 0.005	-0.005	s_3	0.765	0.753 ± 0.004	-0.012
c_4	-0.570	-0.561 ± 0.007	0.009	s_4	0.644	0.637 ± 0.007	-0.007
c_5	-0.842	-0.835 ± 0.004	0.007	s_5	-0.152	-0.162 ± 0.005	-0.010
c_6	-0.626	-0.617 ± 0.004	0.009	s_6	-0.574	-0.568 ± 0.004	0.006
c_7	-0.006	0.002 ± 0.005	0.008	s_7	-0.766	-0.754 ± 0.005	0.012
c_8	0.410	0.409 ± 0.003	-0.001	s_8	-0.386	-0.386 ± 0.004	-0.000

The most important formula is (Equation 1.46),

$$M_{i,j} = \frac{N_{D,\bar{D}}}{2S_f^2}(K_iK_{\bar{j}} + K_{\bar{i}}K_j - 2\sqrt{K_iK_{\bar{j}}K_{\bar{i}}K_j}(c_ic_j + s_is_j)), \tag{3.3}$$

where $M_{i,j}$ is the number of events with D in the i-th bin and D' in the j-th bin, K_i is the number of flavor tagged $K^0_S\pi^+\pi^-$ events in the i-th bin, S_f is the number of flavor tags.

We take the following steps to extract c_i and s_i:

1. Count K_i from flavor tagged $K^0_S\pi^+\pi^-$ samples. Count $M_{i,j}$ from correlated $K^0_S\pi^+\pi^-$ vs. $K^0_S\pi^+\pi^-$ sample.
2. Combine $M_{i,j}$, $M_{\bar{i},\bar{j}}$ together (same with $M_{\bar{i},j}$ and $M_{i,\bar{j}}$) since $M_{i,j} = M_{\bar{i},\bar{j}}$ ($M_{\bar{i},j} = M_{i,\bar{j}}$).
3. Since there is no preference which one is the first $K^0_S\pi^+\pi^-$ or the second $K^0_S\pi^+\pi^-$ in one event, $M_{i,j}$ should equal $M_{j,i}$, then we can fold the upper half of $M_{i,j}$ into the lower half.
4. Background subtraction.
5. Efficiency correction.
6. Using Minuit to extract c_i's and s_i's.

c_i, s_i are obtained by minimizing the negative logarithmic likelihood function

$$-2\log\mathcal{L} = -2\sum_{i,j}\log P(M_{i,j}, \langle M_{i,j}\rangle), \tag{3.4}$$

where $P(M, \langle M\rangle)$ is the Poisson probability to get M events with the expected number of $\langle M\rangle$ events. For 8 bin case, there are 72 equations with 16 unknowns , so each of the free parameters is constrained by many bins.

For Monte Carlo test, we generate about 100 $K^0_S\pi^+\pi^-$ vs. $K^0_S\pi^+\pi^-$ samples using the BaBar model. Firstly we checked generator level results. The generator level results are shown in Table 3.16.

The fit results after fully reconstruction are shown in Fig. 3.4. The pull distributions of c_i and s_i are shown in Fig. 3.5 and Fig. 3.6, the central values and widths are shown in Table 3.17.

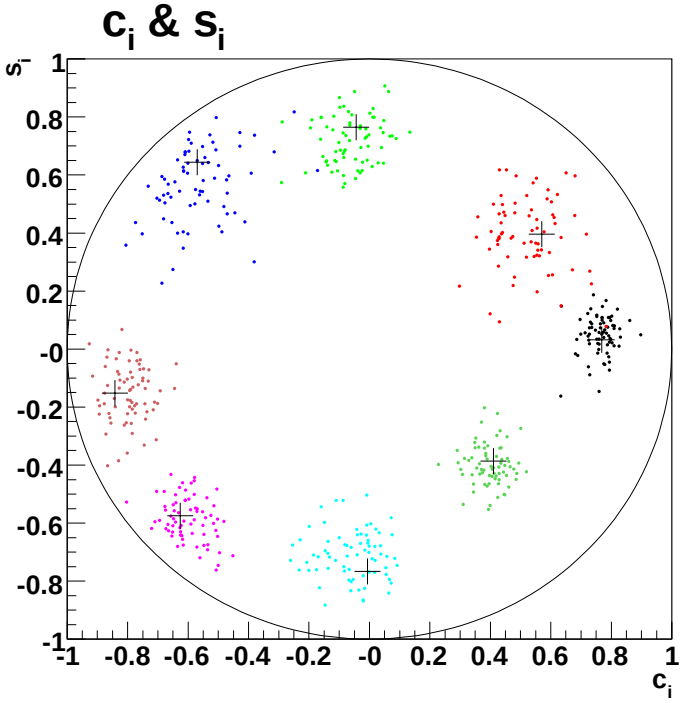

Figure 3.4: c_i and s_i extracted from 100 $K^0_S\pi^+\pi^-$ vs. $K^0_S\pi^+\pi^-$ Monte Carlo samples. Crosses are input values. Points are fitted results, different colors correspond different bins.

Table 3.17: Central value and width for c_i and s_i pull distributions.

	Mean	Width		Mean	Width
c_1	0.031 ± 0.127	1.077 ± 0.090	s_1	0.217 ± 0.114	0.967 ± 0.081
c_2	0.067 ± 0.131	1.110 ± 0.093	s_2	0.078 ± 0.123	1.046 ± 0.087
c_3	-0.139 ± 0.133	1.131 ± 0.094	s_3	-0.056 ± 0.145	1.231 ± 0.103
c_4	0.270 ± 0.117	0.991 ± 0.083	s_4	-0.259 ± 0.117	0.995 ± 0.083
c_5	0.092 ± 0.101	0.856 ± 0.071	s_5	-0.025 ± 0.117	0.991 ± 0.083
c_6	0.025 ± 0.120	1.018 ± 0.085	s_6	-0.019 ± 0.117	0.993 ± 0.083
c_7	0.067 ± 0.127	1.075 ± 0.090	s_7	0.069 ± 0.120	1.019 ± 0.085
c_8	-0.056 ± 0.123	1.044 ± 0.087	s_8	-0.175 ± 0.122	1.031 ± 0.086

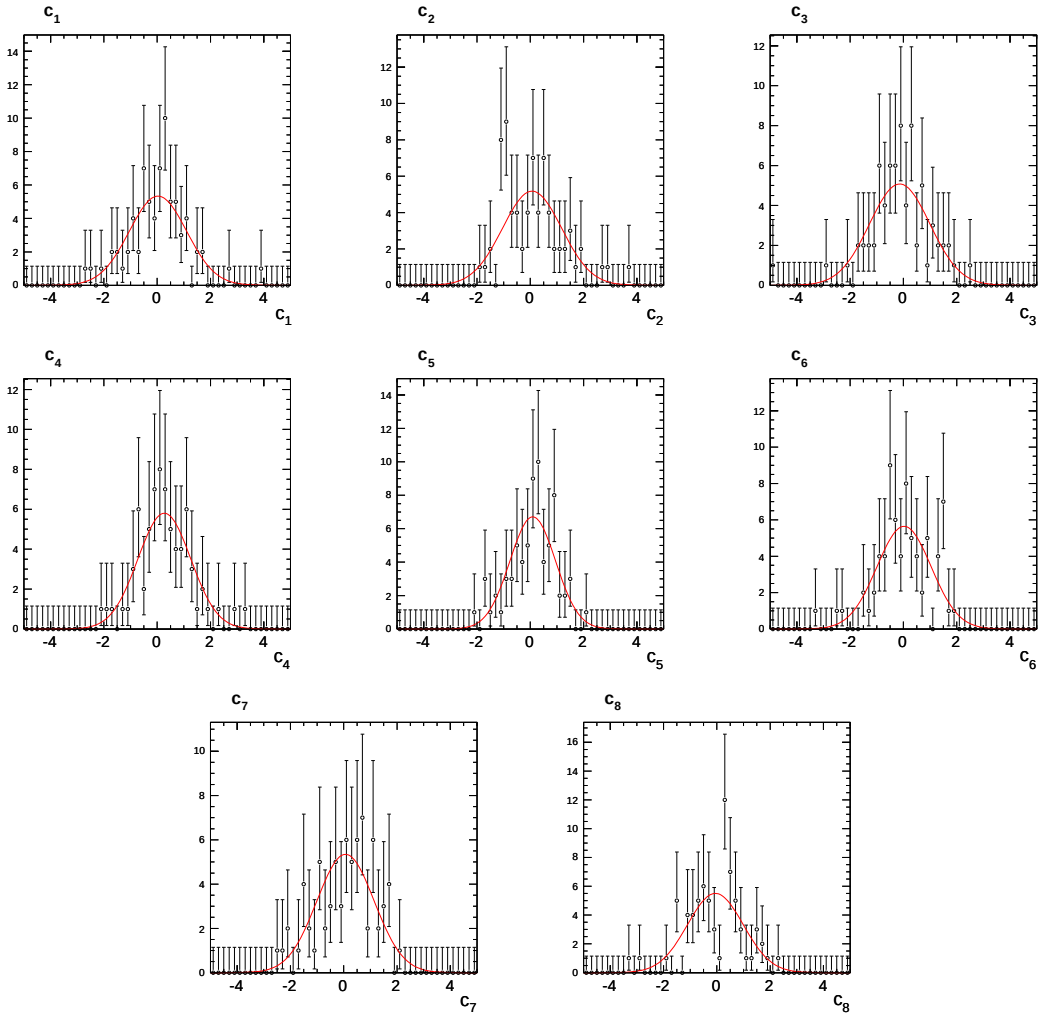

Figure 3.5: c_i pull distributions fitted with a Gaussian function for 100 $K^0_S\pi^+\pi^-$ vs. $K^0_S\pi^+\pi^-$ Monte Carlo samples.

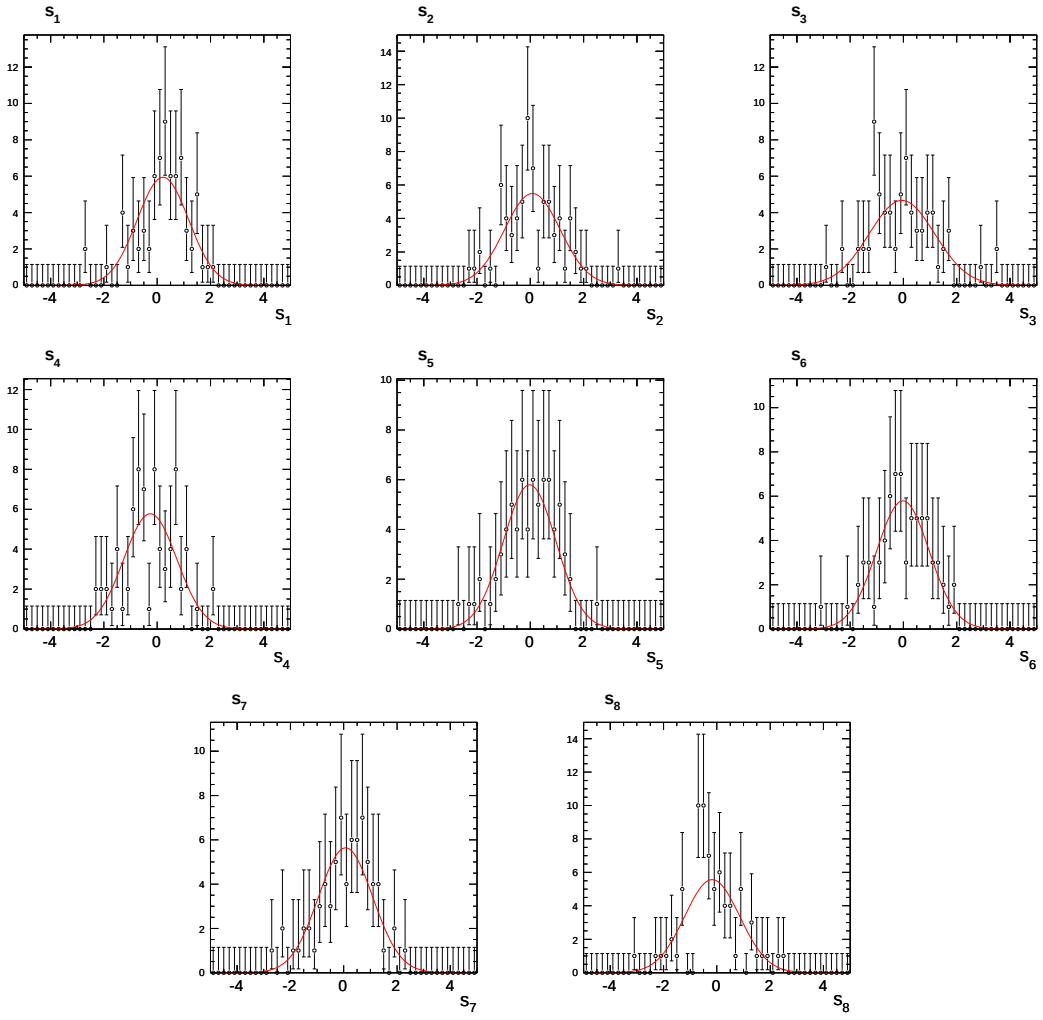

Figure 3.6: s_i pull distributions fitted with a Gaussian function for 100 $K^0_S\pi^+\pi^-$ vs. $K^0_S\pi^+\pi^-$ Monte Carlo samples.

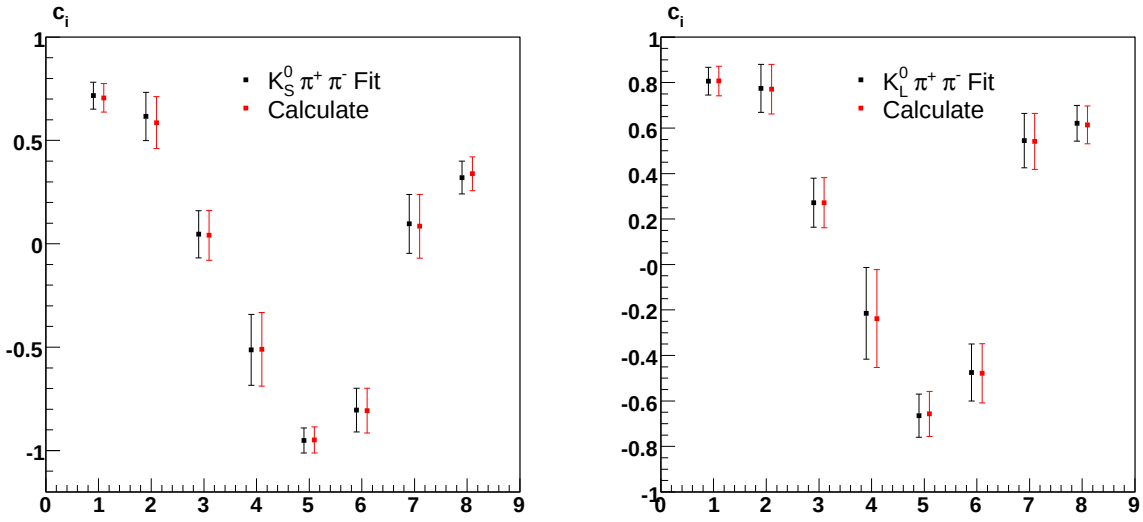

Figure 3.7: Results from fitting and calculations comparison. CP tagged $K^0_S\pi^+\pi^-$ results are shown in the upper plot. CP tagged $K^0_L\pi^+\pi^-$ results are shown in the lower plot.

3.4 Fit

3.4.1 Fitter test for CP tagged $K^0_{S,L}\pi^+\pi^-$

In order to do a global fit, we switched from calculation using formula 1.34 to fit for CP tagged $K^0_{S,L}\pi^+\pi^-$ data samples. This provides us a good test for our fitter. The comparison between calculation and fitting is shown in Fig. 3.7, for both CP tagged $K^0_S\pi^+\pi^-$ data and CP tagged $K^0_L\pi^+\pi^-$ data.

The tiny difference between calculation and fitting is caused by the procedure difference (e.g. in calculation, separate efficiencies are used in upper and lower half of the Dalitz plot, while in fitting, the averaged efficiencies are used.). The fit results also show slight smaller statistical errors, this is because the fitter only considered the statistical error of CP tagged $K^0_{S,L}\pi^+\pi^-$ samples, it ignored the statistical error associated with flavor tagged $K^0_{S,L}\pi^+\pi^-$ samples. This part of statistical error will be considered separately later.

Using CP tagged $K^0_{S,L}\pi^+\pi^-$ samples, we can get c_i and c'_i without any correlations, so the differences between c_i and c'_i can give us a good test for our predictions on the differences discussed in Section 1.5. The comparison between measured $\Delta c_i = c'_i - c_i$ and predictions is shown in Fig. 3.8. The data agrees with predictions well.

3.4.2 Global Fit

Following the mechanism presented in Section 1.6, using all the available data, a global fit is performed to extract the parameters (c_i, s_i), (c'_i, s'_i). From Monte Carlo studies, we found Doubly Cabibbo Suppressed Decay in $K^-\pi^+$, $K^-\pi^+\pi^0$, $K^-\pi^+\pi^+\pi^-$ modes has significant effect when used in $K^0_S\pi^+\pi^-$ vs. $K^0_{S,L}\pi^+\pi^-$ fit, but has relatively small effect when used in CP tagged

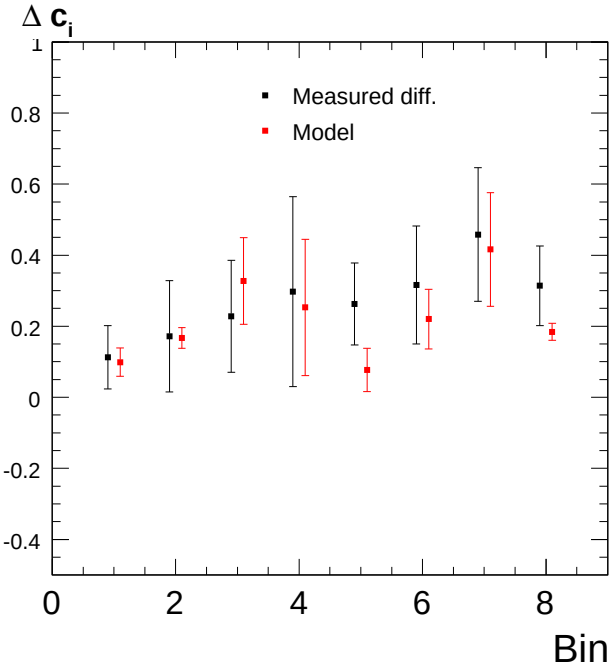

Figure 3.8: $\Delta c_i = c_i' - c_i$ for the eight bins. Black points are CP tagged $K^0_{S,L}\pi^+\pi^-$ data results. Red points are model predictions.

$K^0_{S,L}\pi^+\pi^-$ fit. So in the global fit, semileptonic $K^-e^+\nu$ tagged $K^0_S\pi^+\pi^-$, and $K^-\pi^+$ tagged $K^0_L\pi^+\pi^-$ samples are used in $K^0_S\pi^+\pi^-$ vs. $K^0_{S,L}\pi^+\pi^-$ fitting. We made corrections to the DCSD decay in $K^-\pi^+$ tagged $K^0_L\pi^+\pi^-$ sample using recent TQCA result on the relative strong phase, $\delta = (22 \pm 16.3)^\circ$. The magnitude of Doubly Cabibbo Suppressed decay, $R_{WS}(K\pi) = (0.377 \pm 0.008 \pm 0.005)\%$, comes from Belle measurement [17]. Using BaBar $D^0 \to K^0_S\pi^+\pi^-$ Dalitz fit amplitude, we can calculate the ratio,

$$|A_{D^0\to K^0_S\pi^+\pi^-}|^2/|A_{D^0\to K^0_S\pi^+\pi^-} + re^{-i\delta}A_{\bar{D}^0\to K^0_S\pi^+\pi^-}|^2,$$

for each bin. Using these ratios, we then made corrections to $K^-\pi^+$ vs. $K^0_{S,L}\pi^+\pi^-$ yields. $K^-\pi^+$, $K^-\pi^+\pi^0$, and $K^-\pi^+\pi^+\pi^-$ tagged $K^0_{S,L}\pi^+\pi^-$ samples are used in CP tagged $K^0_{S,L}\pi^+\pi^-$ fit, the effect of Doubly Cabibbo Suppressed Decay is studied as systematic error.

The results of (c_i, s_i), (c_i', s_i') from the global fit are shown in Fig. 3.9, and Table 3.18.

The correlation matrix for (c_i, s_i) is shown in Table 3.19.

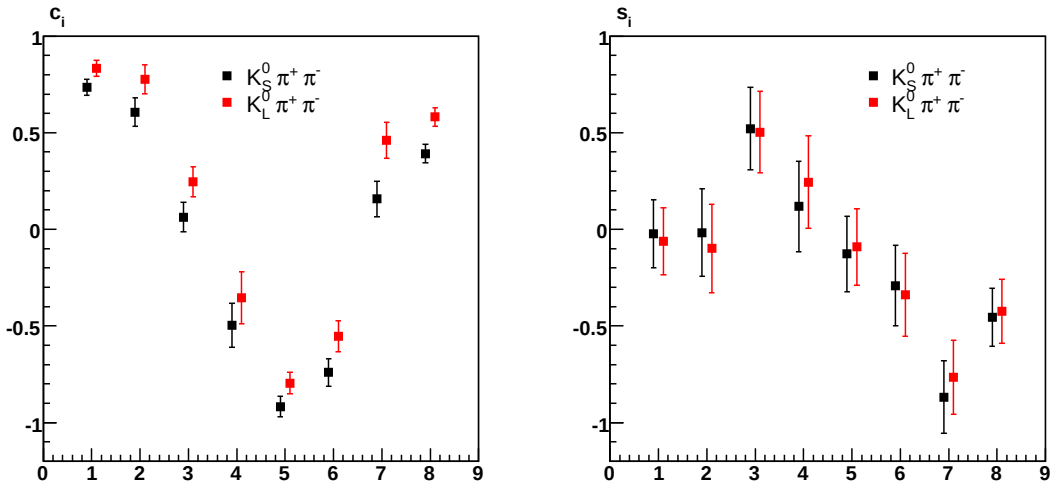

Figure 3.9: Fit results for the global fit. (c_i, c_i') are shown in the left plot, (s_i, s_i') are shown in the right plot. Black points are (c_i, s_i), red points are (c_i', s_i')

Table 3.18: Fit results for the global fit

	c_i	c_i'	s_i	s_i'
1	0.742±0.041	0.839±0.041	-0.022±0.168	-0.059±0.165
2	0.607±0.073	0.776±0.073	0.009±0.220	-0.071±0.223
3	0.064±0.077	0.251±0.078	0.548±0.198	0.529±0.200
4	-0.492±0.113	-0.347±0.135	0.124±0.227	0.252±0.233
5	-0.918±0.053	-0.796±0.056	-0.118±0.194	-0.082±0.197
6	-0.743±0.071	-0.548±0.080	-0.296±0.203	-0.344±0.208
7	0.156±0.092	0.481±0.094	-0.870±0.183	-0.768±0.189
8	0.398±0.047	0.586±0.048	-0.438±0.146	-0.405±0.158

Table 3.19: Correlation Matrix for c_i and s_i. Parameter 1 represents c_1, parameter 2 represents c_2, $\cdots$, parameter 9 represents s_1, $\cdots$, etc..

	1	2	3	4	5	6	7	8	9	10	11	12	13	14	15	16
1	1.000	-0.028	-0.006	0.035	0.078	0.019	0.016	-0.023	0.018	-0.000	0.005	0.004	-0.002	-0.008	0.006	0.002
2	-0.028	1.000	-0.013	0.009	-0.019	0.072	0.014	-0.024	0.007	-0.031	0.008	0.005	0.001	-0.015	0.009	0.003
3	-0.006	-0.013	1.000	0.002	0.005	-0.006	-0.019	0.008	-0.060	0.011	-0.014	-0.014	0.003	0.067	-0.041	-0.038
4	0.035	0.009	0.002	1.000	0.004	-0.001	0.006	0.004	-0.004	-0.007	0.001	0.036	-0.010	0.004	0.000	-0.001
5	0.078	-0.019	0.005	0.004	1.000	-0.082	0.036	0.051	0.037	-0.010	0.023	0.010	0.023	-0.029	0.020	0.013
6	0.019	0.072	-0.006	-0.001	-0.082	1.000	0.016	0.015	0.007	0.032	-0.003	-0.001	-0.045	-0.034	0.004	-0.000
7	0.016	0.014	-0.019	0.006	0.036	0.016	1.000	0.019	0.118	-0.008	0.049	0.022	0.007	-0.098	0.065	0.016
8	-0.023	-0.024	0.008	0.004	0.051	0.015	0.019	1.000	0.052	-0.007	0.041	0.009	0.013	-0.032	0.017	0.054
9	0.018	0.007	-0.060	-0.004	0.037	0.007	0.118	0.052	1.000	-0.091	0.355	0.167	0.226	-0.479	0.354	0.166
10	-0.000	-0.031	0.011	-0.007	-0.010	0.032	-0.008	-0.007	-0.091	1.000	-0.188	-0.146	-0.136	0.119	-0.155	-0.087
11	0.005	0.008	-0.014	0.001	0.023	-0.003	0.049	0.041	0.355	-0.188	1.000	0.263	0.366	-0.264	0.294	0.463
12	0.004	0.005	-0.014	0.036	0.010	-0.001	0.022	0.009	0.167	-0.146	0.263	1.000	0.078	-0.157	0.231	0.155
13	-0.002	0.001	0.003	-0.010	0.023	-0.045	0.007	0.013	0.226	-0.136	0.366	0.078	1.000	-0.285	0.228	0.177
14	-0.008	-0.015	0.067	0.004	-0.029	-0.034	-0.098	-0.032	-0.479	0.119	-0.264	-0.157	-0.285	1.000	-0.393	-0.091
15	0.006	0.009	-0.041	0.000	0.020	0.004	0.065	0.017	0.354	-0.155	0.294	0.231	0.228	-0.393	1.000	0.018
16	0.002	0.003	-0.038	-0.001	0.013	-0.000	0.016	0.054	0.166	-0.087	0.463	0.155	0.177	-0.091	0.018	1.000

Chapter 4

Systematics

4.1 CP violation and D^0, $\bar{D}^0$ mixing

The effect of CP violation and $D^0 \leftrightarrow \bar{D}^0$ mixing is negligible for this analysis [10].

4.2 Statistics of flavor tagged $K^0_{S,L}\pi^+\pi^-$

In the maximum log likelihood fit, the fitter only takes the statistical error of $M_{i,j}$ into account. The statistical error from $K_i, K_{\bar{i}}$ need to be studied separately. We vary each $K_i, K_{\bar{i}}, K'_i, K'_{\bar{i}}$ one at a time by its statistical error, then make a new fit. The quadrature sum of all the variations is shown in Table 4.1.

Table 4.1: Errors on $(c_i, s_i), (c'_i, s'_i)$ due to flavor tagged $K^0_{S,L}\pi^+\pi^-$ statistics.

	1	2	3	4	5	6	7	8
c_i	0.010	0.015	0.015	0.019	0.010	0.015	0.019	0.009
s_i	0.034	0.032	0.045	0.033	0.034	0.029	0.036	0.024
c'_i	0.010	0.015	0.011	0.013	0.009	0.012	0.017	0.009
s'_i	0.034	0.033	0.042	0.029	0.033	0.031	0.037	0.028

4.3 Momentum resolution

We use the relative strong phase difference to define the bins, this gives both narrow and unusual bins in Dalitz phase space. Asymmetric events migration among bins might give us systematic shift, so the results of this analysis are very sensitive to the momentum resolution. The systematic error is studied by smearing the momentum of Monte Carlo samples according CLEO detector momentum resolution many times, the width of the variation is taken as the systematic error. CLEO detector has 0.6% resolution at 1 GeV, better resolution at lower energy. We use 0.6% as the resolution for all the momentum range. We repeat the fit 200 times

Table 4.2: Systematic study for momentum resolution

	Mean	Width		Mean	Width
c_1	0.727 ± 0.001	0.008 ± 0.000	s_1	0.059 ± 0.001	0.017 ± 0.001
c_2	0.581 ± 0.001	0.014 ± 0.001	s_2	0.423 ± 0.002	0.031 ± 0.002
c_3	-0.078 ± 0.001	0.010 ± 0.001	s_3	0.713 ± 0.001	0.018 ± 0.001
c_4	-0.541 ± 0.001	0.017 ± 0.001	s_4	0.631 ± 0.002	0.027 ± 0.001
c_5	-0.898 ± 0.001	0.010 ± 0.001	s_5	-0.182 ± 0.000	0.028 ± 0.000
c_6	-0.623 ± 0.001	0.011 ± 0.001	s_6	-0.569 ± 0.001	0.016 ± 0.001
c_7	0.046 ± 0.001	0.015 ± 0.001	s_7	-0.752 ± 0.002	0.021 ± 0.001
c_8	0.413 ± 0.001	0.008 ± 0.000	s_8	-0.379 ± 0.001	0.017 ± 0.001
c'_1	0.840 ± 0.000	0.007 ± 0.000	s'_1	-0.047 ± 0.002	0.023 ± 0.001
c'_2	0.737 ± 0.001	0.015 ± 0.001	s'_2	0.284 ± 0.003	0.036 ± 0.002
c'_3	0.291 ± 0.001	0.010 ± 0.001	s'_3	0.661 ± 0.002	0.025 ± 0.001
c'_4	-0.338 ± 0.001	0.018 ± 0.001	s'_4	0.730 ± 0.003	0.040 ± 0.002
c'_5	-0.743 ± 0.001	0.009 ± 0.000	s'_5	-0.137 ± 0.002	0.028 ± 0.001
c'_6	-0.344 ± 0.001	0.012 ± 0.001	s'_6	-0.626 ± 0.002	0.022 ± 0.001
c'_7	0.416 ± 0.001	0.017 ± 0.001	s'_7	-0.718 ± 0.002	0.028 ± 0.001
c'_8	0.589 ± 0.001	0.007 ± 0.000	s'_8	-0.434 ± 0.002	0.024 ± 0.001

for the fully simulated Monte Carlo sample, then fit the distributions with a Gaussian function, the central values and widths are shown in Table 4.2.

4.4 $K^0_{S,L}\pi^+\pi^-$ finding efficiencies

From Equation 1.34 and Equation 1.46, we can see that the systematics associated with $K^0_{S,L}\pi^+\pi^-$ finding will cancel since they appear on both left hand side and right hand side. In claiming the systematic error cancel, we made the assumption that the systematics are uniform in the Dalitz space. If the systematics are not uniform, they won't cancel since the events population densities for flavor tagged and CP tagged $K^0_{S,L}\pi^+\pi^-$ are not the same. A systematic study as a function of Dalitz phase space seems not feasible, in stead, we randomly vary the efficiency of each bin according a Gaussian distribution (width is taken as 0.02) and repeat this process for many times to see the changes. The widths of the results are taken as systematic errors. The central values and widths of 200 tests to real data are shown in Table 4.3.

4.5 Tag side yields

The systematics study for single tag fitting is done by releasing the fixed parameters. The difference between the new results and the old results, which are shown in Table 4.4, is taken as systematic error for the yields fit.

For tags with peaking background, we take 20% of Table 2.5 as the estimation of the systematics for the peaking background subtraction.

Table 4.3: Systematics due to $K^0_{S,L}\pi^+\pi^-$ finding efficiencies.

	Mean	Width		Mean	Width
c_1	0.744 ± 0.000	0.004 ± 0.000	s_1	-0.024 ± 0.001	0.018 ± 0.001
c_2	0.607 ± 0.001	0.007 ± 0.000	s_2	0.011 ± 0.001	0.012 ± 0.001
c_3	0.065 ± 0.000	0.011 ± 0.000	s_3	0.546 ± 0.001	0.019 ± 0.001
c_4	-0.493 ± 0.001	0.008 ± 0.000	s_4	0.124 ± 0.000	0.010 ± 0.000
c_5	-0.918 ± 0.000	0.005 ± 0.000	s_5	-0.119 ± 0.001	0.013 ± 0.001
c_6	-0.744 ± 0.001	0.008 ± 0.000	s_6	-0.294 ± 0.001	0.018 ± 0.001
c_7	0.157 ± 0.001	0.010 ± 0.001	s_7	-0.871 ± 0.001	0.013 ± 0.001
c_8	0.398 ± 0.000	0.006 ± 0.000	s_8	-0.438 ± 0.001	0.012 ± 0.001
c'_1	0.839 ± 0.000	0.006 ± 0.000	s'_1	-0.061 ± 0.001	0.018 ± 0.001
c'_2	0.777 ± 0.000	0.006 ± 0.000	s'_2	-0.069 ± 0.001	0.012 ± 0.001
c'_3	0.251 ± 0.001	0.009 ± 0.000	s'_3	0.530 ± 0.001	0.015 ± 0.001
c'_4	-0.348 ± 0.001	0.009 ± 0.000	s'_4	0.252 ± 0.001	0.009 ± 0.000
c'_5	-0.796 ± 0.000	0.004 ± 0.000	s'_5	-0.082 ± 0.001	0.012 ± 0.001
c'_6	-0.549 ± 0.000	0.007 ± 0.000	s'_6	-0.342 ± 0.001	0.018 ± 0.001
c'_7	0.481 ± 0.001	0.011 ± 0.001	s'_7	-0.769 ± 0.001	0.013 ± 0.001
c'_8	0.585 ± 0.000	0.006 ± 0.000	s'_8	-0.405 ± 0.001	0.013 ± 0.001

Table 4.4: Systematics study for Tag yields. M_{bc} is required within 1.860 GeV/c^2 and 1.870 GeV/c^2.

Modes	Nominal	Release Fixed Parameters
$K^-\pi^+$	144563.4±403.1	144094.4±401.0
$K^-\pi^+\pi^0$	258938.0±580.6	259933.5±758.1
$K^-\pi^+\pi^+\pi^-$	220831.3±540.6	221171.4±672.1
$\pi^+\pi^-$	5950.4 ± 111.6	6004.3 ± 148.8
K^+K^-	12867.4 ± 125.8	12920.9 ± 138.0
$K^0_S\pi^0\pi^0$	6562.3 ± 130.9	6684.7 ± 190.0
$K^0_S\pi^0$	19058.7 ± 150.1	19004.0 ± 153.8
$K^0_S\eta$	2792.9 ± 69.4	2788.7 ± 75.7
$K^0_S\omega$	8512.4 ± 107.1	8584.3 ± 145.5

Table 4.5: $K^0_S\pi^+\pi^-$ background estimation using $M_{K^0_S}$ sidebands.

Mode	Signal Region	Sideband	Fraction
$K^-\pi^+$	1447	38	0.026
$K^-\pi^+\pi^0$	2776	54	0.019
$K^-\pi^+\pi^+\pi^-$	2250	34	0.015
K^+K^-	124	0	0.000
$\pi^+\pi^-$	62	1	0.016
$K^0_S\pi^0\pi^0$	56	0	0.000
$K^0_S\pi^0$	189	3	0.016
$K^0_S\eta$	39	2	0.051
$K^0_S\omega$	83	1	0.012
$K^-e^+\nu$	1195	22	0.018
All	8221	155	0.019

4.6 $K^0_S\pi^+\pi^-$ background

Though we used ΔE and K^0_S mass sidebands for the tag side backgrounds subtraction, we didn't apply any background subtraction for $K^0_S\pi^+\pi^-$ signal side, which is believed to be small since we made K^0_S flight significance requirement. The background level in signal side is estimated from K^0_S mass sideband. The K^0_S mass distributions for different tag modes after tag side ΔE sideband subtraction are shown in Fig. 4.1, which show very clean signal. The signal region and sideband yields are shown in Table 4.5. On average, there is 1.9% background in the signal side.

The systematics due to this part of background are estimated using Quantum Correlated Monte Carlo results. Signal side background events are read out from Quantum Correlated Monte Carlo samples. We calculate the fractions of backgrounds in each bin. The backgrounds in data are calculated according these fractions. A new fit is made with these background events subtracted, and the differences in results are taken as systematic errors.

4.7 $K^0_L\pi^0$ yield

For $K^0_L\pi^0$ vs. $K^0_S\pi^+\pi^-$ mode, we need to use $N_{D^0,\bar{D}^0} \times \mathcal{B}_{K^0_L\pi^0}$ to get the number of $K^0_L\pi^0$ single tags. $N_{D^0,\bar{D}^0}$ is calculated from cross section, which is taken from published 281 pb^{-1} D hadronic paper [14], and luminosity. The official total luminosity is 818 ± 8 pb^{-1}. The branching fraction of $K^0_L\pi^0$ is taken from [15].

The background has not been subtracted for $K^0_L\pi^0$ vs. $K^0_S\pi^+\pi^-$ when we do the global fit. The background level for $K^0_L\pi^0$ is estimated from Quantum Correlated Monte Carlo, which is $4.1 \pm 0.5\%$ (excluding the signal side background, which is studied separately). There is $K^0_S\pi^0$ background, which has the opposite CP. We double the effect of this part of background. The resulted background level is 5.76%. We vary the yields of $K^0_L\pi^0$ vs. $K^0_S\pi^+\pi^-$ by 5.76% and take the difference as the systematic error.

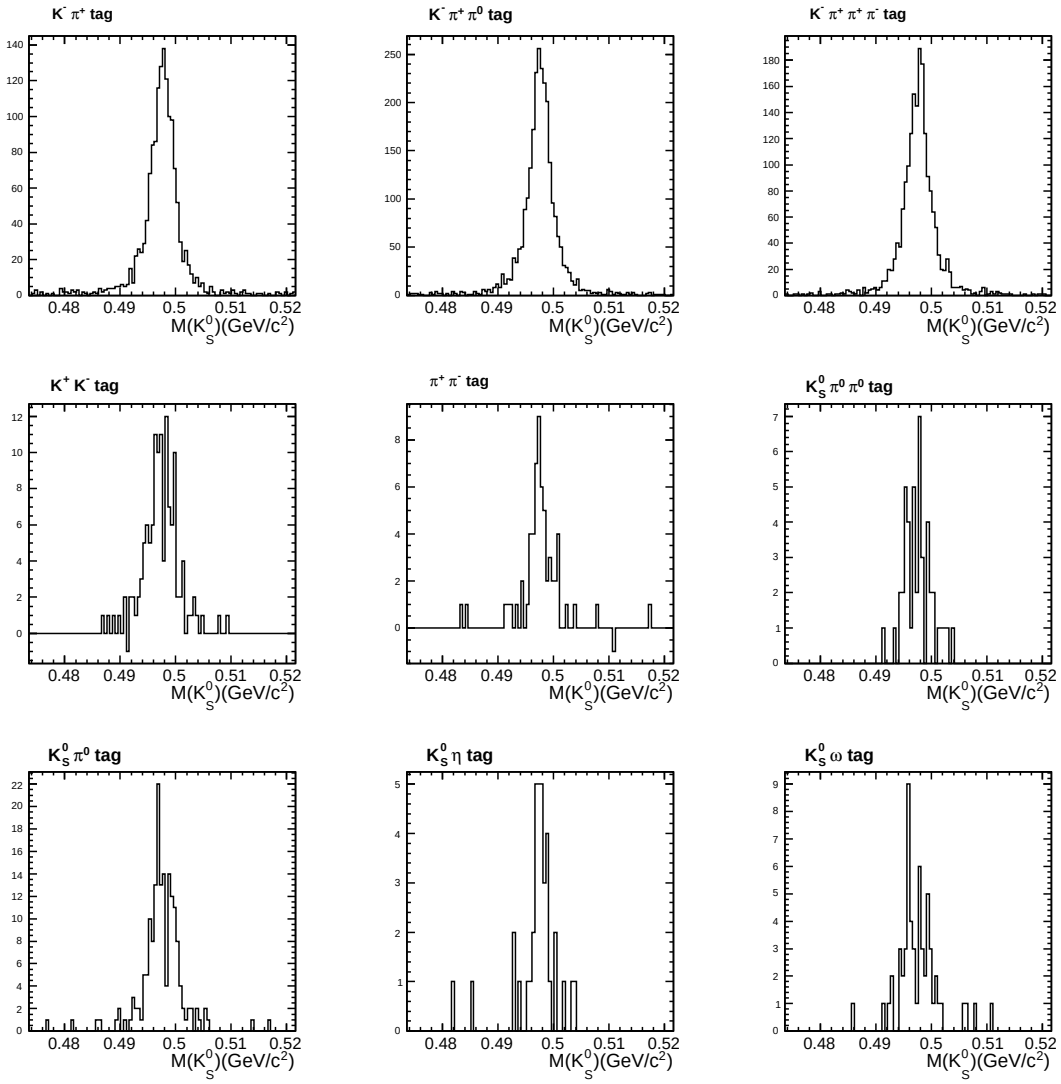

Figure 4.1: K^0_S mass distributions for $K^0_S\pi^+\pi^-$ vs. tag modes. Tag mode ΔE sideband subtraction applied.

Table 4.6: Ratio of $|A_{D^0}|^2/|A_{D^0}+re^{-i\delta}A_{\bar{D}^0}|^2$ for each bin of $K^-\pi^+$ vs. $K^0_{S,L}\pi^+\pi^-$ sample.

	1	2	3	4	5	6	7	8
$R_i(K^0_S\pi\pi)$	1.033	1.002	0.971	0.938	0.933	0.960	1.009	1.030
$R_{\bar{i}}(K^0_S\pi\pi)$	1.132	1.169	1.039	0.921	0.848	0.850	0.933	1.027
$R_i(K^0_L\pi\pi)$	1.030	1.000	0.974	0.941	0.926	0.965	1.005	1.024
$R_{\bar{i}}(K^0_L\pi\pi)$	1.115	1.162	1.113	0.960	0.846	0.862	0.939	1.013

4.8 $K^0_L\pi^0$ systematics

We made 5±3.8% π^0 efficiency correction to $K^0_L\pi^0$ vs. $K^0_S\pi^+\pi^-$ double tag efficiencies. From our previous study in [16], the systematics associated with $K^0_L\pi^0$ selection is about 2.5%, combine with the 3.8% π^0 correction systematics, the total systematics for $K^0_L\pi^0$ selection is less than 5%. We conservely take 5% as the uncertainties for the $K^0_L\pi^0$ vs. $K^0_S\pi^+\pi^-$ yields.

4.9 Doubly Cabibbo suppressed decay for flavor modes

We identify the flavor of $D^0/\bar{D}^0 \to K^0_{S,L}\pi^+\pi^-$ from the tag side using $K^-\pi^+$, $K^-\pi^+\pi^0$, $K^-\pi^+\pi^+\pi^-$, and $K^-e^+\nu$ tags. For $K^-\pi^+$, $K^-\pi^+\pi^0$, and $K^-\pi^+\pi^+\pi^-$ tags, there are Doubly Cabibbo suppressed decays which have opposite flavor. We made corrections to $K^-\pi^+$ vs. $K^0_{S,L}\pi^+\pi^-$ yields using recent TQCA results on the relative strong phase, $\delta = (22 \pm 16.3)^\circ$, where δ is defined as,

$$\frac{< K^+\pi^-|D^0 >}{< K^+\pi^-|\bar{D}^0 >} \equiv re^{-i\delta}.$$

The magnitude of Doubly Cabibbo Suppressed decay, $R_{WS}(K\pi) = (0.377 \pm 0.008 \pm 0.005)\%$, comes from Belle measurement [17], [18]. Using BaBar $D^0 \to K^0_S\pi^+\pi^-$ Dalitz fit amplitude, we can calculate the ratio, $|A_{D^0\to K^0_S\pi^+\pi^-}|^2/|A_{D^0\to K^0_S\pi^+\pi^-} + re^{-i\delta}A_{\bar{D}^0\to K^0_S\pi^+\pi^-}|^2$ for each bin, which is shown in Table 4.6. Using these ratios, we made corrections to $K^-\pi^+$ vs. $K^0_{S,L}\pi^+\pi^-$ yields. The systematics from the strong phase δ are shown in Table 4.7. Systematics from r is negligible since it is precisely measured.

For $K^-\pi^+\pi^0$, and $K^-\pi^+\pi^+\pi^-$ tag modes, there are no relative strong phase measurements, so we consider four cases, $\delta = (0^\circ, 90^\circ, 180^\circ, 270^\circ)$, and take maximum variations among the four cases as the systematic errors. The results are shown in Table 4.8.

4.10 Multi-candidate selection

For $K^0_S\pi^+\pi^-$ vs. $K^0_{S,L}\pi^+\pi^-$ samples, one need to worry about the wrong combinations of the pions since all the pions have similar momentum spectrum. This issue usually give multiple candidates in a single event. For $K^0_S\pi^+\pi^-$ vs. $K^0_S\pi^+\pi^-$, our best candidate is selected with the largest K^0_S flight significance (sum of the first K^0_S flight significance and the second K^0_S flight significance), which is proved to be better than selections based on other variables, such as

Table 4.7: Systematics on corrections to $K^-\pi^+$ vs. $K^0_{S,L}\pi^+\pi^-$ samples. The strong phase is increased and decreased by a standard deviation. The maximum of the two cases is taken as systematic error

	1	2	3	4	5	6	7	8
$\delta + \Delta\delta$	-0.001	0.001	-0.001	-0.001	-0.000	0.001	-0.001	-0.001
$\delta - \Delta\delta$	0.002	0.001	0.004	0.001	-0.000	0.001	0.003	0.001
Δc_i Max.	0.002	0.001	0.004	0.001	-0.000	0.001	0.003	-0.001
$\delta + \Delta\delta$	0.021	-0.004	0.031	0.017	0.015	-0.005	0.024	0.016
$\delta - \Delta\delta$	-0.018	0.003	-0.027	-0.012	-0.012	0.003	-0.017	-0.014
Δs_i Max.	0.021	-0.004	0.031	0.017	0.015	-0.005	0.024	0.016
$\delta + \Delta\delta$	-0.002	0.000	0.001	0.000	0.000	0.001	-0.004	-0.001
$\delta - \Delta\delta$	0.002	0.001	-0.000	-0.000	0.001	-0.001	0.004	0.001
$\Delta c'_i$ Max.	0.002	0.001	0.001	0.000	0.001	0.001	0.004	0.001
$\delta + \Delta\delta$	0.020	-0.005	0.028	0.014	0.013	-0.005	0.024	0.018
$\delta - \Delta\delta$	-0.017	0.004	-0.025	-0.010	-0.011	0.003	-0.017	-0.015
$\Delta s'_i$ Max.	0.020	-0.005	0.028	0.014	0.013	-0.005	0.024	0.018

Table 4.8: Systematics due to Doubly Cabibbo Suppressed Decay in $K^-\pi^+\pi^0$, $K^-\pi^+\pi^+\pi^-$ tag modes. We select $r = 0.06$, $\delta = 0°, 90°, 180°, 270°$, the maximum among the four cases is selected as the systematic error.

	1	2	3	4	5	6	7	8
$\delta = 0°$	-0.008	-0.009	-0.002	-0.013	-0.014	-0.010	-0.003	-0.000
$\delta = 90°$	-0.001	0.012	0.005	-0.011	0.001	0.012	-0.010	-0.005
$\delta = 180°$	0.009	0.012	0.003	0.013	0.014	0.012	0.005	0.000
$\delta = 270°$	0.002	-0.008	-0.001	0.011	-0.002	-0.010	0.013	0.005
Δc_i Max.	0.009	0.012	0.005	-0.013	0.014	0.012	0.013	0.005
$\delta = 0°$	-0.002	0.001	-0.001	-0.001	0.000	0.003	-0.001	0.000
$\delta = 90°$	-0.003	0.001	-0.003	0.000	0.001	0.002	-0.001	-0.001
$\delta = 180°$	0.003	-0.001	0.001	0.002	-0.001	-0.003	0.002	0.000
$\delta = 270°$	0.004	0.000	0.001	0.002	-0.001	-0.002	0.002	0.001
Δs_i Max.	0.004	0.001	-0.003	0.002	-0.001	-0.003	0.002	0.001
$\delta = 0°$	-0.011	-0.010	-0.004	-0.009	-0.013	-0.008	-0.003	-0.000
$\delta = 90°$	-0.001	0.012	0.007	-0.014	0.002	0.013	-0.013	-0.005
$\delta = 180°$	0.010	0.012	0.004	0.009	0.014	0.009	0.004	0.001
$\delta = 270°$	0.002	-0.008	-0.006	0.013	-0.002	-0.013	0.014	0.005
$\Delta c'_i$ Max.	-0.011	0.012	0.007	-0.014	0.014	-0.013	0.014	0.005
$\delta = 0°$	-0.002	0.001	-0.001	-0.001	0.001	0.003	-0.001	0.000
$\delta = 90°$	-0.003	0.001	-0.002	0.000	0.001	0.002	-0.001	-0.001
$\delta = 180°$	0.003	-0.000	0.001	0.002	-0.001	-0.003	0.002	-0.000
$\delta = 270°$	0.004	0.001	0.001	0.002	-0.001	-0.002	0.002	0.001
$\Delta s'_i$ Max.	0.004	0.001	-0.002	0.002	-0.001	-0.003	0.002	-0.001

average ΔE or M_{bc}. Though better than others, this selection criteria can't guarantee always picking the right one from the multiple candidates. A systematic study is needed.

In $K^0_S\pi^+\pi^-$ vs. $K^0_S\pi^+\pi^-$ Monte Carlo, there are 9290 entries for 8677 events. Assume at most 2 entries for a single event, which is mostly true, about 7.2% events have 2 candidates.

The systematic study is done using signal Monte Carlo. In Table 4.9 and Table 4.10, we show the ratio of true events, which is identified using Monte Carlo truth table, to the number of reconstructed events in each bin for $K^0_S\pi^+\pi^-$ vs. $K^0_S\pi^+\pi^-$ and $K^0_S\pi^+\pi^-$ vs. $K^0_L\pi^+\pi^-$, respectively. A new fit is made with each $M_{i,j}$ ($M_{i,\bar{j}}$) times the ratio shown in Table 4.9 and Table 4.10. The difference between this fit and the nominal fit is taken as systematic error.

Table 4.9: The ratio of true events to reconstructed events for $K^0_S\pi^+\pi^-$ vs. $K^0_S\pi^+\pi^-$ Monte Carlo. All numbers are in percentage.

$M_{i,j}$	0	1	2	3	4	5	6	7
0	95.44							
1	102.26	114.29						
2	100.13	97.28	90.62					
3	101.94	100.00	88.89	62.50				
4	101.69	99.67	100.32	96.67	83.87			
5	97.49	100.26	100.19	100.00	102.06	92.45		
6	103.91	109.30	100.00	105.15	95.12	99.14	95.29	
7	98.33	97.69	101.23	94.79	98.09	103.96	99.77	100.70
$M_{i,\bar{j}}$	0	1	2	3	4	5	6	7
0	100.85							
1	98.20	106.79						
2	101.06	95.39	101.02					
3	97.33	101.33	101.63	97.14				
4	102.58	103.91	101.47	96.63	92.86			
5	101.72	101.92	98.90	91.35	104.80	98.49		
6	101.98	102.17	102.16	107.50	99.32	99.67	104.87	
7	101.28	102.24	94.98	95.21	100.12	100.28	101.76	97.39

4.11 K^0_S flight significance cut

We applied K^0_S flight significance requirement to all $K^0_S\pi^+\pi^-$ candidates, except for $K^0_S\pi^+\pi^-$ vs. $K^0_S\pi^+\pi^-$ events.

First, we studied the systematics for the K^0_S flight significance requirement. $K^-\pi^+$, $K^-\pi^+\pi^0$ and $K^-\pi^+\pi^+\pi^-$ tag modes vs. $K^0_S\pi^+\pi^-$ samples are used. Tag side ΔE sideband and signal side K^0_S mass sideband are used for background subtraction. Both data and signal MC results are shown in Table 4.11. Due to the statistics, we combine the three tag modes and find that there is 1.5% difference between data and MC.

We estimate the systematic error on (c_i, s_i) and (c'_i, s'_i) by varying $K^0_S\pi^+\pi^-$ vs. $K^0_S\pi^+\pi^-$ efficiency by 1.5%, the difference is taken as the systematic error.

Table 4.10: The ratio of true events to reconstructed events for $K^0_S\pi^+\pi^-$ vs. $K^0_L\pi^+\pi^-$ Monte Carlo. All numbers are in percentage.

$M_{i,j}$	0	1	2	3	4	5	6	7
0	100.13	101.69	100.88	96.69	104.84	88.50	104.91	99.72
1	102.16	101.55	102.18	92.54	96.83	80.00	103.73	103.42
2	101.53	103.54	100.00	98.82	104.92	89.63	97.18	104.02
3	94.17	98.00	100.79	100.00	105.21	96.39	88.24	106.58
4	87.50	104.76	99.28	103.49	102.04	104.51	94.94	105.26
5	89.96	80.95	95.50	100.00	103.69	97.67	105.90	101.40
6	97.11	95.93	97.58	103.12	102.35	98.40	104.80	105.13
7	99.33	96.54	96.76	104.00	101.06	98.20	102.33	104.31
$M_{i,\bar{j}}$	0	1	2	3	4	5	6	7
0	97.79	112.88	97.70	96.34	95.92	92.06	104.51	100.68
1	97.85	104.74	95.59	90.82	103.14	98.70	99.63	105.27
2	96.78	101.58	97.53	101.81	105.73	95.28	104.88	100.33
3	93.64	152.08	93.79	102.22	111.48	99.46	107.54	92.51
4	90.83	91.67	102.57	100.63	101.83	103.06	96.86	109.80
5	98.72	104.60	98.71	105.42	103.23	97.33	107.56	96.60
6	103.17	99.74	101.56	97.36	105.54	103.56	104.77	96.47
7	98.92	101.11	97.35	101.15	107.35	95.84	102.42	104.21

4.12 $K^0_S\pi^+\pi^-$ vs $K^0_S\pi^+\pi^-$ background

The major background for $K^0_S\pi^+\pi^-$ vs $K^0_S\pi^+\pi^-$ comes from nonresonant four charged pions decay. We have subtracted that part of background from Monte Carlo study. The residue backgrounds (about 30%) are not subtracted in the fit. We study the systematics from generic Monte Carlo. We identify the backgrounds (excluding $\pi^+\pi^-\pi^+\pi^-$) by consulting Monte Carlo truth, then count the number of background events in each bin. The ratios of yields with background subtracted to the original yields are shown in Table 4.12. A new fit is made with the data yields time this table. The difference is taken as systematic error.

4.13 Partial reconstruction

Some of the $K^0_S\pi^+\pi^-$ vs $K^0_S\pi^+\pi^-$ events are partially reconstructed by identifying a missing pion. The background level is about 20% with some four charged pions peaking background. The peaking background has been subtracted from Monte Carlo study in the fit. The rest backgrounds are considered here as systematic errors.

From Table 2.12, there is 15.4% non-peaking backgrounds in the signal region. The systematic errors on c_i are estimated by subtracting 15.4% signals from the partially reconstructed events. Since this part of background is only a very small fraction for the full data sample, we assume the backgrounds are uniformly distributed over the Dalitz plot.

Table 4.11: Systematic study for K^0_S flight significance cut. Tag side ΔE sideband and signal side K^0_S mass sideband are used for background subtraction.

Data	No cut	$f_{sig} > 2$	ratio(%)
$K^-\pi^+$	1078	955	88.6±1.0
$K^-\pi^+\pi^0$	1859	1707	91.8±0.6
$K^-\pi^+\pi^+\pi^-$	1368	1223	89.4±0.8
Total	4305	3885	90.2±0.5
Generic MC	No cut	$f_{sig} > 2$	ratio(%)
$K^-\pi^+$	6842	6265	91.6±0.3
$K^-\pi^+\pi^0$	12811	11706	91.4±0.2
$K^-\pi^+\pi^+\pi^-$	10134	9321	92.0±0.3
Total	29787	27292	91.6±0.2

4.14 $N_{D^0/\bar{D}^0}$

The total number of $D^0/\bar{D}^0$ is calculated from luminosity, which is 818 ± 8 pb^{-1}, and cross section. A systematic study is performed for all the associated errors.

4.15 Backgrounds from non-$D^0/\bar{D}^0$

Continuum Monte Carlo is checked for non-$D^0/\bar{D}^0$ backgrounds. No significant peaking background is seen for double tagged $K^0_S\pi^+\pi^-$ samples. The yields for double tagged $K^0_L\pi^+\pi^-$, and $K^0_L\pi^0$ vs. $K^0_S\pi^+\pi^-$ are shown in Table 4.13. The $M^2_{missing}$ distributions are shown in Fig. 4.2. These yields are already sideband subtracted. The continuum Monte Carlo sample used here is about 4.6 times of the real data. For K^+K^-, $\pi^+\pi^-$, $K^0_S\eta$ modes, the contribution are negligible. For other modes, there are 1∼2% contributions. A systematic study is performed assuming the background is uniform distributed in the Dalitz plot.

4.16 $K^0_L\pi^+\pi^-$ backgrounds

We use $M^2_{missing}$ sidebands to subtract $K^0_L\pi^+\pi^-$ backgrounds. The missing mass sideband is the best way to estimate the background distributions in the Dalitz plot, however, there still might be some difference. To be conservative, we made a new fit assuming the backgrounds of $K^0_L\pi^+\pi^-$ are uniformly distributed in the Dalitz phase space. The differences between the new fit and the nominal fit are taken as systematic errors. The systematics for flavor tagged, CP-even tagged, CP-odd tagged, and $K^0_S\pi^+\pi^-$ tagged $K^0_L\pi^+\pi^-$ samples are considered separately.

4.17 Fit constrain

In the global fit, Δc_i and Δs_i are constrained using a χ^2 term. The errors on Δc_i and Δs_i are studied from BaBar, Belle, and CLEO $D^0 \to K^0_S\pi^+\pi^-$ Dalitz fit results. For a systematic

Table 4.12: Ratios of yields with background subtracted to the original yields.

$M_{i,j}$	0	1	2	3	4	5	6	7
1	0.948							
2	0.948	0.979						
3	0.860	0.877	0.952					
4	0.882	0.969	0.929	0.857				
5	0.933	0.989	0.797	0.955	0.906			
6	0.916	0.868	0.914	0.864	0.987	0.938		
7	0.988	0.964	0.927	0.818	0.949	0.929	0.878	
8	0.957	0.920	0.870	0.898	0.855	0.866	0.890	0.974
$M_{i,\bar{j}}$	0	1	2	3	4	5	6	7
1	0.955							
2	0.950	0.947						
3	0.974	0.977	0.968					
4	0.944	0.944	0.948	1.000				
5	0.994	0.973	1.000	0.903	0.960			
6	0.984	0.984	0.971	0.959	0.988	0.967		
7	0.974	0.969	0.988	0.977	0.991	0.982	0.962	
8	0.976	0.987	0.977	0.964	0.973	0.983	0.989	0.979

Table 4.13: Peaking yields from continuum Monte Carlo. The yields are already sideband subtracted.

	$K^-\pi^+$	$K^-\pi^+\pi^0$	$K^-\pi^+\pi^+\pi^-$	K^+K^-	$\pi^+\pi^-$	$K^0_S\pi^0$	$K^0_S\eta$	$K^0_S\pi^+\pi^-$
$K^0_L\pi^+\pi^-$	87	253	89	2	-1	40	1	46
$K^0_L\pi^0$	/	/	/	/	/	/	/	26

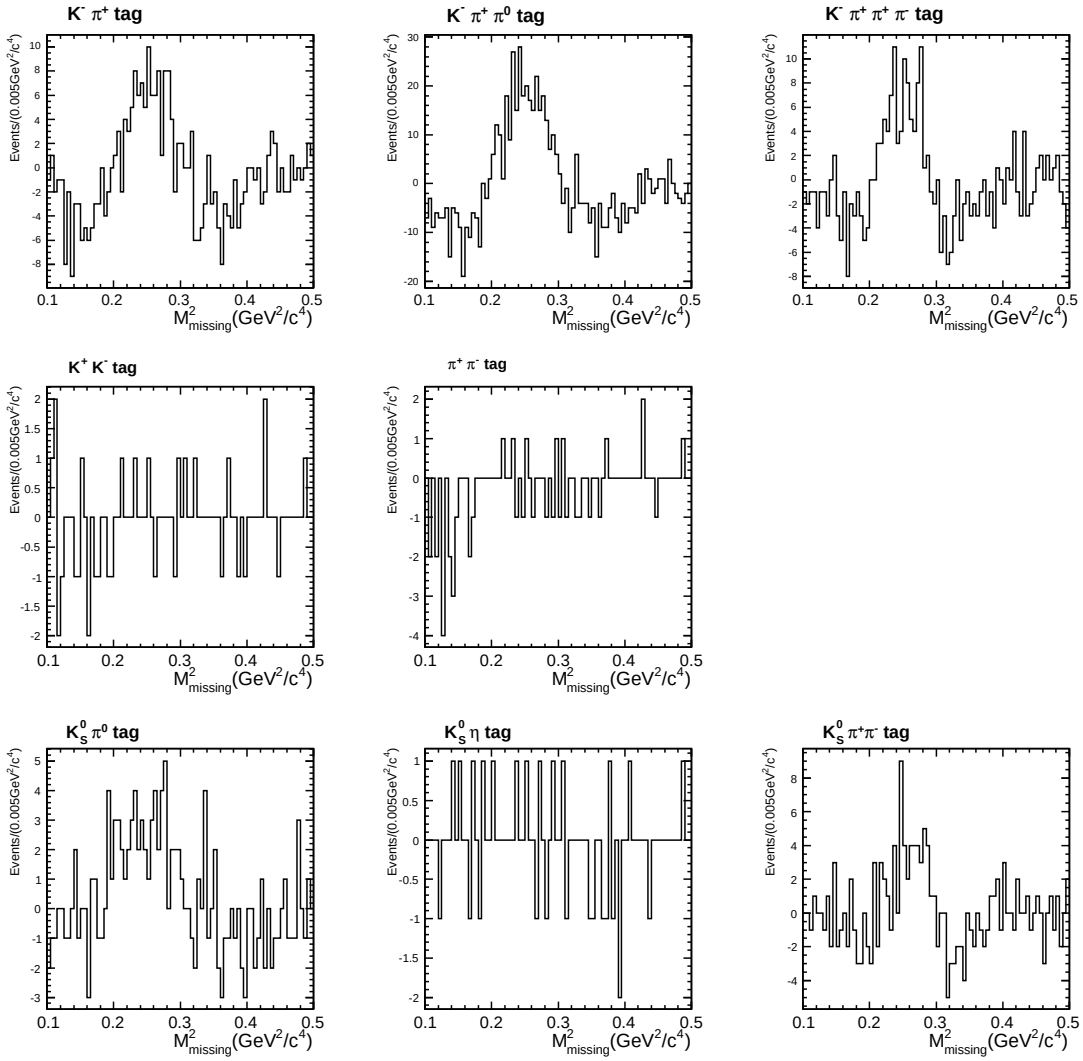

Figure 4.2: Sideband subtracted $K_L^0\pi^+\pi^-$ $M^2_{missing}$ distributions in continuum Monte Carlo.

study, we release the constrain by a factor of 2, i.e. increase the errors by a factor of 2. A new fit is made and the difference is taken as systematic error.

4.18 All systematics

All the systematics are grouped together in Table 4.14, Table 4.15, Table 4.16, and Table 4.17. The following items are considered:

- Item 1: Uncertainties from momentum resolution.
- Item 2: Uncertainties from efficiency systematics.
- Item 3∼8: Uncertainties from CP modes single tag numbers.
- Item 9: Uncertainties from $\mathcal{B}_{K^-e^+\nu}$.
- Item 10: Uncertainties from number of flavor tags.
- Item 11: Uncertainties from total number of $D^0/\bar{D}^0$.
- Item 12: Uncertainties from $\mathcal{B}_{K^0_L\pi^0}$.
- Item 13: Uncertainties from $K^0_L\pi^0$ systematics.
- Item 14: Uncertainties from $K^0_L\pi^0$ backgrounds.
- Item 15: Uncertainties from $K^0_S\pi^0\pi^0$ vs. $K^0_S\pi^+\pi^-$ peaking backgrounds
- Item 16: Uncertainties from $K^0_S\pi^0$ vs. $K^0_S\pi^+\pi^-$ peaking backgrounds.
- Item 17: Uncertainties from $K^0_S\eta$ vs. $K^0_S\pi^+\pi^-$ peaking backgrounds.
- Item 18: Uncertainties from $K^0_S\omega$ vs. $K^0_S\pi^+\pi^-$ peaking backgrounds.
- Item 19: Uncertainties from $K^0_S\pi^+\pi^-$ backgrounds.
- Item 20: Uncertainties from $K^0_S\pi^0$ vs. $K^0_L\pi^+\pi^-$ peaking backgrounds.
- Item 21: Uncertainties from $K^0_S\eta$ vs. $K^0_L\pi^+\pi^-$ peaking backgrounds.
- Item 22: Uncertainties from $K^0_S\pi^+\pi^-$ vs. $K^0_S\pi^+\pi^-$ multi-candidate selection.
- Item 23: Uncertainties from K^0_S flight significance cut.
- Item 24: Uncertainties from $K^0_S\pi^+\pi^-$ vs. $K^0_S\pi^+\pi^-$ residue backgrounds.
- Item 25: Uncertainties from $K^0_S\pi^+\pi^-$ vs. $K^0_S\pi^+\pi^-$ partial reconstruction.
- Item 26: Uncertainties from $K^0_S\pi^+\pi^-$ vs. $K^0_L\pi^+\pi^-$ multi-candidate selection.
- Item 27: Uncertainties from flavor tags vs. $K^0_L\pi^+\pi^-$ background consideration.

- Item 28: Uncertainties from CP-even tags vs. $K^0_L\pi^+\pi^-$ background consideration.
- Item 29: Uncertainties from CP-odd tags vs. $K^0_L\pi^+\pi^-$ background consideration.
- Item 30: Uncertainties from $K^0_S\pi^+\pi^-$ vs. $K^0_L\pi^+\pi^-$ background consideration.
- Item 31: Uncertainties from flavor tagged $K^0_L\pi^+\pi^-$ non-$D/\bar{D}$ events.
- Item 32: Uncertainties from CP tagged $K^0_L\pi^+\pi^-$ non-$D/\bar{D}$ events.
- Item 33: Uncertainties from $K^0_S\pi^+\pi^-$ vs. $K^0_L\pi^+\pi^-$ non-$D/\bar{D}$ events.
- Item 34: Uncertainties from $K^0_L\pi^0$ vs. $K^0_S\pi^+\pi^-$ non-$D/\bar{D}$ events.
- Item 35: Uncertainties from $K^-\pi^+$ Doubly Cabibbo Suppressed Decay.
- Item 36: Uncertainties from $K^-\pi^+\pi^0$, $K^-\pi^+\pi^+\pi^-$ Doubly Cabibbo Suppressed Decay.
- Item 37: Flavor tagged $K^0_{S,L}\pi^+\pi^-$ statistical error.

The total systematic uncertainty is the quadrature sum of all the above systematic uncertainties.

Table 4.14: Systematic errors for c_i.

	c_1	c_2	c_3	c_4	c_5	c_6	c_7	c_8
p resolution	0.008	0.014	0.010	0.017	0.010	0.011	0.015	0.008
Efficiency	0.004	0.007	0.011	0.008	0.005	0.008	0.010	0.006
$N_{K^+K^-}$	-0.000	0.000	0.001	-0.000	-0.000	0.000	0.001	-0.001
$N_{\pi^+\pi^-}$	-0.000	0.000	0.001	-0.000	-0.001	0.000	0.001	-0.001
$N_{K^0_S\pi^0\pi^0}$	0.000	0.001	0.001	0.000	-0.000	0.001	0.001	0.000
$N_{K^0_S\pi^0}$	-0.000	0.000	-0.000	-0.000	-0.000	0.001	-0.000	-0.000
$N_{K^0_S\eta}$	-0.000	0.000	0.000	-0.000	-0.000	0.001	-0.000	-0.000
$N_{K^0_S\omega}$	-0.001	-0.000	-0.000	-0.001	-0.001	-0.000	-0.001	-0.001
$\mathcal{B}_{K^-e^+\nu}$	0.001	0.003	0.004	0.003	0.001	0.002	0.004	0.002
N_{flavor}	-0.000	0.000	0.000	-0.001	-0.001	0.000	-0.000	-0.001
$N_{D^0/\bar{D}^0}$	0.001	0.002	0.003	0.002	0.000	0.002	0.003	0.001
$\mathcal{B}_{K^0_L\pi^0}$	0.005	0.007	0.013	0.010	0.004	0.008	0.015	0.006
$K^0_L\pi^0$ sys.	0.004	0.005	0.009	0.008	0.003	0.006	0.009	0.006
$K^0_L\pi^0$ BG.	0.004	0.006	0.011	0.009	0.004	0.006	0.010	0.007
$K^0_S\pi^0\pi^0$ vs. $K^0_S\pi^+\pi^-$	0.001	0.001	0.004	0.002	0.001	0.002	0.002	0.001
$K^0_S\pi^0$ vs. $K^0_S\pi^+\pi^-$	-0.001	-0.001	-0.001	-0.001	-0.001	-0.000	-0.002	-0.001
$K^0_S\eta$ vs. $K^0_S\pi^+\pi^-$	-0.000	0.000	-0.000	-0.001	-0.000	0.000	-0.000	-0.001
$K^0_S\omega$ vs. $K^0_S\pi^+\pi^-$	-0.001	-0.000	-0.001	-0.002	-0.000	-0.001	-0.001	-0.001
Signal side	-0.001	-0.001	-0.008	-0.026	-0.013	-0.005	0.003	-0.002
$K^0_S\pi^0$ vs. $K^0_L\pi^+\pi^-$	0.001	0.002	0.001	0.001	0.001	0.002	0.001	0.001
$K^0_S\eta$ vs. $K^0_L\pi^+\pi^-$	-0.000	0.000	0.001	0.000	-0.000	0.001	0.000	-0.000
Multi. Candidate (1)	0.000	-0.000	0.002	-0.005	-0.000	-0.000	-0.003	-0.000
K^0_S cut	-0.000	0.000	0.001	0.000	0.000	0.001	0.001	0.000
$K^0_S\pi^+\pi^-$ BG.	0.001	0.001	0.004	0.002	0.001	0.003	0.000	-0.002
Partial Reconst.	0.000	0.001	0.001	-0.004	-0.001	0.001	0.000	-0.001
Multi. Candidate (2)	0.001	0.003	0.000	-0.004	-0.005	-0.006	-0.001	0.001
$K^0_L\pi^+\pi^-$ BG.(1)	0.005	0.011	0.002	0.002	0.001	0.002	0.006	0.001
$K^0_L\pi^+\pi^-$ BG.(2)	-0.000	0.001	-0.000	0.010	-0.007	-0.003	-0.003	0.001
$K^0_L\pi^+\pi^-$ BG.(3)	0.002	0.015	0.003	-0.005	-0.000	0.001	-0.002	0.001
$K^0_L\pi^+\pi^-$ BG.(4)	0.004	-0.004	-0.000	-0.021	-0.015	-0.011	-0.016	0.005
Constrain	0.001	0.003	0.041	0.024	-0.023	0.011	0.028	-0.004
Non-$D/\bar{D}$ (1)	0.001	0.003	0.002	0.001	0.000	0.001	0.003	0.001
Non-$D/\bar{D}$ (2)	0.007	0.015	0.002	0.004	0.002	0.004	0.003	0.003
Non-$D/\bar{D}$ (3)	-0.000	0.000	-0.002	-0.004	-0.003	-0.003	-0.002	-0.001
Non-$D/\bar{D}$ (4)	0.006	0.007	0.003	0.003	0.001	0.002	0.004	0.002
DCSD (1)	0.009	0.012	0.005	-0.013	0.014	0.012	0.013	0.005
DCSD (2)	0.002	0.001	0.004	0.001	-0.000	0.001	0.003	-0.001
Flavor stat.	0.010	0.015	0.015	0.019	0.010	0.015	0.019	0.009
Sum	0.022	0.038	0.052	0.056	0.039	0.033	0.050	0.020

Table 4.15: Systematic errors for s_i.

	s_1	s_2	s_3	s_4	s_5	s_6	s_7	s_8
p resolution	0.017	0.031	0.018	0.027	0.028	0.016	0.021	0.017
Efficiency	0.018	0.012	0.019	0.010	0.013	0.018	0.013	0.012
$N_{K^+K^-}$	0.001	0.000	0.000	0.000	-0.000	-0.000	0.000	0.000
$N_{\pi^+\pi^-}$	0.001	0.000	0.000	0.000	-0.000	-0.000	0.000	0.000
$N_{K^0_S\pi^0\pi^0}$	0.001	0.000	0.000	0.000	-0.000	-0.000	0.000	0.000
$N_{K^0_S\pi^0}$	0.000	0.000	-0.000	0.000	-0.001	0.000	0.000	0.000
$N_{K^0_S\eta}$	0.000	0.000	-0.000	0.000	-0.000	0.000	0.000	0.000
$N_{K^0_S\omega}$	0.000	0.000	-0.000	0.000	-0.000	0.000	0.000	0.000
$\mathcal{B}_{K^-e^+\nu}$	-0.004	0.000	-0.006	-0.004	-0.005	0.002	-0.005	-0.002
N_{flavor}	0.000	0.000	-0.000	0.000	-0.000	-0.000	0.000	0.000
$N_{D^0/\bar{D}^0}$	-0.000	0.000	-0.001	-0.001	-0.002	-0.000	-0.001	-0.000
$\mathcal{B}_{K^0_L\pi^0}$	0.004	-0.000	0.003	0.002	-0.000	-0.003	0.002	0.001
$K^0_L\pi^0$ sys.	0.003	-0.000	0.002	0.002	-0.000	-0.002	0.001	0.001
$K^0_L\pi^0$ BG.	0.003	-0.000	0.003	0.002	-0.000	-0.003	0.002	0.001
$K^0_S\pi^0\pi^0$ vs. $K^0_S\pi^+\pi^-$	0.001	0.000	0.000	0.001	-0.000	-0.000	0.000	0.000
$K^0_S\pi^0$ vs. $K^0_S\pi^+\pi^-$	0.000	0.000	-0.000	0.000	-0.000	0.000	0.000	0.000
$K^0_S\eta$ vs. $K^0_S\pi^+\pi^-$	0.000	0.000	-0.000	0.000	-0.000	-0.000	0.000	0.000
$K^0_S\omega$ vs. $K^0_S\pi^+\pi^-$	0.000	0.000	-0.000	0.000	-0.000	0.000	0.000	0.000
Signal side	0.001	0.000	-0.001	-0.002	-0.000	-0.000	0.000	0.001
$K^0_S\pi^0$ vs. $K^0_L\pi^+\pi^-$	0.001	0.000	-0.000	0.000	-0.001	-0.000	0.000	0.000
$K^0_S\eta$ vs. $K^0_L\pi^+\pi^-$	0.000	0.000	-0.000	0.000	-0.000	0.000	0.000	0.000
Multi. Candidate (1)	-0.003	-0.003	0.015	0.004	0.002	0.003	-0.010	0.006
K^0_S cut	-0.000	0.000	0.000	0.000	-0.001	0.001	0.000	0.001
$K^0_S\pi^+\pi^-$ BG.	-0.009	0.011	-0.038	-0.024	-0.011	0.001	-0.019	-0.013
Partial Reconst.	-0.000	0.004	-0.001	0.003	0.003	0.005	0.002	-0.004
Multi. Candidate (2)	0.035	0.017	0.029	0.011	0.024	-0.026	0.024	0.007
$K^0_L\pi^+\pi^-$ BG.(1)	-0.011	-0.008	-0.012	-0.009	-0.003	-0.002	-0.009	-0.005
$K^0_L\pi^+\pi^-$ BG.(2)	-0.000	-0.001	0.000	0.002	-0.000	0.000	0.000	0.000
$K^0_L\pi^+\pi^-$ BG.(3)	-0.000	-0.001	-0.001	0.001	0.002	0.000	0.000	0.000
$K^0_L\pi^+\pi^-$ BG.(4)	0.065	0.016	0.035	0.041	0.012	-0.043	0.008	-0.010
Constrain	0.037	0.008	0.040	0.025	0.007	-0.030	0.014	-0.004
Non-$D/\bar{D}$ (1)	-0.002	-0.001	-0.002	-0.001	-0.002	-0.000	-0.002	-0.001
Non-$D/\bar{D}$ (2)	0.002	-0.001	0.001	0.001	-0.001	-0.001	0.001	0.000
Non-$D/\bar{D}$ (3)	0.004	0.001	0.005	0.005	0.003	-0.003	0.002	0.001
Non-$D/\bar{D}$ (4)	0.002	-0.001	0.001	0.001	-0.000	-0.002	0.001	0.000
DCSD (1)	0.004	0.001	-0.003	0.002	-0.001	-0.003	0.002	0.001
DCSD (2)	0.021	-0.004	0.031	0.017	0.015	-0.005	0.024	0.016
Flavor stat.	0.034	0.032	0.045	0.033	0.034	0.029	0.036	0.024
Sum	0.096	0.054	0.096	0.074	0.057	0.070	0.062	0.041

Table 4.16: Systematic errors for c_i'.

	c_1'	c_2'	c_3'	c_4'	c_5'	c_6'	c_7'	c_8'
p resolution	0.007	0.015	0.010	0.018	0.009	0.012	0.017	0.007
Efficiency	0.006	0.006	0.009	0.009	0.004	0.007	0.011	0.006
$N_{K^+K^-}$	-0.001	-0.001	-0.002	-0.001	-0.000	-0.001	-0.002	-0.001
$N_{\pi^+\pi^-}$	-0.001	-0.000	-0.002	-0.001	-0.000	-0.001	-0.001	-0.001
$N_{K^0_S\pi^0\pi^0}$	-0.000	0.000	0.000	0.000	0.000	0.000	0.000	0.000
$N_{K^0_S\pi^0}$	0.000	-0.000	0.001	0.002	0.001	0.001	0.002	0.000
$N_{K^0_S\eta}$	-0.000	-0.000	0.000	0.000	0.000	0.001	0.001	-0.000
$N_{K^0_S\omega}$	-0.001	-0.001	-0.001	-0.000	0.000	-0.000	-0.000	-0.001
$\mathcal{B}_{K^-e^+\nu}$	0.001	0.002	0.003	0.003	0.002	0.003	0.003	0.002
N_{flavor}	-0.001	-0.000	-0.000	-0.000	0.000	0.000	0.000	-0.000
$N_{D^0/\bar{D}^0}$	0.001	0.001	0.001	0.001	0.001	0.001	0.001	0.001
$\mathcal{B}_{K^0_L\pi^0}$	0.004	0.006	0.005	0.005	0.003	0.004	0.005	0.006
$K^0_L\pi^0$ sys.	0.002	0.004	0.003	0.004	0.003	0.003	0.003	0.005
$K^0_L\pi^0$ BG	0.003	0.005	0.004	0.005	0.003	0.003	0.003	0.006
$K^0_S\pi^0\pi^0$ vs. $K^0_S\pi^+\pi^-$	0.000	0.000	0.001	0.001	0.001	0.001	0.001	0.001
$K^0_S\pi^0$ vs. $K^0_S\pi^+\pi^-$	-0.001	-0.001	-0.001	-0.001	-0.000	-0.000	-0.000	-0.001
$K^0_S\eta$ vs. $K^0_S\pi^+\pi^-$	-0.001	-0.000	-0.000	-0.000	0.000	0.000	0.000	-0.000
$K^0_S\omega$ vs. $K^0_S\pi^+\pi^-$	-0.001	-0.001	-0.001	-0.001	0.000	-0.000	-0.000	-0.001
Signal side	-0.002	-0.001	-0.005	-0.012	-0.007	-0.003	-0.001	-0.002
$K^0_S\pi^0$ vs. $K^0_L\pi^+\pi^-$	0.002	0.002	0.003	0.003	0.002	0.003	0.004	0.001
$K^0_S\eta$ vs. $K^0_L\pi^+\pi^-$	-0.000	-0.000	0.001	0.001	0.000	0.000	0.001	-0.000
Multi. Candidate (1)	-0.000	-0.001	0.000	-0.002	0.000	-0.000	-0.001	0.000
K^0_S cut	-0.000	-0.000	0.000	0.000	0.001	0.000	0.000	0.000
$K^0_S\pi^+\pi^-$ BG.	0.000	0.001	0.002	0.001	0.001	0.002	0.001	-0.001
Partial Reconst.	-0.000	0.000	0.000	-0.002	-0.000	0.000	-0.000	-0.001
Multi. Candidate (2)	0.003	0.003	0.000	-0.004	-0.002	-0.004	-0.000	0.001
$K^0_L\pi^+\pi^-$ BG.(1)	0.007	0.012	-0.002	0.001	0.001	0.000	0.009	0.001
$K^0_L\pi^+\pi^-$ BG.(2)	-0.000	0.000	-0.005	0.035	-0.012	-0.006	-0.009	0.001
$K^0_L\pi^+\pi^-$ BG.(3)	0.004	0.016	0.007	-0.017	0.000	-0.001	-0.007	0.002
$K^0_L\pi^+\pi^-$ BG.(4)	0.003	-0.004	0.011	-0.025	-0.013	-0.012	0.003	0.006
Constrain	-0.003	0.006	-0.046	-0.047	0.032	-0.022	-0.028	0.006
Non-$D/\bar{D}$ (1)	0.002	0.003	0.001	0.000	0.000	0.000	0.003	0.001
Non-$D/\bar{D}$ (2)	0.011	0.016	0.005	0.006	0.003	0.004	0.008	0.004
Non-$D/\bar{D}$ (3)	-0.000	-0.000	-0.001	-0.003	-0.002	-0.002	-0.001	-0.001
Non-$D/\bar{D}$ (4)	0.004	0.006	0.001	0.002	0.001	0.001	0.001	0.002
DCSD (1)	-0.011	0.012	0.007	-0.014	0.014	-0.013	0.014	0.005
DCSD (2)	0.002	0.001	0.001	0.000	0.001	0.001	0.004	0.001
Flavor stat.	0.010	0.015	0.011	0.013	0.009	0.012	0.017	0.009
Sum	0.024	0.039	0.053	0.074	0.043	0.036	0.045	0.020

Table 4.17: Systematic errors for s'_i.

	s'_1	s'_2	s'_3	s'_4	s'_5	s'_6	s'_7	s'_8
p resolution	0.023	0.036	0.025	0.040	0.028	0.022	0.028	0.024
Efficiency	0.018	0.012	0.015	0.009	0.012	0.018	0.013	0.013
$N_{K^+K^-}$	0.001	0.000	0.000	0.001	-0.000	-0.000	0.001	0.000
$N_{\pi^+\pi^-}$	0.001	0.000	0.000	0.001	-0.000	-0.000	0.001	0.000
$N_{K^0_S\pi^0\pi^0}$	0.001	0.000	-0.000	0.001	-0.000	-0.000	0.000	0.000
$N_{K^0_S\pi^0}$	0.000	0.001	-0.000	0.000	-0.000	0.000	0.000	0.000
$N_{K^0_S\eta}$	0.000	0.001	-0.000	0.000	-0.000	-0.000	0.000	0.000
$N_{K^0_S\omega}$	0.000	0.001	-0.000	0.000	-0.000	0.000	0.000	0.000
$\mathcal{B}_{K^-e^+\nu}$	-0.004	0.001	-0.006	-0.003	-0.004	0.002	-0.005	-0.002
N_{flavor}	0.000	0.000	-0.000	0.000	-0.000	-0.000	0.000	0.000
$N_{D^0/\bar{D}^0}$	-0.000	0.001	-0.001	-0.000	-0.002	-0.000	-0.001	-0.001
$\mathcal{B}_{K^0_L\pi^0}$	0.004	-0.000	0.002	0.002	-0.000	-0.004	0.002	0.000
$K^0_L\pi^0$ sys.	0.003	0.000	0.002	0.002	-0.000	-0.003	0.001	0.001
$K^0_L\pi^0$ BG.	0.003	0.000	0.002	0.002	-0.000	-0.003	0.002	0.001
$K^0_S\pi^0\pi^0$ vs. $K^0_S\pi^+\pi^-$	0.001	0.001	0.000	0.001	-0.000	-0.001	0.000	0.000
$K^0_S\pi^0$ vs. $K^0_S\pi^+\pi^-$	0.000	0.001	-0.000	0.000	-0.000	0.000	0.000	0.000
$K^0_S\eta$ vs. $K^0_S\pi^+\pi^-$	0.000	0.000	-0.000	0.000	-0.000	-0.000	0.000	0.000
$K^0_S\omega$ vs. $K^0_S\pi^+\pi^-$	0.000	0.000	-0.000	0.000	-0.000	0.000	0.000	0.000
Signal side	0.001	0.000	-0.000	-0.002	-0.000	-0.000	0.001	0.001
$K^0_S\pi^0$ vs. $K^0_L\pi^+\pi^-$	0.001	0.001	-0.000	0.000	-0.001	-0.000	0.000	0.000
$K^0_S\eta$ vs. $K^0_L\pi^+\pi^-$	0.000	0.001	-0.000	0.000	-0.000	-0.000	0.000	0.000
Multi. Candidate (1)	-0.003	-0.002	0.013	0.004	0.002	0.002	-0.009	0.006
K^0_S cut	-0.000	0.001	-0.000	0.001	-0.001	0.001	0.000	0.001
$K^0_S\pi^+\pi^-$ BG.	-0.009	0.012	-0.035	-0.021	-0.010	0.002	-0.018	-0.015
Partial Reconst.	-0.000	0.004	-0.001	0.003	0.003	0.005	0.002	-0.003
Multi. Candidate (2)	0.037	0.018	0.029	0.006	0.024	-0.026	0.024	0.008
$K^0_L\pi^+\pi^-$ BG.(1)	-0.011	-0.008	-0.011	-0.008	-0.002	-0.001	-0.009	-0.006
$K^0_L\pi^+\pi^-$ BG.(2)	-0.000	-0.000	0.000	0.003	-0.000	0.000	0.000	0.000
$K^0_L\pi^+\pi^-$ BG.(3)	-0.000	-0.001	-0.001	0.001	0.002	0.001	0.000	0.000
$K^0_L\pi^+\pi^-$ BG.(4)	0.067	0.015	0.029	0.038	0.006	-0.043	0.006	-0.011
Constrain	0.022	-0.039	0.007	-0.000	-0.009	-0.058	0.035	0.035
Non-$D/\bar{D}$ (1)	-0.002	-0.001	-0.002	-0.001	-0.002	-0.000	-0.002	-0.001
Non-$D/\bar{D}$ (2)	0.002	-0.001	0.000	0.001	-0.001	-0.001	0.001	0.000
Non-$D/\bar{D}$ (3)	0.004	0.002	0.005	0.005	0.003	-0.003	0.002	0.001
Non-$D/\bar{D}$ (4)	0.002	-0.000	0.001	0.001	-0.000	-0.002	0.001	0.000
DCSD (1)	0.004	0.001	-0.002	0.002	-0.001	-0.003	0.002	-0.001
DCSD (2)	0.020	-0.005	0.028	0.014	0.013	-0.005	0.024	0.018
Flavor stat.	0.034	0.033	0.042	0.029	0.033	0.031	0.037	0.028
Sum	0.095	0.070	0.082	0.069	0.055	0.088	0.073	0.060

Chapter 5

Conclusion

The final results are shown in Fig. 5.1 and Table 5.1. In Table 5.1, the first error is statistical error, the second error is systematic error. The correlation matrix among c_i, s_i is shown in Table 3.19.

For s_i and s_i', they have two-fold ambiguities, we choose the one predicted by the isobar model.

The impact on γ measurement of the input c_i and s_i measured in this analysis is studied using Monte Carlo samples. Assuming plenty of $B^{\pm} \to \tilde{D}^0 K^{\pm}$ data, we found the uncertainty on γ due to CLEO-c results is about 2°, which is much lower than the model dependent uncertainty. The results presented here can be used by LHCb and future Super-B factories to improve the determination of γ.

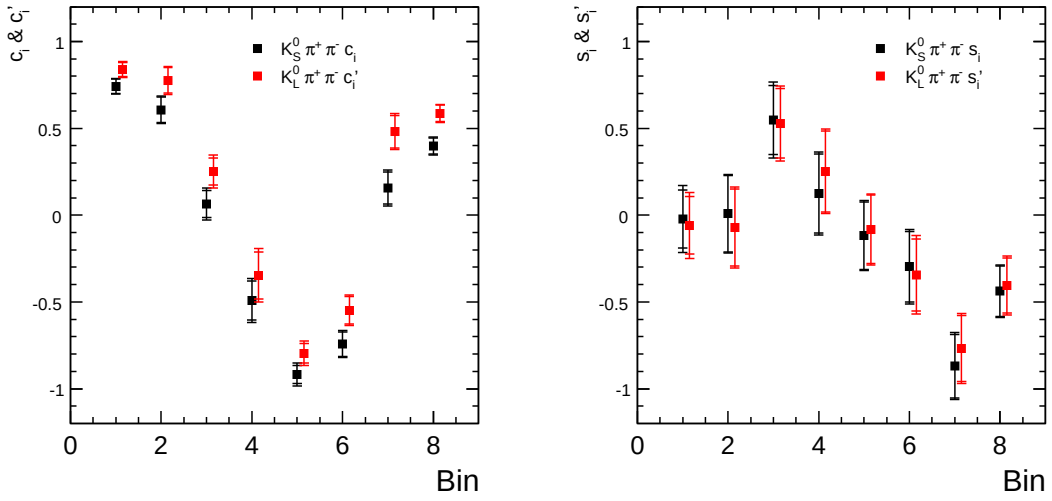

Figure 5.1: Final results. (c_i, c_i') are shown in the left plot, (s_i, s_i') are shown in the right plot. Inner errors are statistical errors, outer errors are the total errors.

Table 5.1: Final results. First error is statistical error, second error is systematic error. (c_i, s_i) are associated with $K^0_S\pi^+\pi^-$, (c'_i, s'_i) are associated with $K^0_L\pi^+\pi^-$

i	c_i	c'_i	s_i	s'_i
1	0.742±0.041±0.022	0.839±0.041±0.024	-0.022±0.168±0.096	-0.059±0.165±0.095
2	0.607±0.073±0.038	0.776±0.073±0.039	0.009±0.220±0.054	-0.071±0.223±0.070
3	0.064±0.077±0.052	0.251±0.078±0.053	0.548±0.198±0.096	0.529±0.200±0.082
4	-0.492±0.113±0.056	-0.347±0.135±0.074	0.124±0.227±0.074	0.252±0.233±0.069
5	-0.918±0.053±0.039	-0.796±0.056±0.043	-0.118±0.194±0.057	-0.082±0.197±0.055
6	-0.743±0.071±0.033	-0.548±0.080±0.036	-0.296±0.203±0.070	-0.344±0.208±0.088
7	0.156±0.092±0.050	0.481±0.094±0.045	-0.870±0.183±0.062	-0.768±0.189±0.073
8	0.398±0.047±0.020	0.586±0.048±0.020	-0.438±0.146±0.041	-0.405±0.158±0.060

Bibliography

[1] B. Aubert *et al.* (BaBar collaboration), Phys. Rev. Lett. **95**, 121802 (2005).

[2] A. Poluektov *et al.* (Belle collaboration), Phys. Rev. D **70**, 072003 (2004); A. Poluektov *et al.* (Belle collaboration), Phys. Rev. D **73**, 112009 (2006).

[3] B. Aubert *et al.* (BaBar collaboration), Phys. Rev. D **71**, 112003 (2005); Phys. Rev. D **73**, 11101 (R) (2006)

[4] F. J. Ronga *et al.* (Belle collaboration), Phys. Rev. D **73**, 092003 (2006).

[5] Werner Sun *et al.* (CLEO Collaboration), CBX 07-31.

[6] R. A. Briere *et al.* (CLEO collaboration), CBX 04-22 (2004); P. Onyisi, *et al.*, CBX 06-11 (2006).

[7] H. Albrecht *et al.* (ARGUS collaboration), Phys. Lett. B **241**, 278 (1990).

[8] B. Sanghi *et al.* (CLEO collaboration), CBX 08-024.

[9] G J. Gounaris and J. J Sakurai, Phys. Rev. Lett. **22**, 244 (1968).

[10] Anjan Giri *et al.*, PRD **68**, 054018 (2003).

[11] A. Bondar *et al.*, hep-ph/0510246, (2006), Eur. Phys. J. C **47**, 347-353 (2006).

[12] David M. Asner (CLEO collaboration), CBX 01-03.

[13] BES Collaboration, Physics Letters B **607** (2005) 243-253.

[14] S. Dobbs *et al.* (CLEO Collaboration), PRD **76**, 112001 (2007).

[15] Q. He *et al.* (CLEO Collaboration), PRL **100**, 091801 (2008).

[16] Q. He *et al.* (CLEO Collaboration), CBX 07-27.

[17] L. M. Zhang *et al.* (Belle Collaboration), PRL **96**, 151801 (2006).

[18] X. C. Tian *et al.* (Belle Collaboration), PRL **95**, 231801(2005).

[19] J. M. Link *et al.* (Focus Collaboration), PRD **75**, 052003 (2007).